UNIVERSIDADE
BEIRA INTERIOR

Collision Dynamics of a Single Droplet onto a Heated Dry Surface: Jet Fuel and HVO Mixtures

(Versão final após defesa)

Pedro Miguel Moreira Pinto

Dissertação para obtenção do Grau de Mestre em
Engenharia Aeronáutica
(Mestrado Integrado)

Orientador: Prof. Doutor André Resende Rodrigues da Silva

abril de 2021

Acknowledgements

First and foremost, I would like to thank my supervisor, Professor André Resende Rodrigues da Silva, for the guidance and counselling provided, and for accepting to be my supervisor in short notice.

I would also like to thank the opportunity to be a part of AEROG - Aeronautics and Astronautics Research Center. This work could not have been done without the resources provided by this laboratory.

I am thankful to all the people that were always present in the laboratory for the support and moments of joy. I would like to especially thank two PhD students, Daniel Vasconcelos and Daniela Ribeiro, for all the patience and extra guidance, all the teachings, all the persistence and, most importantly, helping me with my work. I can not thank them enough for everything they did for me.

I am grateful for the lab technician, Mr. Rui Manuel Tomé Paulo, who helped me building some parts of the experimental facility.

I would like to thank my friends that were a part of my life in these five years, specially my best friends for hearing me on the ups and downs of this work, for helping me in many situations and for always being by my side through all my academic life.

Last but not least, I would like to thank my parents and my siblings for all the support and encouragement over the course of five years of studies.

Resumo

A preocupação com o ambiente levou o ser humano a desenvolver novos combustíveis alternativos para reduzir a poluição e mitigar a emissão de gases de efeito de estufa. O setor de transporte aéreo e a queima de combustíveis fósseis é responsável por grande parte da poluição. Por conseguinte, introduzir novas formas sustentáveis de fornecer energia, como os biocombustíveis, é de elevada importância. Contudo, de modo a tornar estes novos meios de energia mais eficientes e seguros, é necessário realizar estudos relativos à injecção de combustíveis nas câmaras de combustão e ao impacto de gotas.

Este estudo é focado numa investigação experimental sobre o impacto de gotas numa superfície sólida quente. O principal objectivo deste trabalho é analisar a influência da temperatura da superfície na morfologia do impacto de uma única gota e observar os possíveis resultados. Para isso, nestes ensaios experimentais foram utilizadas misturas de Jet Fuel e HVO (Óleo Vegetal Hidroprocessado). Os fluidos utilizados foram: água (como grupo de controlo), 100% Jet A-1, 75% Jet A-1 e 25% NExBTL, 50% Jet A-1 e 50% de NExBTL, e 100% NExBTL. Estas misturas seguem os requisitos da aviação civil, no qual têm que conter um mínimo de 50% de jet fuel.

O presente trabalho estuda os efeitos de impacto de uma gota em função da temperatura da superfície para diferentes fluidos. A energia de impacto foi mantida constante. Portanto, o número de Weber nesta experiência foi fixado em $We = 320$, tendo variado ou o diâmetro da gota ou a velocidade de impacto. Além disso, foram escolhidas diferentes temperaturas da superfície, que variam entre $T_w = 25$ºC e $T_w = 330$ºC, para procurar obter cada fenómeno de impacto e caracterizar a morfologia do mesmo. As dinâmicas de impacto foram capturadas utilizando uma câmara digital de alta velocidade e as imagens foram processadas digitalmente. Foi possível observar os regimes de calor para todos os fluidos, bem como alguns adicionais para as misturas de 75% jet fuel - 25% HVO e 50% jet fuel - 50% HVO.

Palavras-chave

Impacto de gotas, Estudo Experimental, Superfície Quente, Jet Fuel, Biocombustíveis, Efeito de Leidenfrost.

Abstract

The concern with the environment led the human being to develop new alternative fuels to reduce pollution and mitigate the emission of greenhouse gases. The air transport sector and the burning of fossil fuels are responsible for a huge portion of the pollution. Therefore, introducing new sustainable ways to provide energy, such as biofuel, is of major importance. However, in order to make these new energy sources more efficient and safer, it is necessary to carry out studies related to the injection of fuel into the combustion chambers, and the impact of droplets.

This study focuses on an experimental investigation of a single droplet impact onto a heated solid surface. The main purpose of this work is to analyse the influence of wall temperature on the impact morphology of a single droplet and observe the possible outcomes. To do so, in these experimental tests, Jet Fuel and HVO (Hydroprocessed Vegetable Oil) mixtures were used. The fluids tested were: water (as a control group), 100% Jet A-1, 75% Jet A-1 and 25% NExBTL, 50% Jet A-1 and 50% NExBTL, and 100% NExBTL.

The present work studies the impact outcomes depending on the working fluids and the wall temperature. The impact energy was kept constant. Therefore, the Weber number in this experiment was set to $We = 320$ by varying the droplet diameter or the impact velocity. Furthermore, different wall temperatures were chosen, that vary from $T_w = 25$ºC to $T_w = 330$ºC, to seek for every possible impact phenomenon and characterise the impact morphology. The impact dynamics were captured using a high-speed digital camera and the images were digitally processed. It was possible to observe the heat regimes for all fluids, as well as two additional regimes for the mixtures of 75% jet fuel - 25% HVO and 50% jet fuel - 50% HVO.

Keywords

Droplet Impact, Experimental Study, Heated Surface, Jet Fuel, Biofuel, Leidenfrost effect.

Contents

List of Figures

List of Tables

Nomenclature

c_p	Specific heat
Ca	Capillary number
D	Diameter
f	Ratio of the lens focal length to the diameter of the entrance pupil
Fr	Froude number
g	Gravity acceleration
h	Magnitude of film thickness
h_{fg}	Latent heat of evaporation
k	Thermal conductivity
K	'K' number
La	Laplace number
L_a	Length of the wall roughness
L_{nd}	Dimensionless length of the wall roughness
Oh	Ohnesorge number
R	Radius
R_a	Surface roughness
R_{nd}	Dimensionless surface roughness
Re	Reynolds number
t	Time
T	Temperature
U	Velocity
We	Weber number

Greek Symbols

β	Spread factor
δ	Thickness of the vapour layer
θ	Contact angle
μ	Viscosity
ξ	Dimensionless height
ρ	Density
σ	Surface tension
τ	Dimensionless time

Subscripts

o	Related to the droplet
f	Related to the fluid
g	Gas phase
in	Related to the needle
l	Liquid phase
v	Vapour
w	Refers to the wall
rec	Receding
max	Maximum
adv	Advancing
stat	Static
r	Residence
c	Critical
sat	Saturation
PR	Pure rebound
PA	Pure adhesion
N	Nukiyama
L,d	Dynamic Leidenfrost
Leid	Leidenfrost
CHF	Critical heat flux
amb	Ambient
contact	Liquid-solid contact

Superscripts

*	Dimensionless parameter

List of Acronyms

ASTM	American Society for Testing and Materials
CHF	Critical heat flux
fps	Frames per second
HVO	Hydroprocessed vegetable oil
JF	Jet fuel
LED	Light-emitting diode
MATLAB	Matrix algorithm
NExBTL	Neste renewable diesel

Chapter 1

Introduction

This study focuses on an experimental investigation on droplet impact onto a heated wall. The main purpose of this work is to analyse the influence of wall temperature on the morphology of a single droplet impact and observe the possible outcomes. This first chapter is divided into three sections. In the first section, a brief motivation for the present study will be provided. In the second section, the objectives of this work will be listed. In the final section, the organisation and the discussed topics of this dissertation will be presented.

1.1 Motivation

Nowadays, there is a scientific consensus that the observed effects of global warming are caused by fossil fuel combustion and emissions of greenhouse gases, such as nitrous oxide (N_2O), carbon dioxide (CO_2) and methane (CH_4). Additionally, the transport sector and the burning of fossil fuels are responsible for a high portion of the pollution. Therefore, developing alternatives to the commonly used combustion fuels is of major importance. Biofuels play an important role here. These are defined as any sort of fuel that is made from organic matter and have many benefits, such as the independence of political/social unstable energy suppliers, energy security, reduced carbon emissions, increase farm income and rural development [1].

In order to improve the effectiveness of biofuels in providing the highest energy possible and optimising the engines that they will be injected into, intensive research needs to be made regarding droplet impact and spray impingement. To be able to introduce biofuels in aviation, this experimental work used jet fuel and biofuel mixtures. However, according to ASTM D7566-20b, the current civil aviation legislation only allows fuel mixtures to have a maximum amount of 50% biofuel, implying that it is always required to have a minimum of 50% jet fuel [2]. Therefore, in this experimental work, the fluids used were H_2O, 100% Jet A-1, 75% Jet A-1 and 25% NExBTL, 50% Jet A-1 and 50% NExBTL, and 100% NExBTL.

1.2 Objectives

As mentioned above, the goal of this experimental study is to analyse the collision dynamics of droplets of different fluids on a heated wall. In order to analyse the effects of surface temperature on the morphology of the droplet, the impact energy was kept constant. Therefore, the objectives established in this dissertation are the following:

- Visualise and analyse the outcome of droplet impact;
- Describe the phenomena observed in detail;
- Observe the influence of wall temperature and different fluid properties and compare them;
- Provide experimental data to be used in the development of mathematical models.

1.3 Overview

This dissertation is divided into five chapters: Introduction, Literature Review, Experimental Methodology, Results and Discussion, and Conclusions and Future Work.

The current chapter introduces this dissertation and contains the motivation, the objectives of this experimental work, and how this work is organised. The second chapter will be aimed towards the literature review and it will contain the most important subjects to know regarding the current work. It will be mainly focused on droplet impact on heated surfaces, with some information on non-heated surfaces as well. The third chapter will explain the experimental procedure and everything related to the experimental work such as the work methodology, calculations of droplet impact energy, and detailed explanations of the materials used. In the fourth section, an analysis of the image visualisation and discussion over the results will be given. A detailed description of the events observed will be given and compared between the fluids. Last, but not least, the fifth chapter will mention the conclusions of this work and possible improvements for future work.

Chapter 2

Literature Review

This chapter will contain the fundamentals to understand the phenomenon of droplet impact. First, an introduction to the importance of this subject and its applications will be given. Afterwards, the main parameters that govern the droplet impact will be explained. Then, a brief explanation of droplet impact on non-heated surfaces will be presented, followed by a detailed analysis of droplet impact on heated surfaces.

2.1 Introduction

The importance of the phenomenon of droplet impact has driven many investigators to comprehend its interactions with mass, momentum, and heat transfer. With newer technology, such as ultra-high-speed imaging, this subject has been widely more covered and investigated. Understanding the phenomena behind droplet impact is key to improve the effectiveness in many industrial applications such as ink-jet printing [3], rapid spray cooling of hot surfaces, such as turbine blades [4], direct fuel injection in combustion engines [5], pesticide spraying of crops [6], fire suppression by sprinklers [7], and many others. In the following topics, the fundamental information for the understanding of droplet impacts will be presented.

2.2 Dimensionless Parameters

According to Liang and Mudawar [8], there are many parameters that influence the phenomenon of droplet impact. These include droplet and fluid physical properties (droplet diameter, D_0, impact velocity, U_0, fluid viscosity, μ_f, fluid density, ρ_f, fluid surface tension, σ), surrounding gas properties (pressure, temperature, flow configuration), and wall characteristics (wettability, diffusivity, surface roughness, and wall temperature, T_w). These parameters combined provide some dimensionless parameters that are used to define the droplet impact. The most used dimensionless numbers are the Reynolds number, Re (equation 2.1), the Weber number, We (equation 2.2), the Ohnesorge number, Oh (equation 2.3), and the Laplace number, La (equation 2.4).

The Reynolds number is the ratio between inertial forces and viscous forces, the Weber number relates the inertial and surface tension forces, the Ohnesorge number represents the ratio of the viscous and surface tension forces, and the Laplace number measures the ratio between the surface tension forces and the momentum-transport (especially dissipation) in-

side a fluid.

$$Re = \frac{\rho_f U_0 D_0}{\mu_f} \quad (2.1)$$

$$We = \frac{\rho_f U_0^2 D_0}{\sigma} \quad (2.2)$$

$$Oh = \frac{\mu_f}{(\rho_f D_0 \sigma)^{\frac{1}{2}}} = \frac{We^{1/2}}{Re} \quad (2.3)$$

$$La = \frac{\rho_f D_0 \sigma}{\mu_f} \quad (2.4)$$

The K number, (equation 2.5), is a dimensionless number that identifies the disintegration and deposition limit on a dry impact. Below the critical value of K, deposition occurs, and above, splash occurs. This number refers to splashing due to the most frequent mechanisms of splashing, which are prompt and corona splashing. [9].

$$K = WeOh^{-0.4} \quad (2.5)$$

Other pertinent parameters are:

$$\rho^* = \frac{\rho_f}{\rho_g} \quad (2.6)$$

$$\mu^* = \frac{\mu_f}{\mu_g} \quad (2.7)$$

$$\tau = \frac{U_0 t}{D_0} \quad (2.8)$$

$$Ca = \frac{\mu_f U_0}{\sigma} \quad (2.9)$$

$$Fr = \frac{U_0^2}{g D_0} \quad (2.10)$$

Where ρ^* (equation 2.6) denotes the ratio of liquid-gas density, μ^* (equation 2.7) is the ratio of liquid-gas viscosity, τ (equation 2.8) corresponds to the non-dimensional time, t represents time after impact, Ca (equation 2.9) stands for the capillary number, and Fr (equation

2.10) corresponds to the Froude number. The capillary number characterises the ratio of viscous forces to surface tension forces, and the Froude number measures the ratio of the inertia force on an element of fluid to the weight of the fluid. In general, gravity effects can be neglected for $Fr \geqslant 10^2$ and, in most cases of droplet impact, they are not relevant [10].

Additionally, another important parameter is the dimensionless temperature, which describes the influence of the wall temperature on the impact outcome. Amiel [11] obtained this temperature, referred as T^* (equation 2.11), from the wall superheat temperature $(T_w - T_{sat})$, which is the difference from the wall temperature, T_w, and the boiling point of the fluid, T_{sat}, and the Leidenfrost temperature (T_{Leid}).

$$T^* = \frac{T_w - T_{sat}}{T_{Leid} - T_{sat}} \quad (2.11)$$

The Leidenfrost temperature is the minimum temperature of the film boiling regime. If the wall temperature is lower than the boiling point, T^* takes a negative value and, above the Leidenfrost temperature, it takes a value higher than 1. The heat flux exchanged between the wall and the droplet is minimal at this temperature.

Opposed to the saturation temperature, the Leidenfrost temperature depends on the nature of the liquid and wall roughness, since roughness tends to increase the number of nucleation sites. The Leidenfrost temperature can be assumed to be constant if the surface roughness, the ambient pressure, the liquid, and the wall materials are kept constant during the experiments. In the following chapters, more information will be provided regarding this temperature.

2.3 Wettability

When a droplet impacts a solid surface, different outcomes may prevail depending on the properties of the liquid-solid interface. One of the most influencing properties that determines the impact phenomenon is the wettability, which is specific for a given liquid/solid/gas system. Wettability describes the ability of a liquid to spread on a solid in a surrounding gas phase and is quantified by the static contact angle, θ_{stat}, as shown in figure 2.1. The contact angle is geometrically defined as the angle formed by a liquid at the three-phase boundary (where a liquid, gas, and solid intersect).

There are three possible cases for the outcome of droplet impact depending on the values of the contact angle. When the static contact angle is zero, $\theta_{stat} = 0^o$, the system is said to be completely wettable. When the static contact angle is smaller than 90^o, $\theta_{stat} < 90^o$, the system is partially wettable, and when the static contact angle is above 90^o, $\theta_{stat} \geq 90^o$, it is a non wettable system [12].

The following two dynamic contact angles are crucial for the understanding of the droplet impact dynamics: the dynamic advancing contact angle, θ_{adv}, and the dynamic receding con-

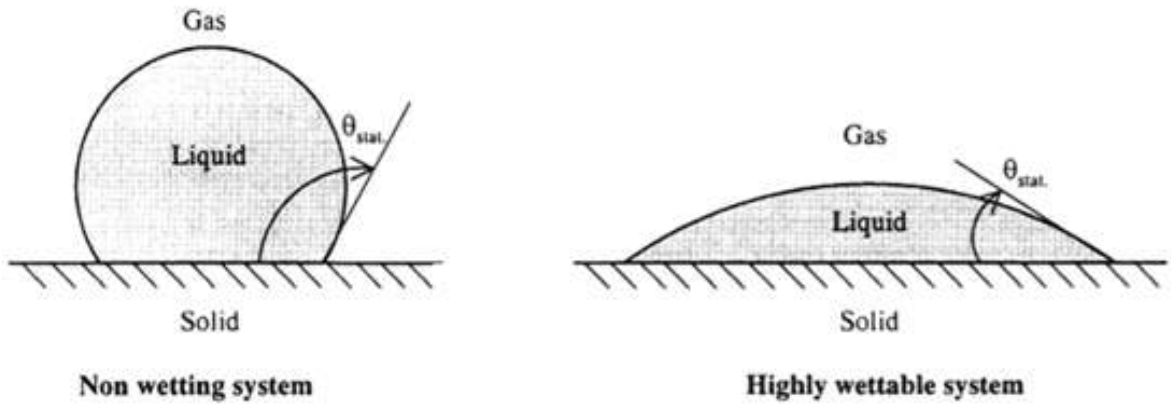

Figure 2.1: Definition of the Static Contact Angle (θ_{stat}). For a non wetting system, θ_{stat} is equal to or higher than 90^{o}, and for a wettable system, θ_{stat} is lower than 90^{o}. The system is completely wettable if $\theta_{stat} = 0^{o}$ [12].

tact angle, θ_{rec}. These two are different from the static contact angle. However, the dynamic contact angles and the static contact angle both depend on the liquid, vapour, the material of the surface, the surface roughness, and any surface impurities. The static contact angle is measured when the droplet hits the surface and stays in a static position. The dynamic advancing contact angle refers to the condition when the interface is advancing towards the vapour phase, i.e., the droplet is spreading and the contact angle increases. The receding contact angle is the opposite. The interface evolves from the solid surface to the liquid phase, i.e., the droplet recedes and the contact angle increases. In fig. 2.2, a visual illustration of the dynamic angles are presented.

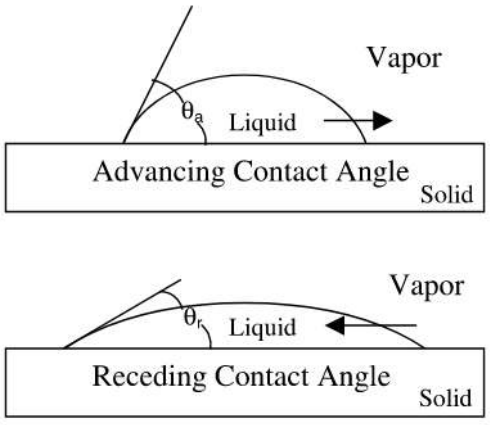

Figure 2.2: Advancing and receding dynamic contact angles, θ_{adv} and θ_{rec}, respectively. Adapted from Bernardin et al. [13].

Bernardin et al. [13] summed up the types of contact angle reported in the literature and investigated the dependence of quasi-static advancing contact angle, θ_{adv}, for a water droplet on a polished aluminium surface. Their results ranged from $25 - 170^{o}$C for wall temperature and $101.3 - 827.4$ kPa for pressure. Two distinct regimes that depend on temperature were identified: a low temperature regime for $T_w < 120^{o}$C, where the static contact angle is rel-

atively constant at $\theta_{stat} = 90^{o}$, and a high temperature regime, $T_w > 120^{o}$C, where contact angle decreases relatively linearly towards zero, according to the relation below:

$$\theta_{stat} = 157.4 - 0.55T_w \quad (2.12)$$

2.4 Boundary Conditions

In this section, an explanation regarding the most common impact targets will be given. Besides the droplet parameters that govern the impact outcomes, the impact target also plays an important role on predicting the collision dynamics. Droplet impact can be classified into three different subtopics based on the impact target: dry solid surface, thin liquid film (also known as pre-wet wall), and deep liquid pool [14]. However, in this dissertation the target that will be addressed is the dry solid surface.

2.4.1 Non-Heated Dry Solid Surface

When a droplet impacts onto a dry non-heated solid surface, the droplet outcome depends on many factors, such as impact energy and surface properties. Earlier phases of the droplet impact are controlled by the Re and We numbers, while in the later stages, the substrate effect is much more important. This means that on a wetting substrate the impact can result in additional spreading, while on a partially wetting substrate, with low surface energy, the droplet may recede. In a non-wetting substrate, the droplet will recede and if the surface is hydrophobic, the droplet may rebound [9]. Additionally, droplet spreading after an impact onto a dry surface can be accompanied by instabilities at the outer rim of the lamella. This phenomenon is termed fingering and the instabilities are called fingers [10].

Rioboo et al. [12] experimentally observed seven possible scenarios of droplet impact on a dry wall: stick, deposition or spreading, prompt splash, corona splash, receding breakup, partial rebound, and complete rebound.

Stick occurs at very low impact energies when the droplet is gently deposited and it adheres to the surface in a nearly spherical form. Deposition or spreading (Fig. 2.3) takes into consideration when the droplet deforms and sticks to the surface during its impacting process, without formation of secondary droplets. This outcome occurs when the impact energy is low and the impact fails to create capillary waves. These waves are generated after droplet impact, where thin liquid sheets grow into a lamella that propagates in the radial direction [15]. The maximum spread factor, $\beta_{max} = \frac{2R_{max}}{D_0}$, which is the ratio of the final lamella diameter at the wall, $2R_{max}$, and the droplet diameter, varies from 1.25 to 5.

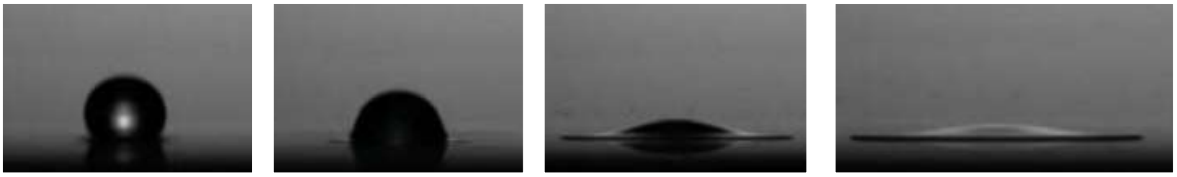

Figure 2.3: Deposition phenomenon according to Rioobo et al. Adapted from Cunha [16]

The prompt splash (Fig. 2.4) occurs when the liquid lamella disintegrates in the periphery into secondary droplets in the spreading phase. It is promoted by a higher impact energy on rough surfaces. At the end, the droplet spreads and stays on the wall.

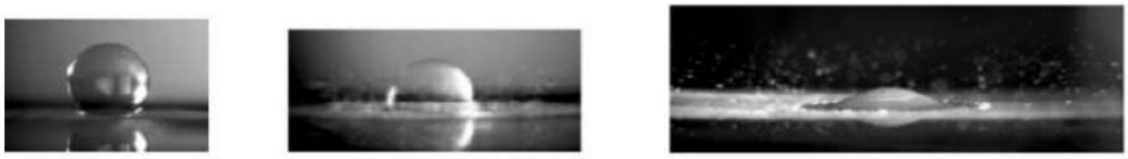

Figure 2.4: Prompt splash phenomenon according to Rioobo et al. [12].

Reducing the surface tension, the liquid lamella can separate from the wall, resulting in corona splash (Fig. 2.5). The corona splash occurs on a smooth surface, where the outer rim of the expanding lamella is lifted off the surface to form a corona shaped structure, from which a high number of secondary droplets are generated. This phenomenon is very characteristic of droplet impacts on liquid films. The corona splash can be inhibited by decreasing ambient pressure.

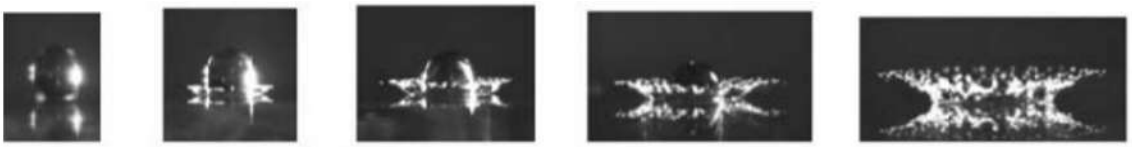

Figure 2.5: Corona splash phenomenon according to Rioobo et al. [12].

Receding breakup (Fig. 2.6) occurs when some tiny droplets detach from the original droplet in the receding phase. The dynamic contact angle decreases as the liquid retracts from its maximum spreading radius. If the limiting value of zero is reached, some droplets are left behind the receding lamella.

Figure 2.6: Receding breakup phenomenon according to Rioobo et al. [12].

Partial rebound and complete rebound (Fig. 2.7 and Fig. 2.8, respectively) only happen when a receding phase is observed. The occurrence of this phase depends on the maximum diameter reached by the spreading droplets and the receding contact angle. For higher energetic impacts, this diameter is larger, and the maximum diameter is even larger than it would be expected, given the static receding contact angle. In this case, the droplet begins to recede.

The difference between whether it is complete or partial rebound is in the dynamic receding contact angle. Knowing that the receding phase is energetic enough in both cases, for lower values of receding contact angle a partial rebound occurs (Fig. 2.7), and for higher values, a complete rebound occurs (Fig. 2.8).

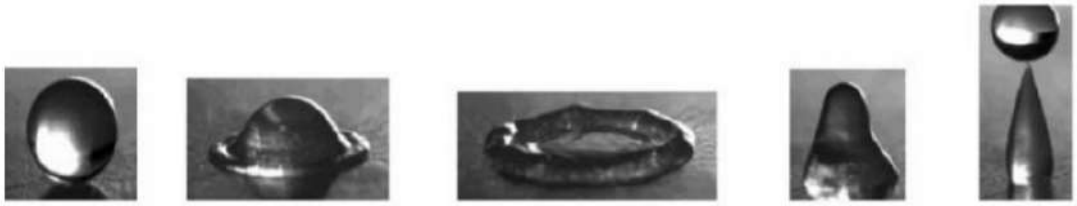

Figure 2.7: Partial rebound phenomenon according to Rioobo et al. [12].

Figure 2.8: Complete rebound phenomenon according to Rioobo et al. [12].

Figure 2.9 is adapted from Ferrão [17] and it represents the outcomes of a droplet impact on a non-heated dry solid surface based on the impact energy.

As discussed above, there are several parameters governing the droplets collision dynamics. The surface roughness is the variation in the height of the surface relative to a reference plane and it is an important aspect to take into account in the outcome of droplet impact. Increasing the roughness amplitude (R_a) promotes the prompt splash. This is due to the spreading lamella being perturbed by the roughness, eventually leading to a breakup [12].

The effect of increasing the impact velocity on rough surfaces is to promote prompt splash. For non-wettable systems, the impact velocity also promotes the receding breakup phenomenon. A higher impact velocity leads to a larger spreading diameter, which results in a higher ve-

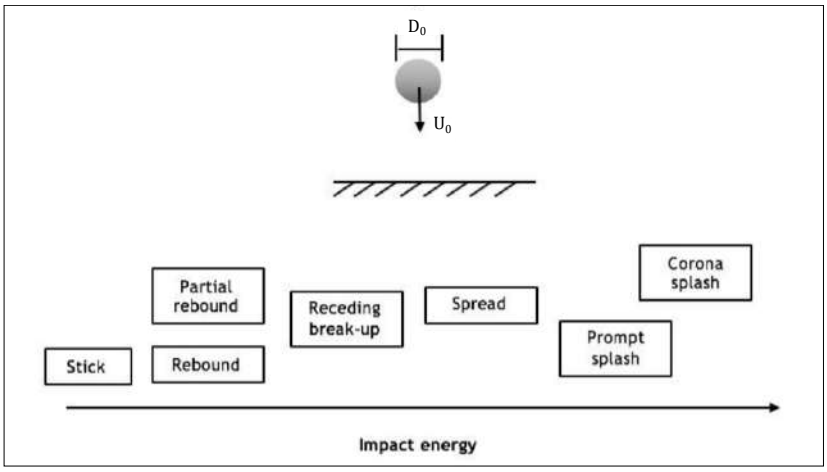

Figure 2.9: Outcomes according to the impact energy. Adapted from Ferrão [17]

locity during the receding phase. Consequently, it leads to a lower dynamic receding contact angle and, therefore, to a higher probability of receding breakup [12].

The droplet diameter plays a major role as well. For the same impact conditions, smaller droplets tend to promote deposition and for larger droplets, corona splash takes place. Furthermore, the corona splash occurs only with the presence of a very smooth surface and is intensified by lower surface tension. For rough surfaces, the prompt splash sets in before a corona can be formed [12].

Increasing the viscosity reduces the probability of all breakup outcomes. According to Almohammadi and Amirfazli [18], for high surface tension fluids at a given droplet velocity, an increase in velocity changes spreading to splashing. However, beyond this limit, an increase in viscosity inhibits the splashing phenomenon.

The surface tension is defined as the elastic-like force existing in the surface of a liquid, that tends to minimise the area of the surface, caused by asymmetries in the intermolecular forces between surface molecules [19]. Usually, values of surface tension are measured when the surface of the liquid is in contact with air. For the same conditions, the surface tension decreases the droplet diameter, and therefore, promotes lower impact energies outcomes. A lower surface tension also promotes corona splash.

In table 2.1, a summary of all the different parameters are shown regarding the effects provided in each outcome of the droplet impact.

Table 2.1: Summary of the effect of each parameter on each outcome. Adapted from Rioobo et al. [12].

Increase of	Deposition	Prompt Splash	Corona Splash	Receding Breakup	Partial Rebound	Complete Rebound
U_0	$\downarrow$	$\uparrow$	$\uparrow$	$\uparrow$	$\uparrow$	$-$
D_0	$\downarrow$	$\uparrow$	$-$	$-$	$-$	$-$
σ	$-$	$\downarrow$	$\downarrow$	$\uparrow$	$\uparrow$	$\uparrow$
μ	$\uparrow$	$\downarrow$	$\downarrow$	$\downarrow$	$-$	$-$
R_a	$\downarrow$	$\uparrow$	$\downarrow$	$-$	$-$	$-$

2.4.2 Heated Dry Solid Surface

The surface temperature is a very important factor that affects the outcomes of the impacting droplets. Nevertheless, the consideration of this factor introduces further complexity to the impact phenomenon. Depending on the surface temperature, distinct heat transfer mechanisms may develop when a droplet impinges a hot surface, depending on wall temperature, T_w, the saturation temperature of the liquid, T_{sat}, and the Leidenfrost temperature, T_{Leid}:

- If $T_w < T_{sat}$, heat transfer is mostly done by conduction from the wall to the liquid and by evaporation due to mass transfer along the liquid-gas interface;
- When $T_w > T_{sat}$, the droplet boils on the heated wall, and tiny bubbles form inside the droplet;
- When $T_w > T_{Leid}$, a thin vapour layer forms between the droplet and the wall, and heat transfer is highly reduced.

Bai and Gosman [20] identified some important temperature ratios:

$$\frac{T_w}{T_{sat}}\,,\ \frac{T_w}{T_{PA}}\,,\ \frac{T_w}{T_N}, \frac{T_w}{T_{PR}}, \frac{T_w}{T_{Leid}}$$

where $T_{sat} < T_{PA} < T_N < T_{PR} < T_{Leid}$

T_{sat} is the saturation temperature (or boiling point), T_N is the Nukiyama temperature at which a droplet reaches its maximum evaporation rate, T_{Leid} is the Leidenfrost temperature or the minimum evaporation temperature. T_{PA} and T_{PR} are termed respectively pure adhesion temperature, below which adhesion occurs at low impact energy and pure rebound temperature, above which bounce occurs at low impact energy.

The wall temperature, T_w, and the impact Weber number are the two most important parameters on determining the regime. It affects both impact dynamics and heat transfer per-

formance. The Leidenfrost temperature is the minimum temperature for the film boiling regime and it is influenced by many parameters, such as surface and liquid properties, and the impact parameters. Based on the increasing pressure in the liquid-solid interface for an impinging droplet, it was established that the Leidenfrost temperature increases for higher droplet velocities [21].

The surface temperature influences the characteristic size of secondary droplets and the splashing threshold. Since the identification of different heat regimes is mostly based on the droplet morphology, some authors define the Leidenfrost temperature as a dynamic property, $T_{L,d}$, which will be discussed in a later topic. In the case of sessile droplet impact, it represents the temperature at which the vapour layer rebounds the droplet, the pure rebound temperature.

2.4.2.1 Regimes of Droplet Impact onto a Heated Wall

Describing the several regimes is quite complex because the phenomena observed must take into account each phase of the boiling regime. There are many studies that address various parameters, such as liquid properties, wall temperature, the disintegration and secondary droplets characteristics, etc. Bertola [22] proposed a classification based on the final outcome instead of the details of the droplet morphology during impact. This includes five main impact regimes for droplet impact onto a dry heated wall (despite the obvious spread/deposition): secondary atomisation, breakup/splashing, rebound, rebound with secondary atomisation, breakup with secondary atomisation (Fig. 2.10).

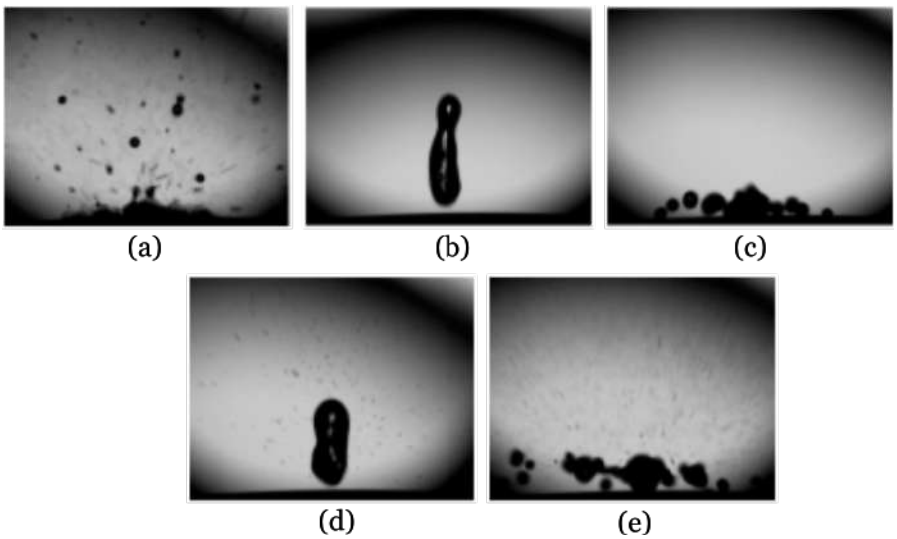

Figure 2.10: Impact outcomes based on the terminology used by Bertola [22]. (a) secondary atomisation; (b) rebound; (c) splashing; (d) rebound with secondary atomisation; (e) breakup with secondary atomisation.

When T_w is above T_{sat}, vapour bubbles created on the heated surface rise by buoyancy and burst on the free surface of the droplet, dispersing a high amount of secondary droplets. The intensity of secondary atomisation varies according to the surface temperature and the Weber number, and the secondary droplets are not uniform in size. Secondary atomisation

depends highly on properties of the surface, specifically its thermal effusivity.

According to Bertola [22], for high surface temperatures for distilled water (above $T_w = 350$°C in an aluminium plate) there are two possible outcomes: droplet rebound for low Weber numbers, and droplet splashing for high Weber numbers. Droplet rebound occurs at high enough temperatures as a result of the formation of a vapour film between the droplet and the surface, which reduces heat transfer. This vapour reduces energy dissipation during droplet spread and recoil. Therefore, promoting rebound. However, if there is an excess in kinetic energy after spread and recoil, the droplet will breakup into smaller droplets which will also remain in the Leidenfrost state. At temperatures lower than $T_w = 350$°C, there are two possible regimes: rebound with secondary atomisation, and splashing with secondary atomisation. This is due to an unstable vapour layer in the solid-liquid interface that allows local contact between the droplet and the surface, where vapour bubbles grow and generate secondary atomisation. This regimes are associated with transition boiling, which will be discussed in the following topics.

However, in this dissertation, the terminology used is based on the evaporation lifetime of a single droplet at different wall temperatures. Ko and Chung [23] proposed four different regimes: film evaporation, nucleate boiling, transition boiling, and film boiling. An illustration of these regimes is presented in figure 2.11. The droplet evaporation time decreases as the surface temperature increases up to the critical heat flux (CHF). Then, the evaporation time rapidly decreases until the Leidenfrost temperature. Beyond this temperature, as the surface temperature increases, the evaporation time slightly decreases. It is important to

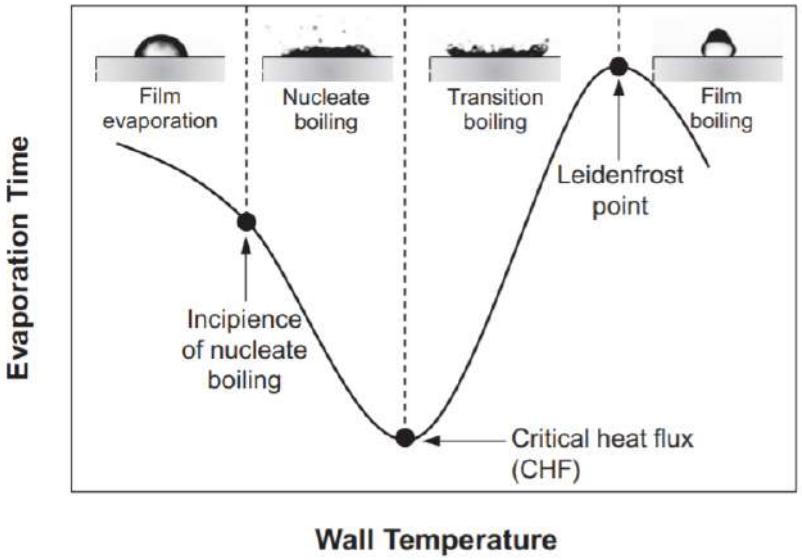

Figure 2.11: Heat transfer regimes of droplet impact onto a hot wall, as reported by Ko and Chung [23].

notice that, in the film evaporation and nucleate boiling regimes, a liquid film is formed on the surface. Therefore, these are considered as wetting regimes. As for the transition and film boiling regimes, they are non-wetting because the vapour layer formed prevents contact

between the droplet and the wall.

2.4.2.1.1 Film Evaporation

This regime takes place when $T_w < T_{sat}$ and heat transfer occurs mainly by conduction from the wall to the liquid and evaporation due to mass transfer along the liquid-gas interface. The saturation temperature is the temperature at which the vapour pressure of a liquid equals the surrounding pressure and the liquid changes into a vapour.

Seki et al. [24] measured the liquid-solid contact temperature, $T_{contact}$ (equation 2.13), using a thin-film thermometer, and compared the results to theoretical values.

$$T_{contact} = \frac{T_w \sqrt{(k\rho\, c_p)_w} + T_f \sqrt{(k\rho\, c_p)_f}}{\sqrt{(k\rho\, c_p)_w} + \sqrt{(k\rho\, c_p)_f}} \quad (2.13)$$

c_p and k represent the specific heat and the thermal conductivity, respectively. For most situations regarding droplet impact onto a heated wall, the heat transfer from the wall to the fluid is higher, $(k\rho c_p)_w \gg (k\rho c_p)_f$, which results in $T_{contact} \cong T_w$. They also found that T_w decreases to $T_{contact}$ right after the initial impact, and $T_{contact}$ increases with higher initial wall temperatures. Additionally, $T_{contact}$ for a water droplet is approximately constant for $100 \ll T_w - T_{sat} \ll 200$°C, but increases for $T_w - T_{sat} \geq 200$°C.

Fig. 2.12 represents a scheme of the three stages of the film evaporation regime: initial, fundamental, and final. The initial stage refers to the droplet impingement phase where, after contact, the droplet spreads and oscillates until it achieves an equilibrium state consisting of a spherical liquid cap.

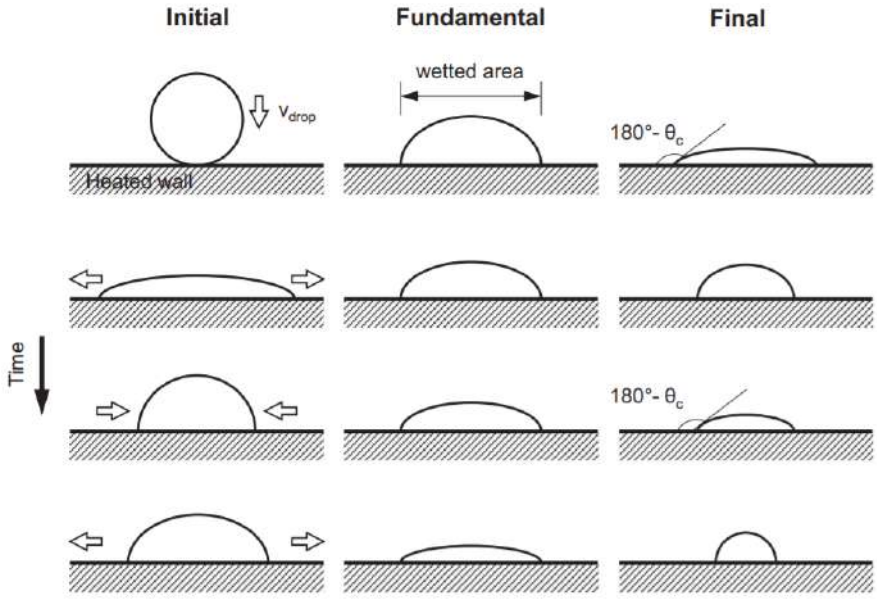

Figure 2.12: Representation of the stages of droplet impact with a heated wall during film evaporation regime. Adapted from Liang and Mudawar [25].

The fundamental stage refers to the evaporation of the spherical cap, while preserving constant wetting area, but with the contact angle and droplet height gradually decreasing. According to di Marzo and Evans [26], the fundamental stage takes about 80% of the total droplet evaporation time. The final stage corresponds to a rapid succession of events, where the spherical cap shrinks laterally into a cap with smaller wetted area. Afterwards, it incurs further evaporation, before shrinking again into a smaller cap and evaporating, and so on, until the liquid is completely evaporated. Droplet heat transfer in this regime is influenced by temperature variations inside the droplet and the wall, the wall heat flux, and the droplet evaporation time.

Chandra et al. [27] reported that reducing the contact angle with the aid of surfactant increases droplet evaporation rate by increasing droplet-wall contact area and decreasing film thickness. Decreasing initial contact angle from $\theta_{stat} = 90^{o}$ to $\theta_{stat} = 20^{o}$ reduces droplet evaporation time by about 50%. After impact, wall temperature is lowest at the impact point and increases in the radial direction.

Liang et al. [28] showed experimentally that impact velocity has little influence on the droplet film evaporation, and stated that the evaporation rate and the average heat flux increases linearly with increasing T_w. They also witnessed the formation of tiny bubbles at the liquid-solid interface inside the droplet, which they suggested to be due to initial gas entrainment.

Fukai et al. [29] concluded that the droplet diameter is highly influenced by T_w in the recoiling stage rather than in the spreading stage. Also, their calculations predict that increasing T_w decreases the maximum diameter of the wetted area and delays the instant that it occurs.

Cui et al. [30] experimentally showed the effects of dissolved gas and solid salts on evaporation heat transfer. On the one hand, dissolved salts were found to reduce the evaporation rate by decreasing the water vapour pressure. On the other hand, dissolved gas has the opposite effect, improving evaporation through the formation of bubbles in the liquid.

2.4.2.1.2 Nucleate Boiling

This region ranges the beginning of boiling, which occurs at a T_w slightly above T_{sat}, to the critical heat flux (CHF) point ($T_{sat} < T_w < T_{CHF}$). In order to predict the beginning of this regime, an accurate measurement of $T_{contact}$ needs to be made and, additionally, when $T_{contact} > T_{sat}$, bubbles begin to nucleate within the bottom of the droplet.

Moita and Moreira [31] found that fluids with smaller surface tension and latent heat tend to reach boiling faster which, in turn, promote liquid droplets breakup and the making of dry surface areas.

Cui et al. [30] experienced with gas and salts dissolved on the droplets. They reported that

the heat transfer is enhanced by a small amount with dissolved carbon dioxide. Dissolving sodium carbonate in the liquid inhibits the bubble coalescence and promotes foaming, which in turn reduces droplet lifetime. Foaming is a subcategory of the nucleate boiling regime, where, as the name suggests, the entire droplet starts to foam (a frothy mass of bubbles forms on the droplet [32]). Dissolving sodium bicarbonate instead of sodium carbonate reduces droplet lifetime even more because it decomposes when heated to produce carbon dioxide, augmenting bubble formation. Salt particles coming out of solution and precipitating inside the droplet enhances bubble nucleation.

Xiong and Yuen [33] found that maximum heat transfer rate occurs at a wall superheat of $T_w - T_{sat} = 50 - 60$°C for pure liquids, and this superheat value does not depend on droplet size for fuel, but decreases slightly with increasing droplet size for water.

The Nukiyama temperature or critical heat flux corresponds to the shortest droplet lifetime and it is the minimum evaporation time. It describes the thermal limit of a phenomenon where a phase change occurs during heating, which suddenly decreases the efficiency of heat transfer, hence causing localised overheating of the heating surface.

Kandlikar and Steinke [34] proved experimentally that CHF in droplet impact is caused by the motion of the liquid-vapour interface, due to a thin vapour layer. Bernardin et al. [35] reported that CHF in water droplets occurs at $T_w = 130$°C, regardless of impact velocity, surface roughness, or impact frequency. Vapour bubbles form close to the wall and move by buoyancy up to the liquid-air interface. The heat is removed by vaporisation and increases to a maximum at the critical heat flux temperature (T_{CHF}).

Nakoryakov et al. [36] experimentally concluded that increasing the surface thickness or decreasing the droplet volume would decrease the droplet evaporation time. Additionally, decreasing surface thickness increases the critical heat flux temperature.

Ahktar et al. [37] identified three different impact regimes for a water droplet impinging a heated stainless-steel wall near CHF ($140 < T_w < 160$°C): droplet adhesion for $We < 15 \pm 5$; droplet spreading without atomisation (until complete evaporation) for $20 \pm 5 < We < 300 \pm 20$; and droplet breakup for $We > 350$.

2.4.2.1.3 Transition Boiling

This regime is between the CHF and the Leidenfrost temperature ($T_{CHF} < T_w < T_{Leid}$). In this regime, according to Rodrigues [38], the rate of bubble generation exceeds the rate of bubble detachment from the hot surface.

Above the temperature corresponding to the local minimum in the boiling curve (Fig. 2.11), the Leidenfrost phenomenon occurs. This phenomenon is characterised by the formation

of a vapour film at the solid-liquid interface, thus decreasing the contact area, which causes a thermal insulation that obstructs the heat flux between the droplet and the wall. Consequently, with increasing values of the temperature, the evaporation time increases, and the heat flux decreases to a local minimum at the Leidenfrost temperature.

2.4.2.1.4 Film Boiling

This regime occurs when wall temperature exceeds the Leidenfrost temperature ($T_w > T_{Leid}$) and a stable vapour film is quickly formed between the droplet and the wall, which greatly decreases liquid-solid contact and culminates in substantial deterioration of heat removal from the wall. This is known as the Leidenfrost phenomenon and it corresponds to the lowest wall temperature on the film boiling regime.

Two different methods were adopted to determine T_{Leid}, the thermodynamic and hydrodynamic. The thermodynamic method defines T_{Leid} as the wall temperature at which the total evaporation time of the droplet is the longest, while the hydrodynamic method relies on temperature measurements to determine when a stable vapour layer begins to form between the droplet and the wall.

Bernardin and Mudawar [39] proposed a new model in 2002 based on surface cavity characterisation, as well as bubble nucleation, growth, and interaction criteria. As T_{Leid} is approached from the bubble boiling regime, several tiny surface cavities become activated, and the growth of bubbles increases. For temperatures equal to or above T_{Leid}, more cavities are created and the bubble growth rate increases enough that the liquid right next to the wall is immediately evaporated, forming a layer of vapour.

Testa and Nicotra [40] proved that the pressure has the same effect in T_{Leid} as in T_{sat}, i.e., when the pressure decreases, T_{Leid} also decreases. Other investigators suggested that, for rough surfaces, T_{Leid} is higher compared to smooth ones. Surface porosity was found to increase T_{Leid}. T_{Leid} is also influenced by surface tension and gravity. Research showed that decreasing contact angle and surface tension also decreases T_{Leid}.

Gottfried et al. [41] found that the T_{Leid} of water does not depend on droplet size but on wall material and the method of droplet deposition on the wall, varying from $T_{Leid} = 150^{o}$C to $T_{Leid} = 210^{o}$C above T_{sat}. However, all other fluids have a T_{Leid} ranging from $T_{Leid} = 100^{o}$C to $T_{Leid} = 105^{o}$C above T_{sat}.

2.4.2.2 Types of Breakup

Senda et al. [42] identified four different types of breakup when a droplet impinges a heated surface (Fig. 2.13), which depend highly on the surface temperature and the droplet Weber number. The liquid used was water and it is assumed that the droplet deforms in a radial

film on the surface. The most common regimes are:

- **N Type**: At a surface temperature above $T_w = 200$°C, the radial film breaks up since vapour blows through the centre of the film. This type is characterised by the droplets being blown upward with the vapour. After this process, a radial film remains on the surface in a separate form.
- **H Type**: With the rise in impact velocity and droplet diameter, the H type breakup appears, and more vapour is blown through the film when compared to the N type. The tiny droplets attributed to blow-through are distributed over the film, but the blow-through of the vapour is weak compared to the N type. The separated films which remain on the surface after vapour blow-through are the N type.
- **V Type**: This type appears at surface temperatures of $T_w = 300 - 400$°C and there is no decrease in the radial film. This film breaks up when it leaves the surface. Further increasing the impact energy, the droplets are ejected radially and the transition is made to the F type.
- **F Type**: The radial film leaves the surface due to the vapour underneath the film that is blown out in the radial direction. Subsequently, this film is torn and broken up into droplets as the diameter of the film increases. Additionally, the vapour passes under the radial film. The behaviour of this vapour can be confirmed in those small droplets dispersed from under radial film in the radial direction, and the dispersing velocity is faster than the film velocity.

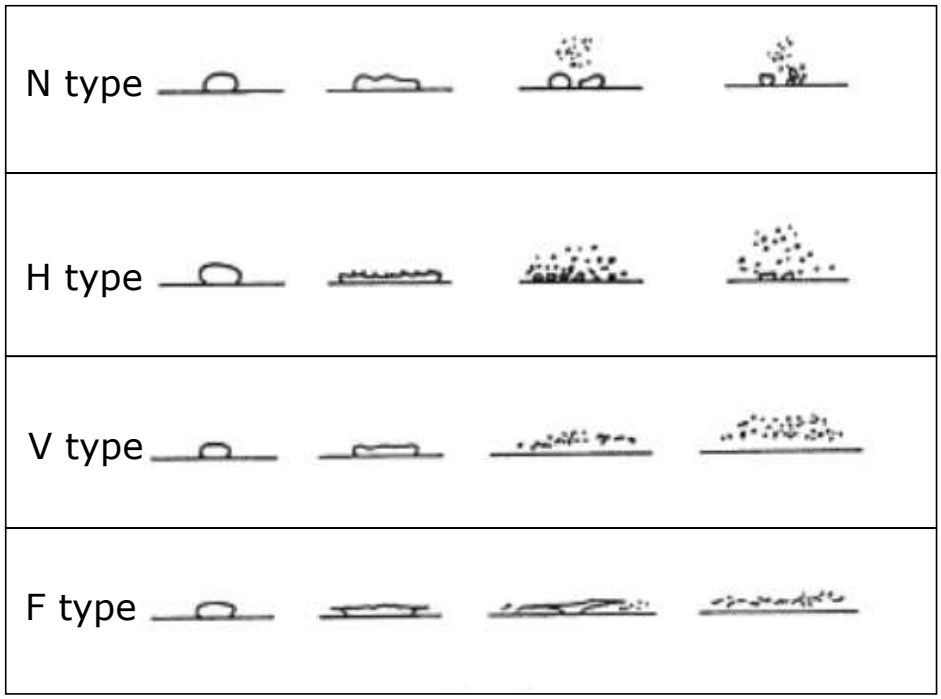

Figure 2.13: Different types of breakup according to Senda et al. [42].

2.4.2.3 Bubble Formation

According to Liang and Mudawar [25], all reports suggested that a single bubble or circular bubble rings are formed in the droplet right after impact, which they attributed to air

entrapment in the solid-liquid interface, regardless of thermal effects. Afterwards, vapour bubbles are formed around the initial air bubbles. Subsequently, due to the boiling of the liquid, isolated vapour bubbles are formed in the rim of the spreading liquid film.

Some investigators refer to bubble boiling as the combination of the nucleation and transition boiling regime. Chaves et al. [43] observed bubble formation in the bubble boiling regime with ethanol droplets, and concluded that the maximum spreading diameter and bubble lifetime depend on We and T_w, and increasing We decreases film thickness and the size of bubbles growing in the spreading liquid film.

According to Chandra [44], when $T_w < T_{sat}$, there are two approaches regarding the formation of bubbles: entrapment of air in the liquid-solid interface during impact, and cavitation inside the liquid caused by a decreasing pressure of the liquid to below its saturation vapour pressure during the jetting process. The air entrapment might occur by the deformation of the liquid during impact. The bubble could be created if a cavity, formed during impact, immediately closes. This deformation can be on the liquid when a droplet impacts a solid surface or in the substrate when a liquid impacts another liquid. Cavitation is the process of rapid formation and collapse of vapour bubbles within the liquid due to isothermal decompression. It is an explanation for the formation of bubbles within a droplet when a moving solid surface impacts a stationary droplet. This occurs mainly when the static pressure becomes smaller than the vapour pressure of the liquid.

One possible method to reduce liquid pressure is a rapid liquid radial jetting along the axis of the droplet and propagation of compression waves after impact, which reflect off the free surface of the droplet and return as expansion waves. The overlay of expansion waves and compression waves result in the formation of regions with high and low pressures.

2.4.2.4 Secondary Atomisation

According to Cossali et al. [45], the secondary droplet atomisation is due to the vapour bubble explosion at the liquid interface of the spreading lamella. The impact velocity, the surface temperature, the impact angle, the surface tension, the viscosity of the liquid, the surface wettability, the effusivity, and surface roughness are the main parameters influencing the process.

Two main regimes of secondary atomisation are expected to exist as a function of wall temperature, which can be related to the two boiling regimes:

- In the bubble boiling regime, the bubbles that are produced by the heat transfer grow and break. The burst of bubbles produces a high amount of small secondary droplets. Here, the formation of secondary droplets begins a few milliseconds after impact, and the droplet ejection is mainly vertical. With a higher surface roughness, spreading appears faster and atomisation is more effective earlier.

- In the film boiling regime, when wall temperature is sufficiently high to generate a vapour film almost immediately after impact, that causes the levitation of the droplet on the wall. The formation of secondary droplets begins right after impact and droplets are ejected radially.

Cossali et al. [46] showed that increasing impact velocity barely decreases droplet size, and surface roughness has a weak influence on bubble formation. Chaves et al. [43] proposed a mechanism for secondary droplet formation in the bubble boiling regime. The formation of secondary droplets is due to the breakup of thin jets caused by explosion of vapour bubbles through the liquid lamella. By increasing T_w, both the jet length and number of secondary droplets increase. Cossali et al. [47] experimentally proved this mechanism and also witnessed another process for formation of tiny droplets: jets ejected above pagoda-like bubbles (Fig. 2.14), which they explained that these bubbles emerge in thick parts of the film, then push the liquid upwards due to high pressure inside the bubble.

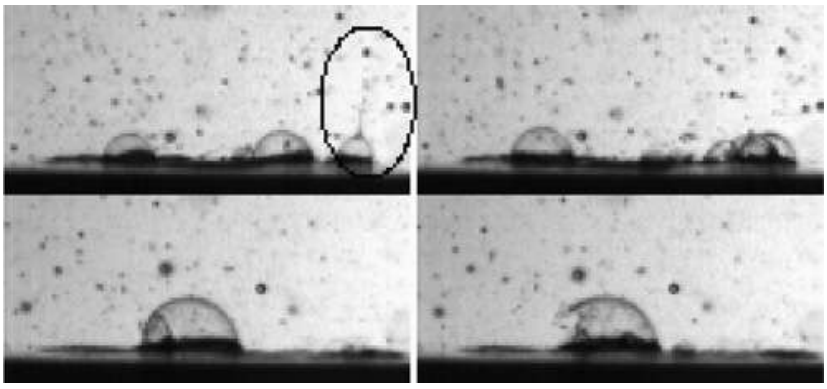

Figure 2.14: Pagoda-like bubbles in the bubble boiling regime. Adapted from Moita and Moreira [48].

2.4.2.5 Dynamic Leidenfrost Temperature

For sessile droplets, gravity is the only mean to impact the droplet on the wall, while for impinging droplets this contact is also due to the droplet momentum, which increases with T_{Leid}. Consequently, to account for this momentum, a new temperature needed to be determined, the Dynamic Leidenfrost temperature, $T_{L,d}$. This $T_{L,d}$ is higher than T_{Leid} and it is the minimum wall temperature at which the vapour layer in the liquid-solid interface causes the droplet to bounce without shattering.

Xiong and Yuen [33] experimentally showed that $T_{L,d}$ is $90 - 120$ºC above T_{sat} for liquid fuels, and $T_{L,d} = 180 - 210$ºC above T_{sat} for water. Wang et al. [49] reported that the droplet rebounds from the heated wall at $T_w < T_{L,d}$ for high impact We. They used spring analogy to explain this, stating that the thin vapour layer behaves as a spring, which contributes to the rebound of the droplet. With lower We, the spring force is weakened due to the dampening effects of viscosity and surface tension.

Bertola and Sefiane [50] suggested that, for water droplets impacting a polished aluminium

surface, the dynamic Leidenfrost temperature is given by the following expression:

$$T_{L,d} = 165 + 30We^{0.38} \quad (2.14)$$

2.4.2.6 Thickness of the Vapour Layer

Biance et al. [51] proved that the thickness of the vapour layer, δ, depends strongly on the droplet radius. The thickness of the vapour layer is much smaller than the droplet radius, $\left(\frac{\delta}{R_0}\right) < 0.02$. They observed two different regimes: stationary and permanent. In the first one, the evaporation of the droplet supplies the vapour film, but it flows due to the weight of the droplet. The vapour film thickness is given by the following expression

$$\delta \sim \left[\frac{\rho_f k_f \mu_f (T_w - T_{sat}) g}{h_{fg} \rho_v \sigma^2}\right]^{\frac{1}{3}} \left(\frac{D_0}{2}\right)^{\frac{4}{3}} \quad (2.15)$$

where the subscript v is referring to the properties of the vapour film. However, Celestini et al. [52] suggested that the vapour thickness increases for smaller droplets, with $\delta \sim (\frac{D_0}{2})^{(-3/2)}$.

2.4.2.7 Droplet Fragmentation

The critical Weber number, We_c, is the limit for a droplet to breakup upon impact. The We_c for a heated wall ($50 < We_c < 80$) is significantly lower compared to an unheated wall ($200 < We_c < 260$) or on a wall with a thin film ($200 < We_c < 260$). Hatta et al. [53] proposed that We_c for disintegration is influenced by several factors, such as liquid type, wall material, and wall superheat. According to Wachters and Westerling [54], there are three types of droplet disintegration. The first is during the initial impact for $We > 80$, the second is the disintegration after it begins to rise from the wall for $30 < We < 80$, and the last is when there is no disintegration for $We < 30$. Akhtar et al. [37] suggested five different impact regimes for water droplets impacting a stainless steel surface at $260 < T_w < 400$°C. Rebound for $We \leqslant 15 \pm 5$, rebound with breakup for $20 \pm 5 < We < 50 \pm 5$, breakup limit for $We = We_c = 60 \pm 10$, typical splash for $60 \pm 10 < We < 350 \pm 20$, prompt splash for $We > 350$.

For a diesel droplet impacting a polished stainless steel surface at $T_w = 450$°C, Chiu and Lin [55] observed three different outcomes. Regular reflection or rebound without breakup, for $We < 15$, breakup with one secondary droplet for $14 \leq We \leq 25$, breakup with more than one secondary droplet for $We \geq 25$.

2.4.2.8 Rebound Mechanism

According to Liang and Mudawar [8], when a low velocity droplet impacts on a wall with $T_w > T_{L,d}$, it will first spread laterally, and then recoil and bounce off the heated wall. Afterwards, the droplet reaches its maximum height and will then fall again due to gravity, repeating

this process several times. If no secondary droplets are formed, this process is known as non-wetting interaction or reflection. Rebound on a heated wall is highly influenced by its temperature because of the formation of the thin vapour layer in the liquid-solid interface.

Biance et al. [56] used spring analogy to explain this rebound phenomenon which they attributed to droplet elasticity (Fig. 2.15). They reported two different regimes of droplet re-

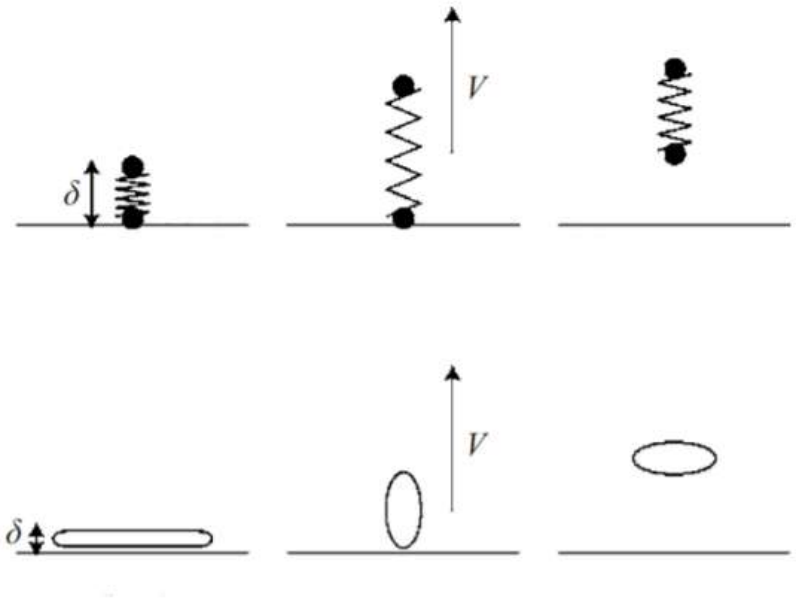

Figure 2.15: Spring analogy used to explain rebound. Adapted from Liang and Mudawar [8].

bound based on the Weber number of the droplet. In the first regime, which happens at high We, the droplet impact inertia is much larger than surface tension, causing the rebound to be less elastic. The droplet loses energy due to dissipation during spreading, and there is a partitioning of energy between droplet oscillation and spreading at rebound. Increasing the droplet velocity, the portion of energy consumed by droplet oscillation increases, which explains the lack of elasticity in this regime. Elasticity also decreases if the droplet diameter exceeds capillary length, $(\frac{\sigma}{g\rho_f})^{1/2}$, which causes the oscillation of the droplet without bouncing, independent of impact velocity.

The second regime, which is associated with low We, corresponds to the quasi-elastic regimes, where the droplet may rebound hundreds of times, returning to the same height in every rebound. Here, the rebound is associated with droplet oscillation, and the droplet maximises its elasticity by adjusting its flight time to oscillation time. Successive bouncing of the droplet reaches a resonant state where energy loss is minimised.

2.4.2.9 Spreading Rate

According to Chandra and Avedisian [44], two dimensions are used to characterise spreading: the diameter of the wetted area and the droplet height above the surface. Normalising these two dimensions over the initial diameter of the droplet, the spread factor, (β), and the

dimensionless height (ξ) are obtained. Spread factor and spread rate $\left(\frac{d\beta}{dt}\right)$ are independent of surface temperature in the initial stages of impact. However, after the initial stages, β depends on the surface temperature and it varies in three different ways:

- If the wall temperature is equal to the ambient temperature, $T_{amb} = T_w$, then β increases until it reaches a maximum. Then, if the Weber number is high enough, it may decrease because of droplet recoiling or evaporation at the contact line;
- If $T_{amb} < T_w < T_{Leid}$, β increases as the droplet spreads out and then decreases as the liquid evaporates or recoils;
- If $T_w > T_{Leid}$, the evolution of β can have many maximums due to recoil/rebound/ evaporation of the droplet from the surface. According to Wachters and Westerling [54], the time period of recoil/impact has been suggested to be of the order of the vibration of a freely oscillating droplet:

$$\tau_r = \frac{\pi}{4}\left[\frac{\rho_f D_0^3}{\sigma}\right]^{1/2} \quad \textbf{(2.16)}$$

τ_r is also known as the residence time of the droplet, which is the duration from the first contact with the surface to first bounce off the wall.

Park et al. [57] experimented on a hydrophobic heated wall and measured a residence time of solid-liquid contact of $\tau_r = 1\ ms$ for $110 < T_w < 210$°C (below $T_{L,d}$), which is the same residence time as in the film boiling regime. However, due to the vapour trapped between the droplet and the surface, they noticed a decrease in residence time to a minimum of $\tau_r = 0.025\ ms$. Negeed et al. [58] suggested that the Weber number and contact angle have a high influence on residence time.

Chapter 3

Experimental Methodology

In this chapter, all the important characteristics related to the installation and the experimental procedures will be described in detail. A diagram with the installation will be presented and afterwards, every component in the experiment will be described regarding their characteristics and specifications. Thereafter, a table with the fluids used and corresponding properties will be provided. With all the components fully described, the next step is to explain the work methodology and describe all the steps in the experiment.

3.1 Experimental Facility

In this dissertation, the installation is made up of four different parts: the image acquisition system (high-speed digital camera), the lighting (LED lamp and a diffusion glass), the pumping system (syringe pump and needles), and the heating system (impact surface and heating device). The camera is placed right in front of the impact surface and the lighting. The pumping system is placed on the side of the assembly. It is composed of a syringe connected to a needle and it is computer-operated to manually choose the desired pumping rate. The impact surface is made of aluminium, and it is positioned between the camera and the lighting lamps. The needles chosen were based on the desired droplet diameter and corresponding Weber number. There are two computers set in a table next to the experimental installation: one is to connect the high-speed digital camera, and the other to connect the data logger and the K-type thermocouples to measure the surface temperature. A diagram of the setup is presented in figure 3.1.

3.1.1 High-Speed Digital Camera

The high-speed digital camera was essential to capture the impact. The camera used is a Photron FASTCAM Mini UX50 with 1.3 Megapixel image resolution at 2000 frames per second (fps), and up to 160000 fps at reduced image resolution. The camera is connected to the computer through an ethernet cable. By making an exposure of a shorter period than the frame rate, the droplets can be seen with better quality. The maximum sensor resolution is 1280x1024 pixels. The lens used was a Tokina AT-X M100 Pro D Macro with a focal length of $100\ mm$, a minimum focusing distance of $0.3\ m$, a minimum aperture of $f/32$ and a maximum aperture of $f/2.8$ (the $'f'$-number is the ratio of the lens focal length to the diameter of the entrance pupil), and a macro ratio of 1:1.

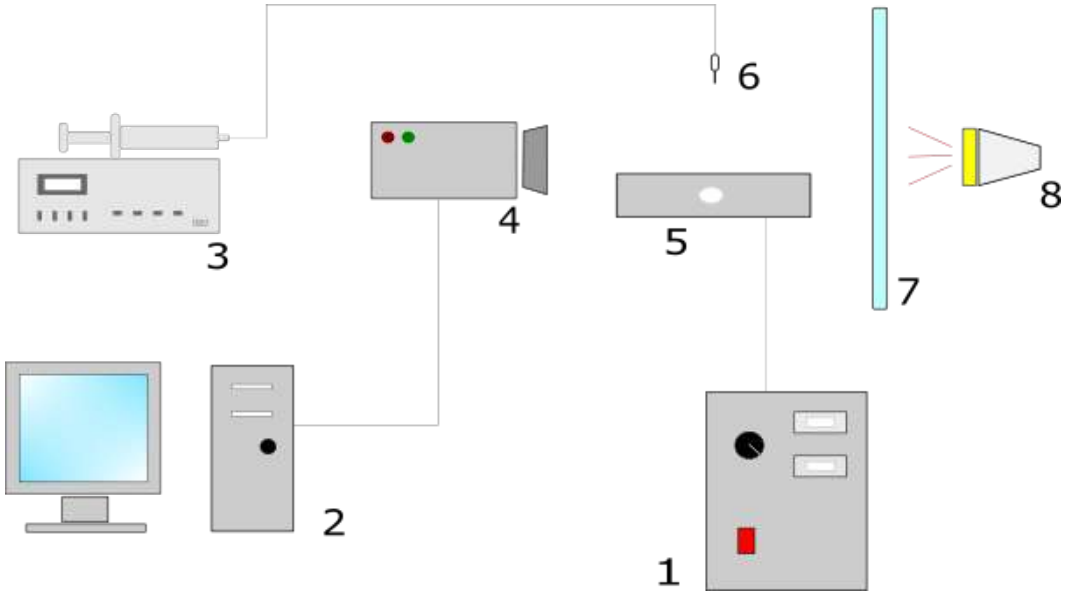

Figure 3.1: Diagram of the experimental setup. 1 - Heating device; 2 - Computers; 3 - Syringe and pump; 4 - High-Speed digital camera; 5 - Impact surface; 6 - Dispensing needle; 7 - Diffusion glass; 8 - LED lamp.

3.1.2 Impact Surface and Heating Device

The impact surface is shown in the figure below (Fig. 3.2 (a)). It is a flat aluminium 5083 surface of size 150 mm x 150 mm x 30 mm. It has four cartridge heaters of 250 W, evenly distanced to uniformly heat the impact surface, so that its temperature is distributed as even as possible. Embedded in the impact surface, there is a type-K thermocouple that controls the temperature that is selected in the heating device. The physical properties are presented in table 3.1 and the blueprint of the impact surface is shown in Appendix A.1. A device that controls the surface temperature is shown in Fig. 3.2 (b). In this device, the desired surface temperature is selected and then the surface temperature heats up until the thermocouple embedded in the surface measures the selected temperature.

Table 3.1: Physical properties of the aluminium impact surface.

Physical Property	**Value**
Density	265 g/cm^3
Melting Point	570 ^oC
Thermal Expansion	$25 \times 10^-6\ /K$
Modulus of Elasticity	72 GPa
Thermal Conductivity	121 $W/m.K$
Electrical Resistivity	$0.058 \times 10^-6\ \Omega.m$

Before starting the droplet impact experiments, the calibration of the impact surface temperature was made. In order to do this, seven different temperatures were selected. The objective is to analyse the deviations of the surface temperature after it stabilises.

Since these tests were made to compare the temperature shown on the heating device to the surface temperature, four additional K-type thermocouples were positioned in the centre of

(a) (b)

Figure 3.2: (a) Aluminium impact surface with four 250W cartridge heaters and one embedded type-K thermocouple. (b) Heating device that controls the selected surface temperature.

the surface and the temperature was measured for ten minutes. Figure 3.3 represents the top view of the impact surface and respective positions of the thermocouples. The centre of the circle corresponds to the droplet impact point, and distanced by $1\ cm$ from the middle are four K-type thermocouples represented by the red crosses. In figure 3.4, an example of the graphs obtained by these measurements is provided. It can be observed that after heating up to the selected temperature, the temperature slightly drops to stabilise at a lower temperature than the selected (in this case, the selected temperature was $T = 50$ºC, and stabilises at around $T_w = 47$ºC). The thermocouple four is measuring a temperature slightly lower than the other three and this was probably due to thermocouple errors. Even though it was slightly different, the standard deviation was still very low and it was still considered constant. The other six temperatures follow the same pattern, in which they reach a peak and then stabilise below the selected temperature. For higher selected temperatures, the difference between the selected temperature and surface temperature is higher. Afterwards, the mean temperature values of the four thermocouples were calculated.

In the table below, table 3.2, it is represented the mean surface temperature for all seven selected temperatures tested as well as the standard deviation, and the range of temperatures the surface stabilises. Additionally, a graph that complements the table is presented in fig. 3.5.

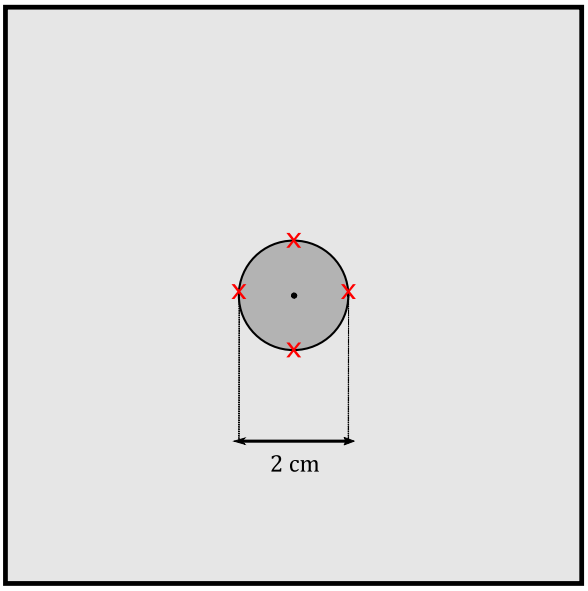

Figure 3.3: Representation of the top view of the impact surface. The centre of the circle represents the droplet impact point and the red crosses the K-type thermocouples.

Table 3.2: Values of the mean surface temperature, the standard deviation and the surface temperature variation after its stabilisation.

Selected Temperature [ºC]	**Mean Surface Temperature [ºC]**	**Standard Deviation [ºC]**	**Surface Temperature Variation [ºC]**
50	47	0.57	[46.4 ; 47.6]
100	91	1.17	[89.8 ; 92.2]
150	135	1.09	[133.9 ; 136.1]
200	180	1.87	[178.1 ; 181.9]
250	224	1.39	[222.6 ; 225.4]
300	267	3.47	[263.5 ; 270.5]
350	315	3.90	[311.1 ; 318.9]

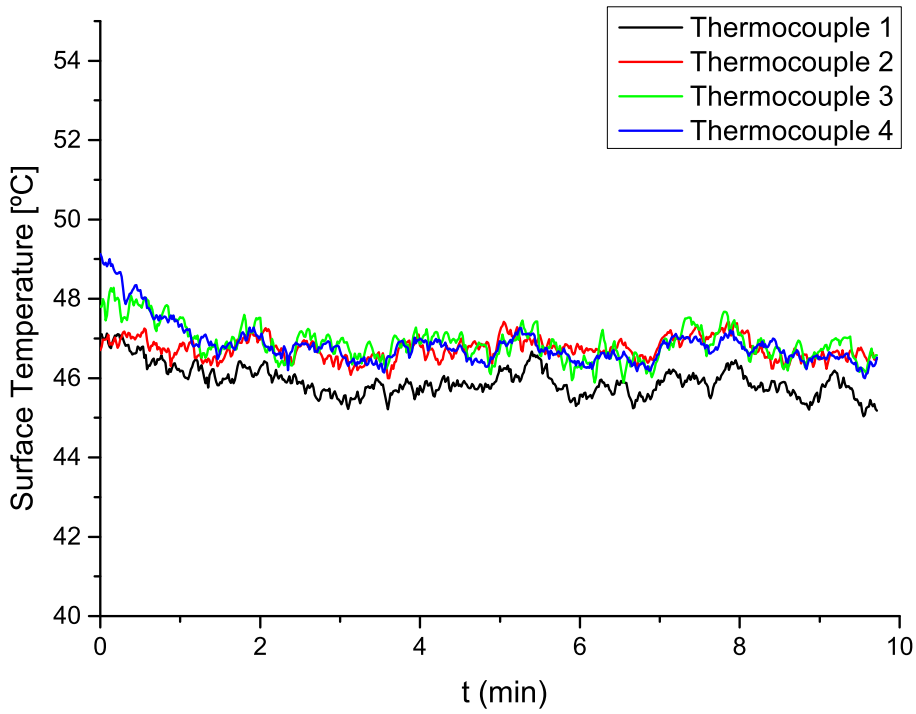

Figure 3.4: Surface temperature measurement with four thermocouples over the course of ten minutes.

3.1.2.1 Droplet Generator

The pump used to produce the droplets is a NE-1000 Programmable Single Syringe Pump. It has a minimum pumping rate of $0.73\ ml/h$ with a $1\ ml$ syringe, up to $2100\ ml/h$ with a $60\ ml$ syringe. The droplet forms at the tip of the needle and detaches when its weight surpasses the surface tension forces.

In these experiments, the pumping rate was sufficiently low ($0.5\ ml/min$) to ensure that the droplet falls only due to gravity. The syringe pump has a needle connected to it through a cable. To ensure the same Weber number, the droplet diameter needed to vary depending on the fluid, therefore, the needles used had different inner diameters. To avoid contamination, there was a single needle, syringe, and tube for each fluid used.

3.1.2.2 Illumination

One of the most important factors for image capture is a good lighting. Having a better illumination makes it possible to capture the impact in better detail and contrast. Therefore, a $20\ W$ LED lamp was positioned right in front of the camera with a diffusion glass between the impact surface and the LED lamp to provide uniform lighting. Besides that, all the windows in the room were sealed and all the lights in the room were turned off, making the LED lamp the only light source in the laboratory.

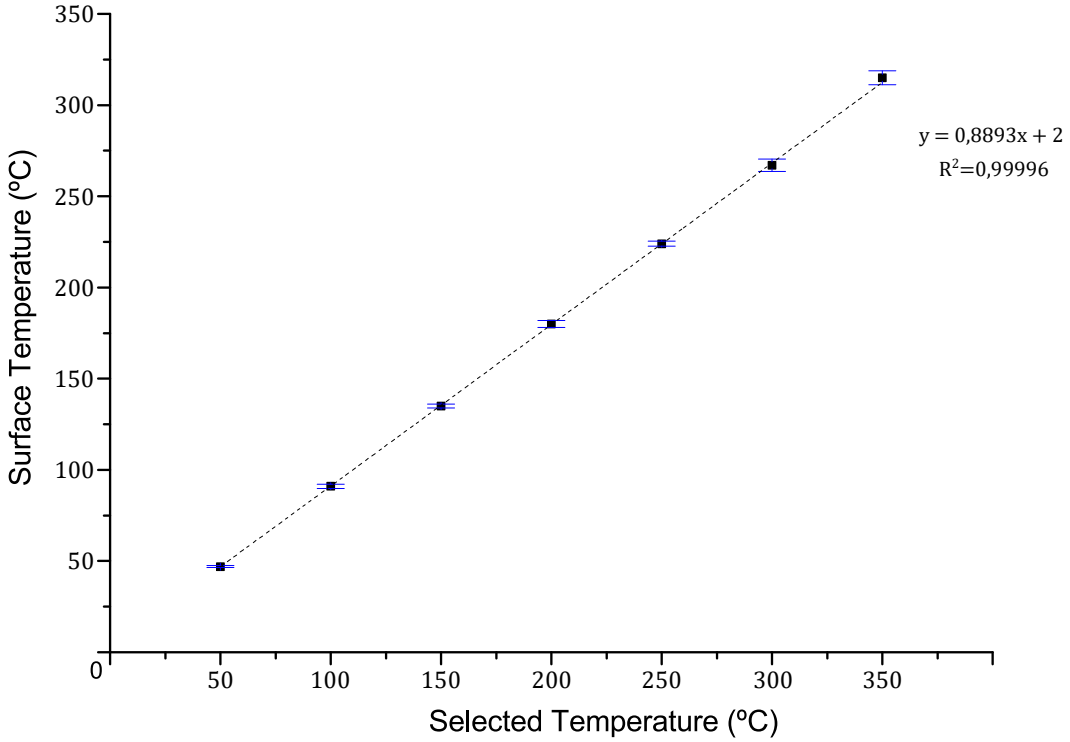

Figure 3.5: Correspondence between the selected temperature and the obtained surface temperature.

3.1.3 Fluid Properties

For this experiment, a total of five different fluids were testes and analysed. The fluids are mostly fuels and mixtures that contain at least 50% jet fuel. The jet fuel chosen was Jet A-1 and the Biofuel was NExBTL. Therefore, the fluids used in these experiments were: H_2O, Jet Fuel (100%), Jet Fuel (75%) - HVO (25%), Jet Fuel (50%) - HVO (50%), and HVO (100%). The fluid properties are derived from Ribeiro [59] and are shown in table 3.3:

Table 3.3: Values of density, (ρ), surface tension, (σ), dynamic viscosity, (μ), flash point, and boiling point for the fluids used. Adapted from Ribeiro [59].

Fluids	**H_2O**	**100% JF**	**75% JF - 25% HVO**	**50% JF - 50% HVO**	**HVO**
$\rho\ [kg/m^3]$ (at 22°C)	1000.0	798.0	795.0	792.4	785.2
$\sigma\ [mN/m]$ (at 22°C)	71.97	25.37	25.53	24.64	26.59
$\mu\ [Pa.s]$ (at 22°C)	0.00100	0.00112	0.00144	0.00179	0.00340
Flash Point (°C)	-	38.5	-	-	77.0
Boiling Point (°C)	100	151.9 - 237.2	-	-	210.5 - 308.0

3.1.4 Work Methodology

The experiments are divided into two parts. In the first one, the image acquisition of the

droplets will be used to calculate the droplet properties, such as the impact velocity and droplet diameter. In the second part, the outcomes were visualised and the impact phenomenon was observed and reported in detail.

Regarding the first part of the experiments, to provide consistency, each case of study was tested ten times. Besides that, before every temperature selected, the temperature of the impact surface was measured with a K-type thermocouple until it stabilises, and for an additional five minutes to guarantee that it did not vary. Also, every five tests made, another report of the temperature would be made to ensure that the temperature would still be the same and no changes were made. Additionally, for every droplet impact, the surface was cleaned using isopropanol. This way, it is guaranteed that all droplet impacts have the same conditions.

As mentioned above, the fluids used were H_2O, Jet Fuel (100%), Jet Fuel (75%) – HVO (25%), Jet Fuel (50%) – HVO (50%), and HVO (100%). To compare the effects of the surface temperature, the Weber number was kept constant for each fluid since it is one of the most important dimensionless numbers when dealing with heated surfaces. In order to reach the same Weber number for different fluids, different needles diameters, and different droplet falling heights had to be chosen.

3.1.4.1 Pixel Sizing

To determine the pixel size, a reference picture was taken before the tests. A needle with an outer diameter of $1.82\ mm$ was used. Knowing this value and measuring the number of pixels in the software MATLAB, the conversion was easily made. With all this done, the pixel size varied from $43.3\ \mu m$ to $46.7\ \mu m$.

3.1.4.2 Droplet Diameter and Impact Velocity

Calculating the droplet diameter and the impact velocity is essential to determine the dimensionless numbers. These two factors will determine the experiments and will influence the dimensionless numbers. In order to obtain these two droplet parameters, two separate MATLAB codes were written.

For both cases, a background image without any droplet was selected. To calculate the droplet diameter, every frame from the first complete droplet to the one before impact was selected. After this selection, every frame is subtracted to the background image, leaving only the droplet in the image. Then, the frames are binarised so that the values obtained are ones and zeros (one correspond to white pixels and zero to black pixels). Afterwards, other MATLAB functions were used to better improve the images, such as removing the noise pixels (pixels that do not belong to the droplet) and filling the area inside the droplet with white pixels. The image below, figure 3.6, represents how the image processing occurs. For all impact conditions, the record rate of the camera was set to 2000 fps and the shutter speed was set to 1/10240 seconds.

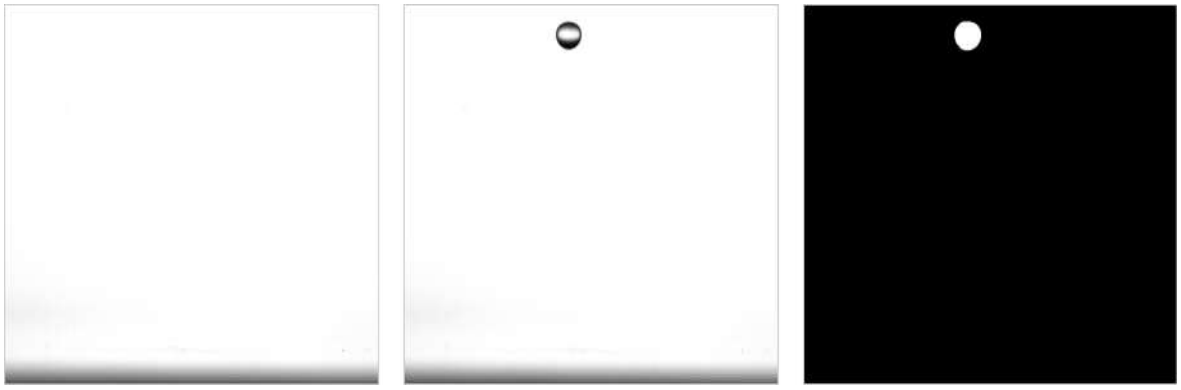

Figure 3.6: The first image represents the background. The second figure is the complete droplet. Lastly, the third image is the image after all the treatment and processing done.

To determine the droplet diameter, the vertical and horizontal length of the droplet for every frame mentioned above were determined and the mean value was calculated. To get a more accurate value, it is necessary to use every possible frame. To calculate the vertical and horizontal length, the number of pixels were counted using a MATLAB algorithm. This way, the column with the most pixels corresponds to the vertical length and the row with the most pixels corresponds to the horizontal length. After calculating this value for every ten tests made, the mean value was calculated, and the diameter obtained. Then, the mean diameter is multiplied by pixel size, so that it can be converted into usable units.

Regarding the calculation of the impact velocity, it is important to notice that the velocity required is the one before impact. Therefore, the centroid position of the droplet right before impact and the previous droplets were found. Then, the distance between them were calculated and divided by the time frames between them. For every test performed, five frames before impact were selected to ensure that the impact velocity did not vary. After all the calculations done, the impact velocity only varied by 0.82% ($\pm 0.01\ m/s$). After that, the value of the velocity is multiplied with pixel size.

Represented in the table below, table 3.4, are the experimental values of the droplet diameter and impact velocity used to obtain similar Weber numbers for all the cases of study.

Table 3.4: Physical properties of the impact droplet for all the fluids used.

Fluid	**Needle Inner Diameter [mm]**	**Droplet Diameter [mm]**	**Impact Velocity [m/s]**	**We**	**Re**
H_2O	1.50	4.0 ± 0.42	2.4 ± 0.33	313	9527
100% JF	0.84	2.9 ± 0.33	1.9 ± 0.30	324	3730
75% JF / 25% HVO	1.50	3.1 ± 0.36	1.8 ± 0.27	313	3081
50% JF / 50% HVO	0.51	2.8 ± 0.28	1.9 ± 0.23	325	2355
100% HVO	1.50	3.1 ± 0.15	1.9 ± 0.25	330	1360

Chapter 4

Results and Discussion

This chapter will be divided into two parts. The first chapter is dedicated to the visualisation and characterisation of the different droplet impact outcomes and phenomenon, and the second chapter includes an analysis of the images obtained that compares the influence of the surface temperature on the different fluids used.

4.1 Image Visualisation

As said before in chapter 2, the terminology adopted in this dissertation is the same Ko and Chong [23] used. Therefore, in the following images, four regimes will be observed for the different fluids: film evaporation, nucleate boiling, transition boiling, and film boiling. Another important aspect to mention is that the dimensionless temperature is calculated using equation 2.8, and $t = 0\ ms$ corresponds to the moment of impact.

4.1.1 Film Evaporation

4.1.1.1 H_2O

At $T_w = 25$ºC (Fig. 4.1), in the film evaporation regime, when the water droplet impacts the surface, a bubble is quickly seen inside the droplet in figure 4.2. This bubble is probably caused by air entrapment in the liquid-solid interface because of the deformation of the droplet at the moment of impact [44]. At $\tau = 3.0$, the lamella reaches its maximum spreading diameter and is followed by a receding stage that is seen from $\tau = 3.0$ to $\tau = 74.4$. During spreading, there are some instabilities at the outer rim of the liquid lamella, which are known as fingers or the fingering phenomenon ($\tau = 3.0$). There is receding breakup seen at $\tau = 74.4$. Afterwards, the droplet oscillates between spreading and receding intermittently until its equilibrium form is established.

In the film evaporation regime, at a temperature slightly lower than T_{sat}, $T_w = 85$ºC (Fig. 4.3), when the droplet impacts, a bubble is immediately formed due to air entrapment. Subsequently, vapour bubbles are formed in the rim of the lamella (Fig. 4.4). The droplet keeps spreading until it reaches its maximum spreading diameter, accompanied with fingering ($\tau = 3.0$). Receding occurs vigorously compared to lower temperatures, because the lamella breaks up into liquid puddles ($\tau = 18.0\ -\ \tau = 30.0$). According to Moita and Moreira [48], this rupture occurs because the vapour-pressure forces at the liquid-solid interface overcome

surface tension forces.

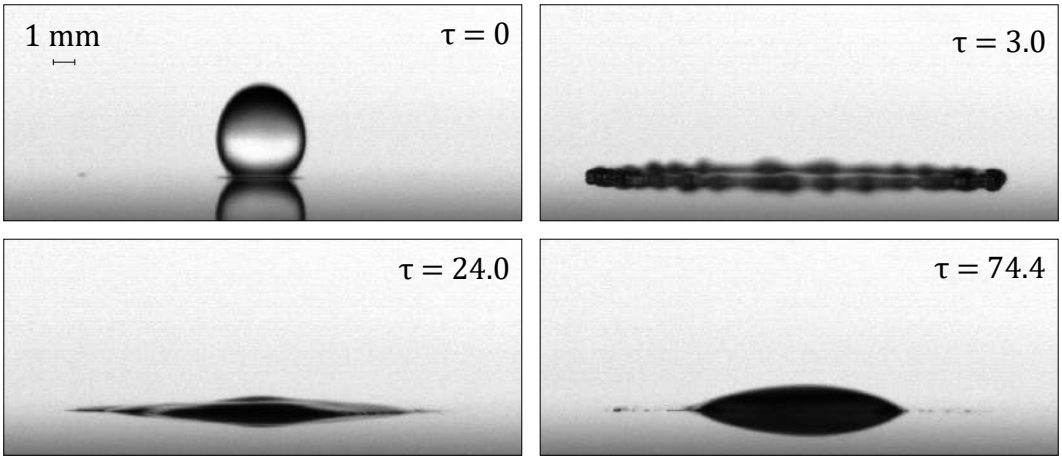

Figure 4.1: Water droplet impact ($We = 313$) onto an aluminium surface within the film evaporation regime ($T_w = 25$ºC).

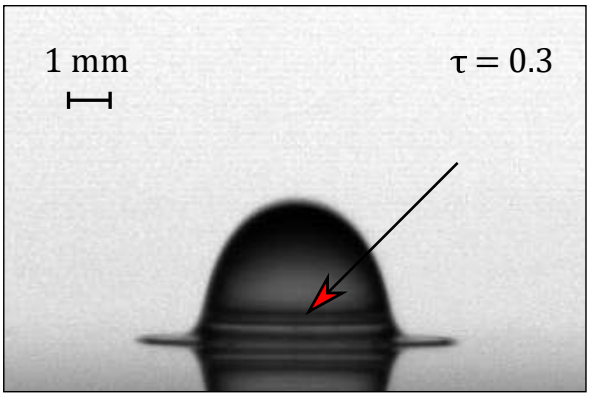

Figure 4.2: Bubble formed right after impact due to air entrapment on a water droplet within the film evaporation regime ($T_w = 25$ºC).

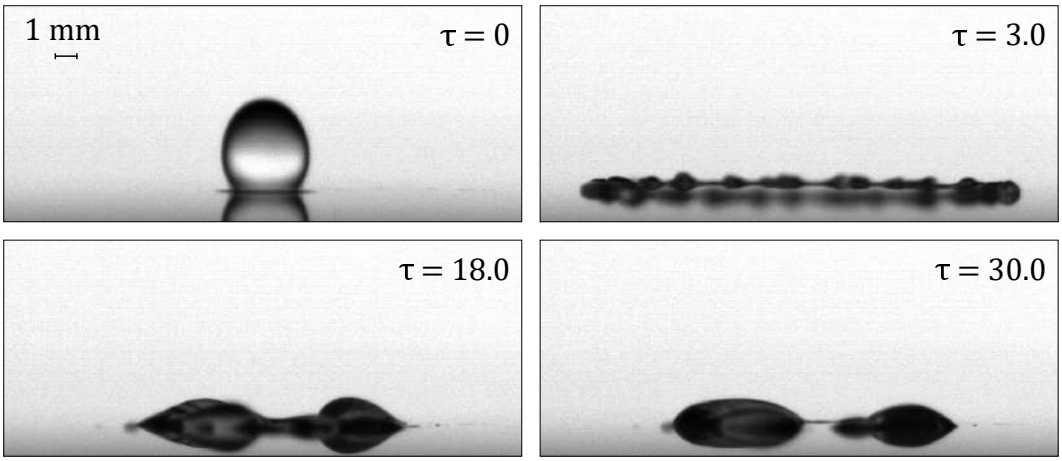

Figure 4.3: Water droplet impact ($We = 313$) onto an aluminium surface within the film evaporation regime ($T_w = 85$ºC).

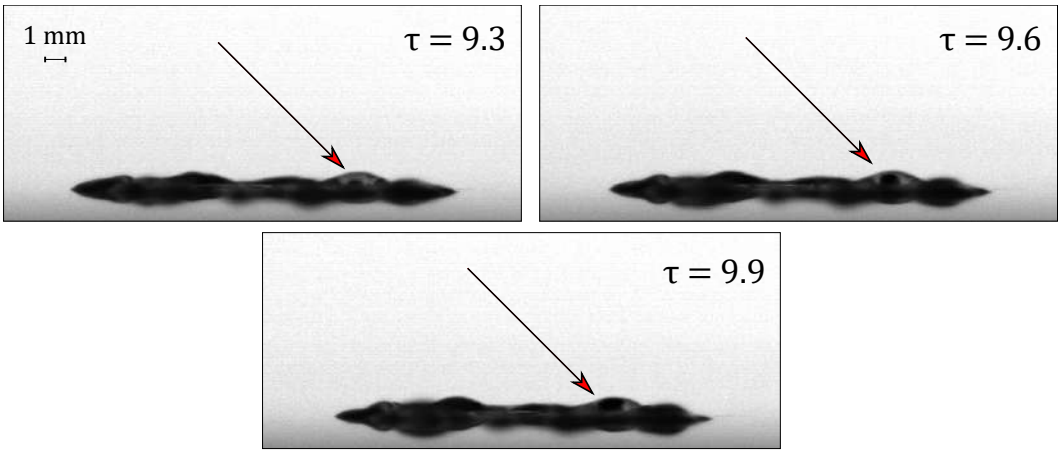

Figure 4.4: Vapour bubbles formation of a water droplet impact ($We = 313$) in the rim of the lamella within the film evaporation regime ($T_w = 85$ºC).

4.1.1.2 100% Jet Fuel

For 100% jet fuel at room temperature (Fig. 4.5), the same spreading phenomenon occurs. Immediately after impact, at $\tau = 0.3$, a bubble is formed due to air entrapment. This phenomenon happened for all the experiments done. The droplet then spreads until it achieves its maximum spreading diameter at $\tau = 6.6$. The receding phase is non-existent, probably due to the lower surface tension compared to water, which means that the droplet will not recede to the lowest surface area possible and will maintain its shape ($\tau = 26.2$). Here, no instabilities such as fingers are seen. As the temperature increases, the same spreading phenomenon occurs for a wall temperature of $T_w = 50$ºC. However, at this temperature, the droplet enters a receding phase, which suggests that a higher wall temperature promotes receding due to the decrease of the fluid viscosity as the temperature increases [60].

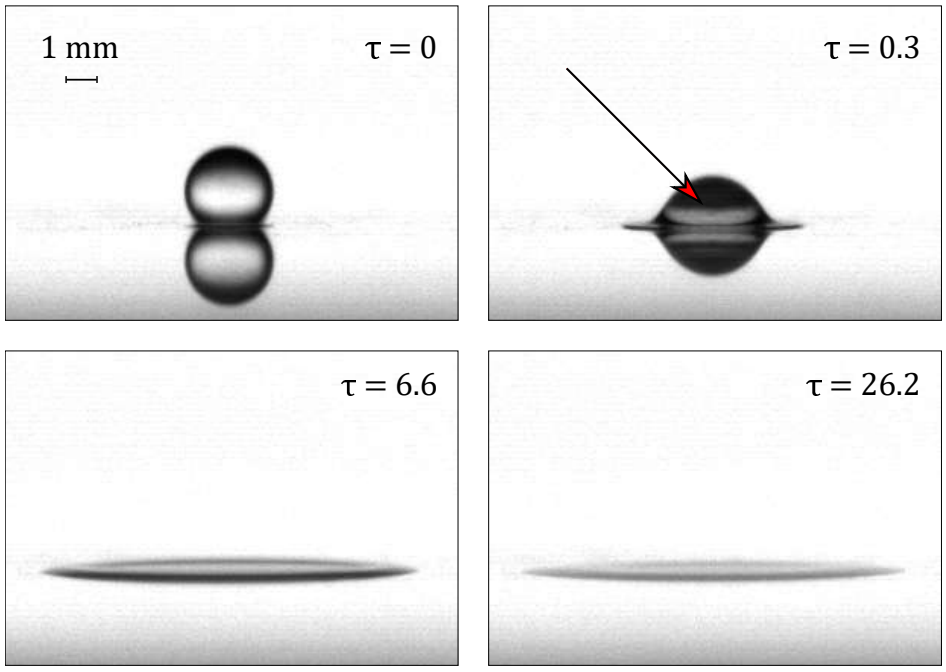

Figure 4.5: 100% jet fuel droplet impact ($We = 324$) onto an aluminium surface within the film evaporation regime ($T_w = 25$ºC).

The same spreading phenomenon occurs until $T_w = 150$ºC (Fig. 4.6). Right after impact, a bubble is seen due to air entrapment at $\tau = 0.3$. At this temperature, instabilities started surging and the droplet would begin spreading with fingering ($\tau = 6.2$). This is probably due to the incipience of boiling and surface tension gradients [43]. At this temperature, there is no receding. However, after the droplet reaches its maximum spreading diameter, it forms puddles and begins evaporating fumes ($\tau = 19.7$). According to Cen et al. [61], this phenomenon is called puffing.

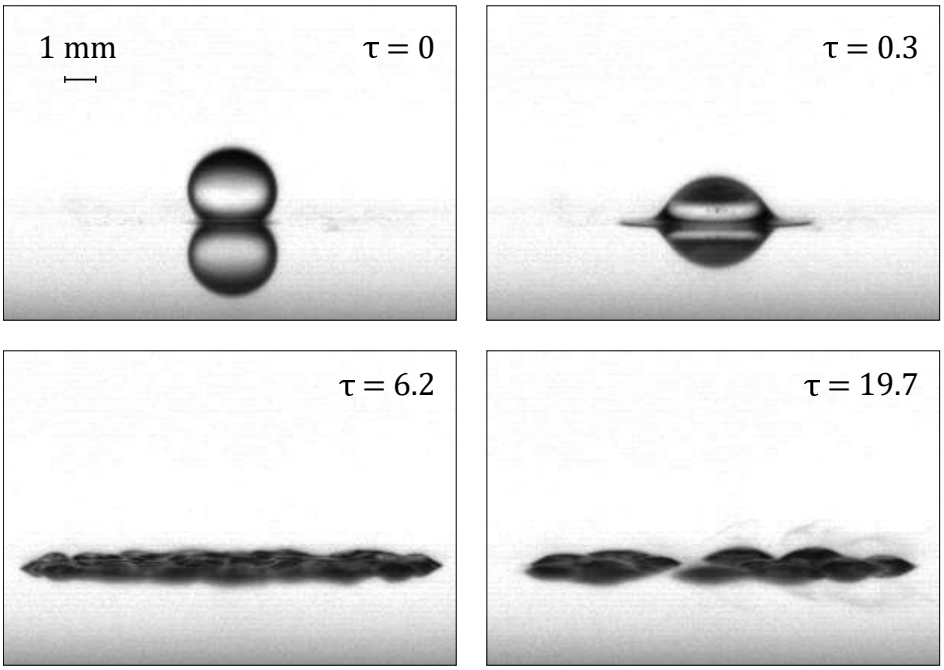

Figure 4.6: 100% jet fuel droplet impact ($We = 324$) within the film evaporation regime ($T_w = 150$ºC).

4.1.1.3 Jet Fuel (75%) - HVO (25%)

For this mixture at room temperature, $T_w = 25$ºC (Fig. 4.7), the same phenomenon happened as it did for the previous fluids. There is air entrapment right after impact ($\tau = 0.3$), and then the droplet will spread without any instabilities until it achieves its maximum spreading diameter, which is maintained until the droplet evaporates ($\tau = 5.8 - \tau = 11.6$). The droplet will not enter a receding phase due to its low surface tension.

At a wall temperature of $T_w = 100$ºC (Fig. 4.8 (a)), the droplet will spread like the previous temperature. However, it will enter a receding phase. The maximum spreading diameter can be seen by the leftover oils that stuck to the wall in the receding phase. When the wall reaches $T_w = 150$ºC (Fig. 4.8 (b)), instabilities due to the boiling of the liquid start appearing. Additionally, puffing occurs and some vapour bubbles form inside the droplet (Fig. 4.8 (c)). Increasing wall temperature to $T_w = 175$ºC (Fig. 4.8 (d)), it occurs the formation of liquid puddles.

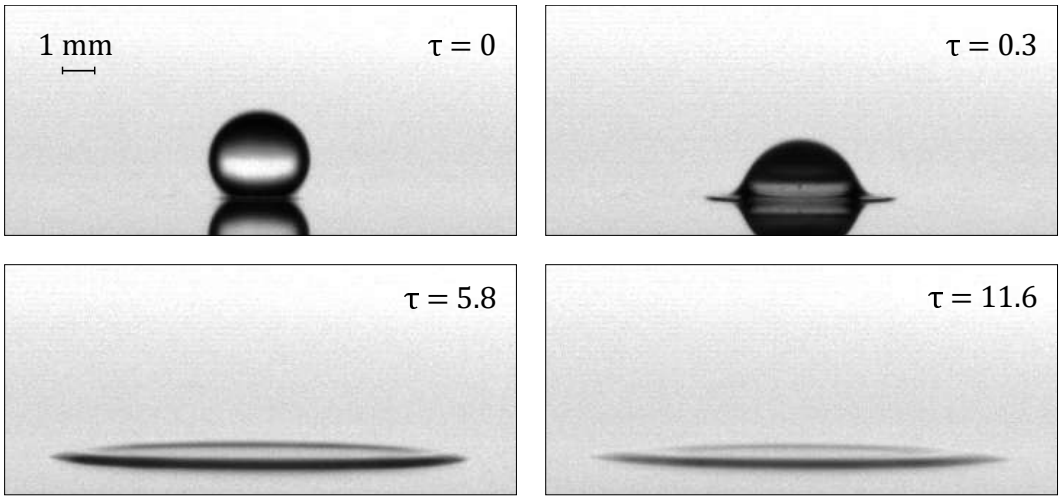

Figure 4.7: Mixture of 75% jet fuel with 25% HVO droplet impact ($We = 313$) onto an aluminium surface within the film evaporation regime ($T_w = 25$ºC).

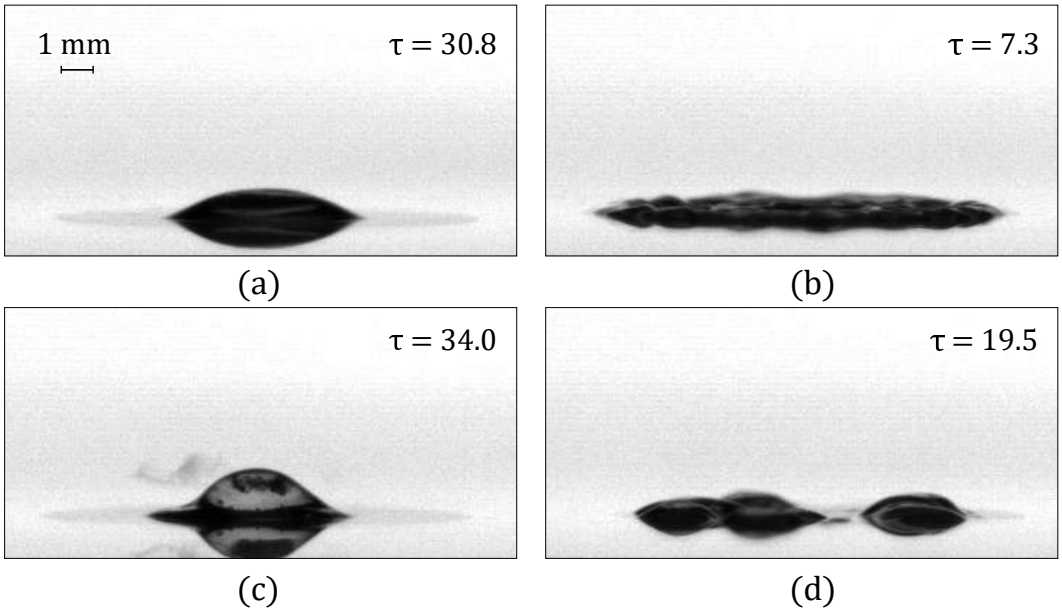

Figure 4.8: 75% jet fuel with 25% HVO droplet impact onto an aluminium surface. (a) Leftover oils in the receding phase in the film evaporation regime ($T_w = 100$ºC). (b) Spreading with fingering within the film evaporation regime ($T_w = 150$ºC). (c) Vapour bubbles forming inside the droplet in the film evaporation regime ($T_w = 150$ºC). (d) Formation of liquid puddles in the film evaporation regime at $T_w = 175$ºC.

4.1.1.4 Jet Fuel (50%) - HVO (50%)

At a wall temperature of $T_w = 25$ºC, for the mixture of 50% jet fuel with 50% HVO, the spreading phenomenon is the same as the other fluids. After impact, a bubble is quickly seen due to air entrapment. No instabilities in the spreading phase were observed and the droplet does not enter a receding phase due to its low surface tension. Increasing the temperature to $T_w = 100$ºC will promote receding and therefore, the droplet will undergo a receding phase. At this temperature, the droplet will oscillate between spreading and receding until it achieves an equilibrium state while slowly evaporating on the heated surface. The droplet spreading diameter is marked by the oils that stuck to the wall on the receding phase, the

same as it occurred for the mixture of 75% Jet Fuel with 25% HVO.

Still in the film evaporation regime, at $T_w = 150^oC$, the same phenomenon occurs. The droplet oscillates until it achieves an equilibrium state, with some vapour bubbles appearing inside the droplet. When $T_w = 180^oC$, fingering appears after the droplet reaches its maximum spreading diameter and enters the receding phase.

Near the nucleate boiling regime ($T_w = 220^oC$) (Fig. 4.9), the droplet starts slowly boiling with puffing. The droplet breaks up into small puddles. These puddles can break and form secondary droplets on the surface, and these secondary droplets might merge into bigger and less secondary droplets. At later stages in this regime, tiny vertical jets constantly burst on top of these puddles, producing some secondary atomisation (Fig. 4.10).

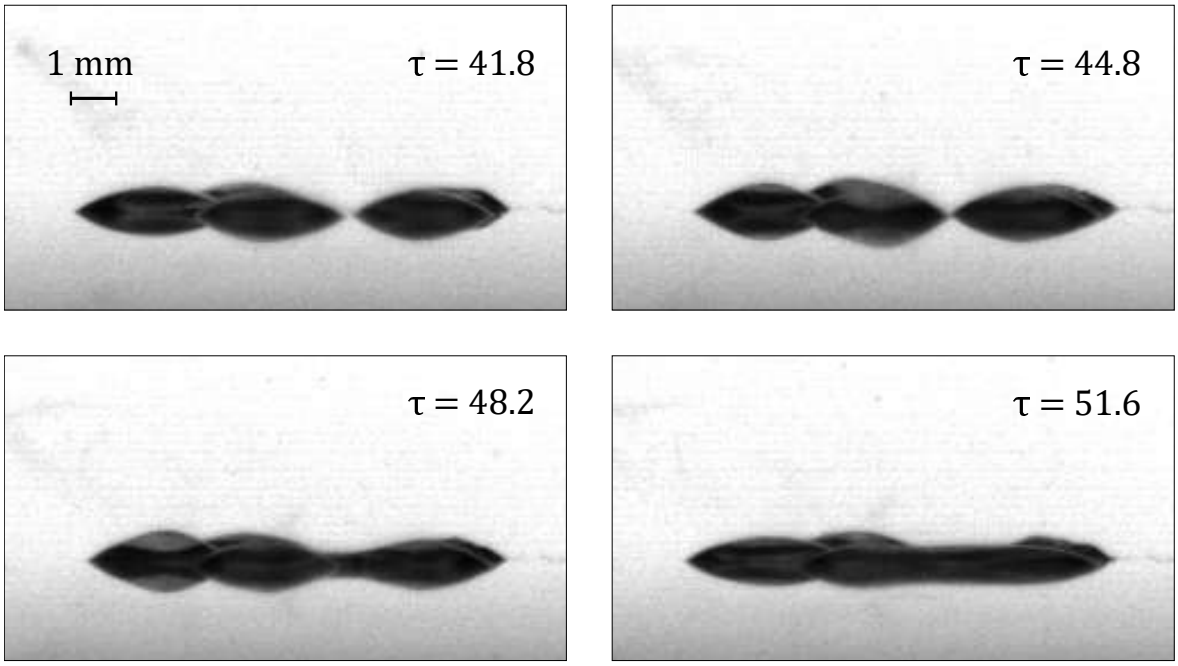

Figure 4.9: Formation of puddles of a mixture of 50% jet fuel with 50% HVO in the film evaporation regime ($T_w = 220^oC$).

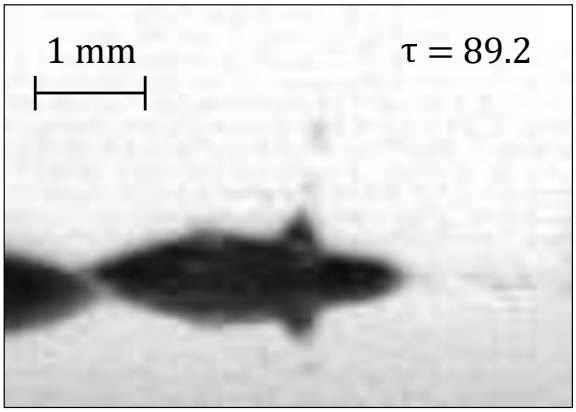

Figure 4.10: Jets bursting on the surface of the puddles of a 50% jet fuel with 50% HVO mixture in the film evaporation regime ($T_W = 220^oC$).

4.1.1.5 100% HVO

The phenomenon with 100% HVO in the film evaporation regime is the same as the fuel mixtures. At ambient temperature, $T_w = 25$°C, the droplet impacts and air entrapment occurs. The droplet spreads without experiencing any instabilities and, afterwards, it does not undergo any receding phase. At a wall temperature of $T_w = 50$°C, a bubble caused by air entrapment is seen again. The droplet spreads and after reaching its maximum spreading diameter, it recedes. Then, it oscillates until it reaches an equilibrium state while slowly evaporating.

When wall temperature is set to $T_w = 100$°C, prompt splash occurs at the moment of impact (Fig. 4.11). Unlike other fluids used, this was the only one that this phenomenon could be observed in this regime. However, increasing wall temperature to $T_w = 130$°C and $T_w = 150$°C, the prompt splash ceased to occur and normal spreading without any instabilities occurred. When the wall temperature was set to 200°C, instabilities started to appear due to the incipience of boiling and at later stages of the impact, puffing occurred as well (Fig. 4.12 (a)). At $T_w = 250$°C when the droplet reaches its maximum spreading diameter, it starts boiling and it eventually breaks into small puddles (Fig. 4.12 (b)). These puddles can break to form bigger and lesser droplets or break into more and smaller secondary droplets. At this temperature, fumes are evaporating from the biofuel but no secondary atomisation. Vapour bubbles can be seen inside the droplet.

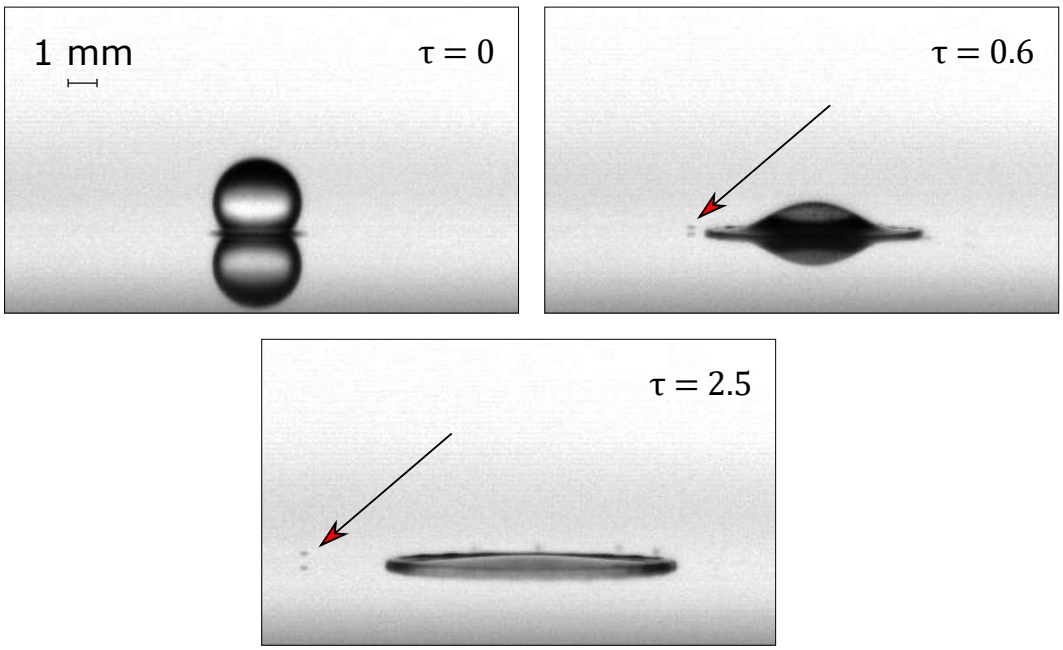

Figure 4.11: 100% HVO droplet prompt splashes onto an aluminium surface within the film evaporation regime ($T_w = 100$°C).

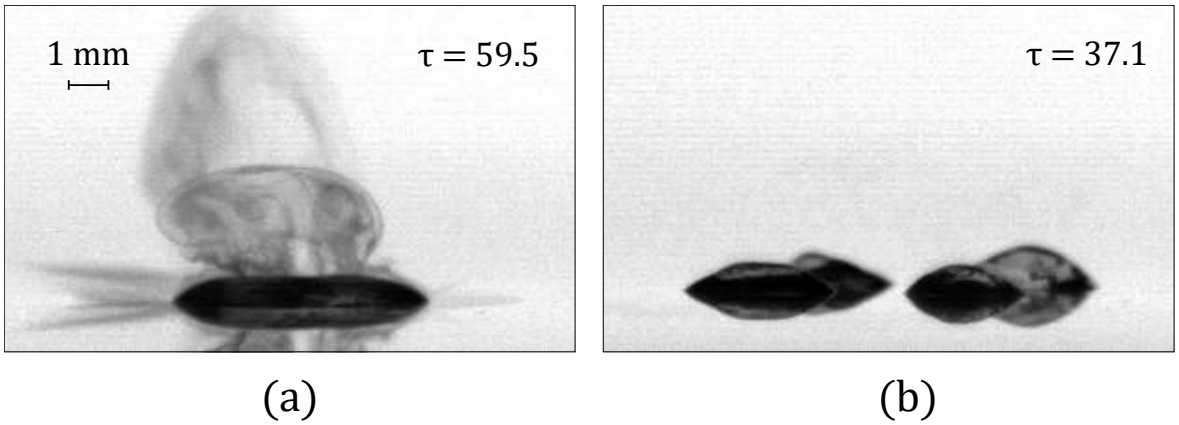

Figure 4.12: (a) Puffing of a 100% HVO droplet within the film evaporation regime ($T_w = 200$°C). (b) Formation of puddles of a 100% HVO droplet in the film evaporation regime ($T_w = 250$°C).

4.1.2 Nucleate Boiling

4.1.2.1 H_2O

In the transition from film evaporation to nucleate boiling regime, $T_w = T_{sat}$ (Fig. 4.13), at the moment of impact, the droplet spreads with fingering until it reaches its maximum spreading diameter ($\tau = 3.0$). Here, the droplet barely recedes. Instead, the formation of puddles is more intense in comparison to $T_w = 85$°C ($\tau = 18.0 - \tau = 36.0$). There is secondary atomisation seen at later stages.

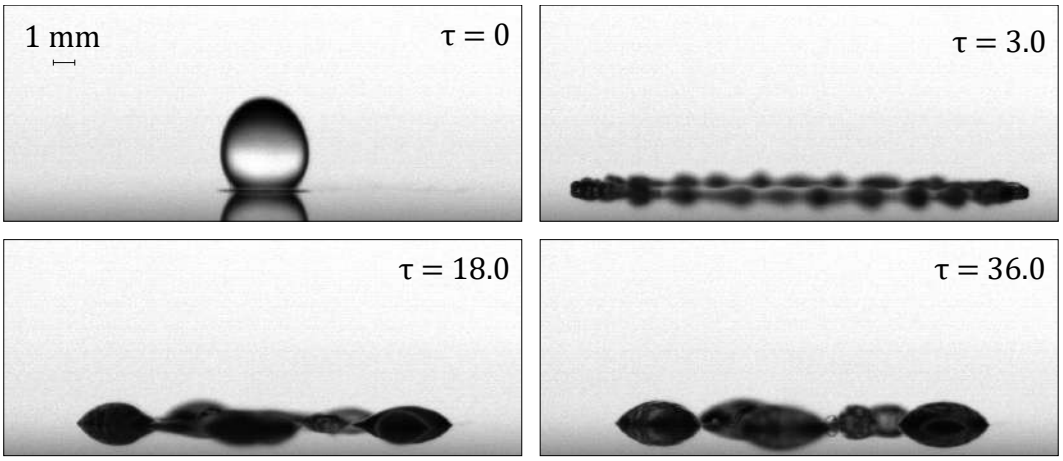

Figure 4.13: Water droplet impact ($We = 313$) onto an aluminium surface within the nucleate boiling regime ($T_w = 100$°C).

In the nucleate boiling regime, $T_w = 110$°C (Fig. 4.14), after impact, the droplet reaches its maximum spreading diameter at $\tau = 3.0$ accompanied with fingering. After that, the droplet breaks into tinier puddles and it begins boiling ($\tau = 15.0$). Afterwards, vapour bubbles form and burst out of the droplet, with gradually increasing secondary atomisation ($\tau = 39.0$). In a later stage of this impact, small jets forming and bursting on the top of the bubbles were reported (Fig. 4.15). This phenomenon was reported by Cossali et al. [47], who identified them as ”pagoda-like” bubbles.

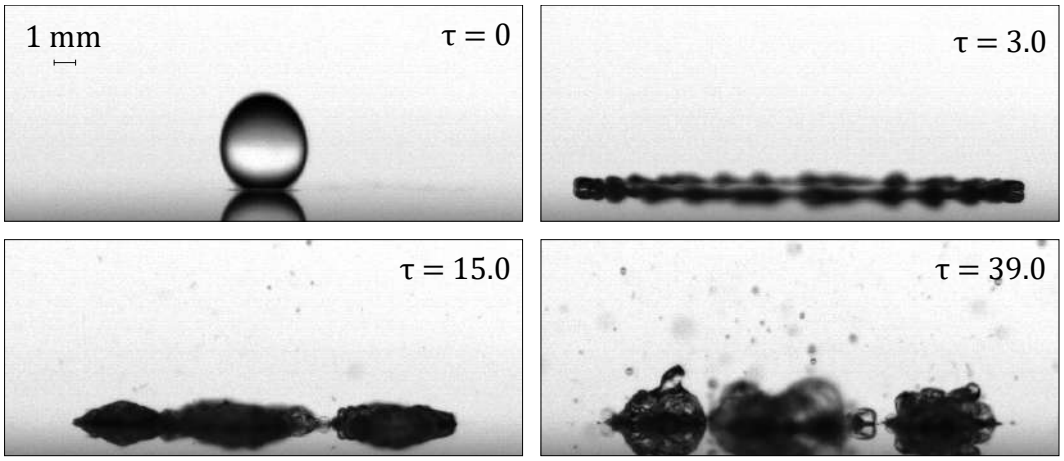

Figure 4.14: Water droplet impact ($We = 313$) onto an aluminium surface within the nucleate boiling regime ($T_w = 110$°C).

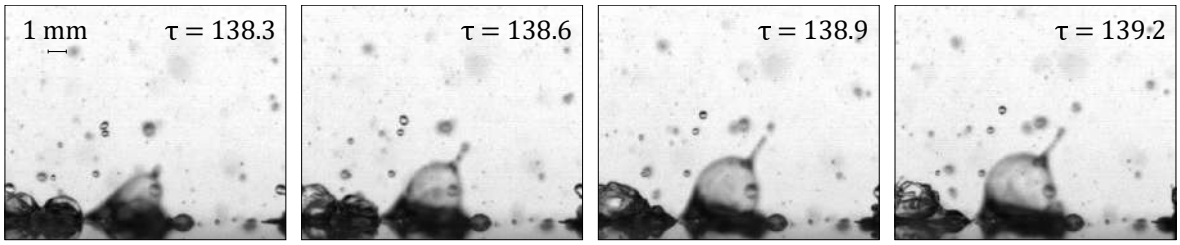

Figure 4.15: Formation of the "pagoda-like" bubbles of a water droplet within the nucleate boiling regime ($T_w = 110$°C).

4.1.2.2 100% Jet Fuel

For jet fuel, at a $T_w = 175$°C (Fig. 4.16), in the nucleate boiling regime, at the moment of impact, vapour bubbles form inside the droplet ($\tau = 0.3$). The droplet then spreads, and a tiny vertical jet is seen at $\tau = 3.3$. According to Cossali et al. [46], the formation of this jet is a boiling induced phenomenon, and a possible explanation is the formation of a pressure wave at the point of impact. This pressure wave is formed because of the rapid formation of vapour bubbles. At $\tau = 13.1$, the droplet boils on the surface, producing secondary atomisation accompanied with puffing. The rupture of the lamella and the formation of puddles is seen at $\tau = 29.5$, while the secondary atomisation grows stronger. In the case of 100% jet fuel, the rupture and formation of puddles is much more intense than on water because of its lower surface tension. As reported for H_2O, pagoda-like bubbles were also observed for this fluid.

4.1.2.3 Jet Fuel (75%) - HVO (25%)

At a wall temperature of $T_w = 200$°C (Fig. 4.17), the nucleate boiling regime is reached for this mixture. However, this temperature is in the transition of the film evaporation to the nucleate boiling regime. After impact, a burst of vapour bubbles is seen at $\tau = 0.6$. Afterwards, the droplet spreads with fingering ($\tau = 2.9$). After reaching the maximum spreading diameter, the droplet does not enter a receding phase. Instead, the droplet will breakup into puddles and boil ($\tau = 40.6$). At the same time, secondary atomisation occurs but is not intense. At later stages of the evaporation, jets breaking up on top of the boiling droplet can be

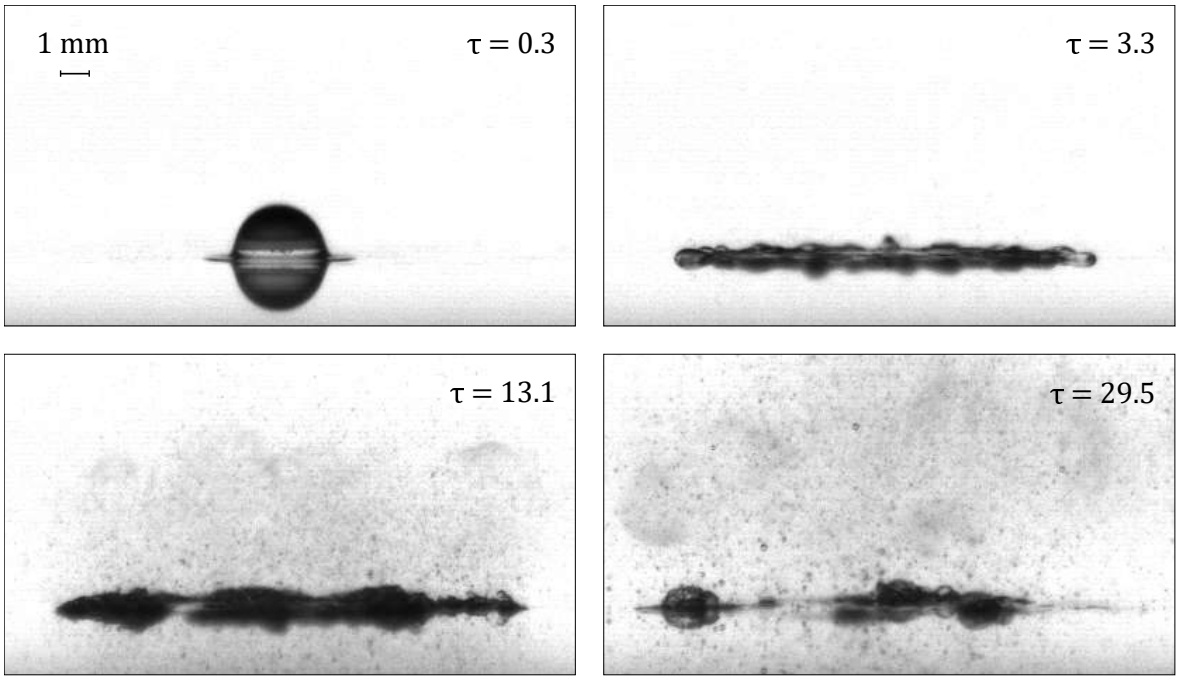

Figure 4.16: 100% jet fuel droplet impact ($We = 324$) onto an aluminium surface within the nucleate boiling regime ($T_w = 175$ºC).

seen producing secondary atomisation (Fig. 4.18).

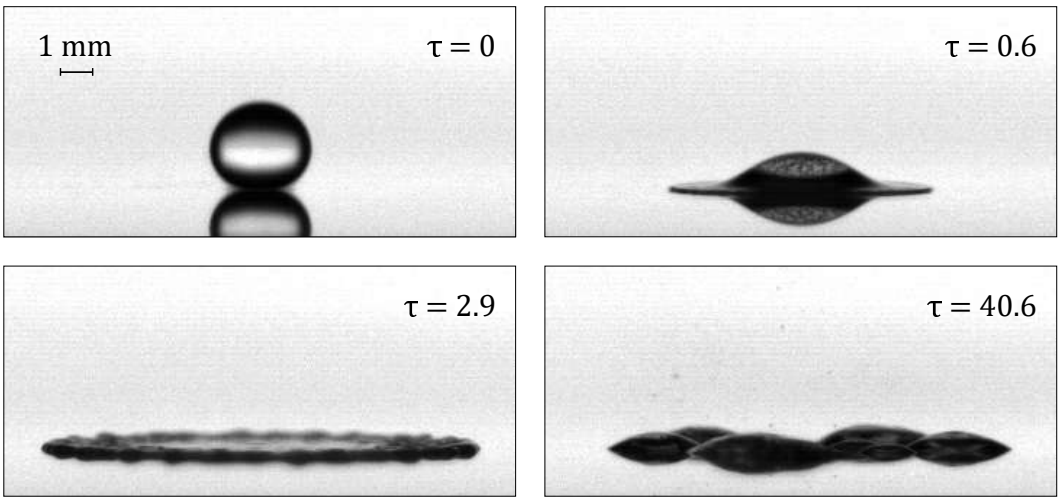

Figure 4.17: Mixture of 75% jet fuel with 25% HVO droplet impact ($We = 313$) onto an aluminium surface within the nucleate boiling regime ($T_w = 200$ºC).

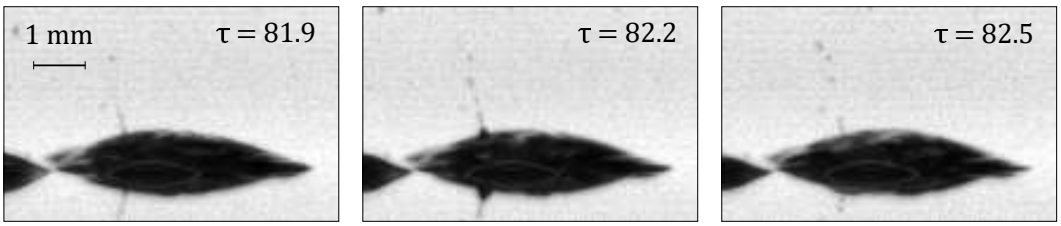

Figure 4.18: Jets bursting on the surface of the puddles of a 75% jet fuel with 25% HVO droplet in the nucleate boiling regime ($T_W = 200$ºC).

When wall temperature reaches $T_w = 220$ºC (Fig. 4.19), a burst of vapour bubbles is quickly

formed at $\tau = 0.3$. At $\tau = 1.5$, the spreading stage with fingering is visible. Afterwards, the droplet will not enter a receding phase. Instead, it will form puddles and boil with more intense secondary atomisation than before and, this time, with puffing ($\tau = 34.8$). At later stages of the impact, the droplet will stop nucleating and enter a film evaporation regime (Fig. 4.20). This can be explained because these two fluids have different boiling points and the surface temperature is in between these two points. The jet fuel has a lower boiling point, therefore, it is in the nucleate boiling regime and it boils earlier than HVO. Afterwards, the remaining droplet left on the heated surface will slowly evaporate.

As the temperature increases until the limit of the transition boiling, a new phenomenon can be seen. When $T_w = 240$ºC, the droplet will initially behave the same way as it did for $T_w = 220$ºC. However, in the later stages, after the jet fuel has evaporated, instead of forming a big single droplet like before, the droplet will breakup into puddles that will slowly evaporate on the heated surface (Fig 4.21). This is because the wall temperature is approaching the nucleate boiling regime for the HVO part of the mixture. Therefore, the puddles start forming just like it did at a $T_w = 250$ºC for the 100% HVO droplet impact in figure 4.12. For this fluid, pagoda-like bubbles were observed for wall temperatures of $T_w = 220$ºC and $T_w = 240$ºC.

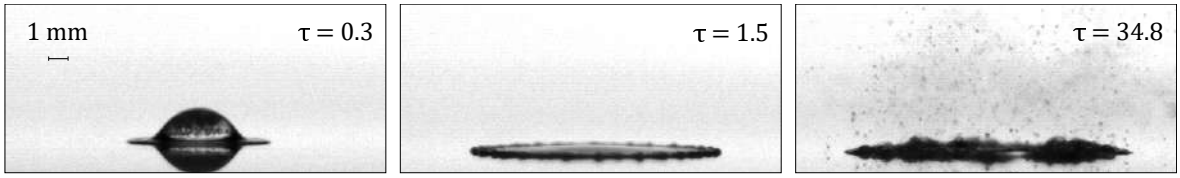

Figure 4.19: Mixture of 75% jet fuel with 25% HVO droplet impact ($We = 313$) onto an aluminium surface within the nucleate boiling regime ($T_w = 220$ºC).

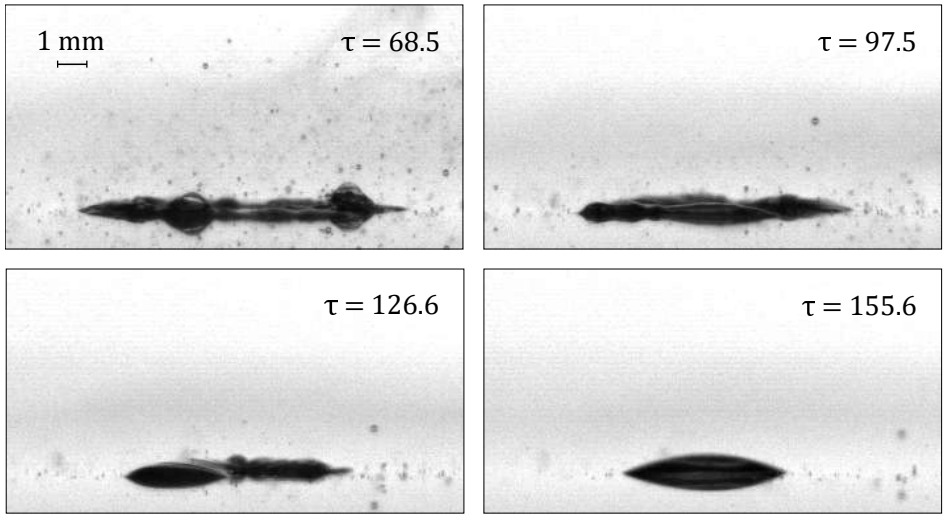

Figure 4.20: Evolution of the 75% jet fuel with 25% HVO mixture droplet impact in the nucleate boiling regime ($T_w = 220$ºC).

4.1.2.4 Jet Fuel (50%) – HVO (50%)

In the nucleate boiling regime, $T_w = 250$ºC (Fig. 4.22), immediately after impact, vapour bubbles form inside the droplet ($\tau = 0.3$). The spreading phase is accompanied with finger-

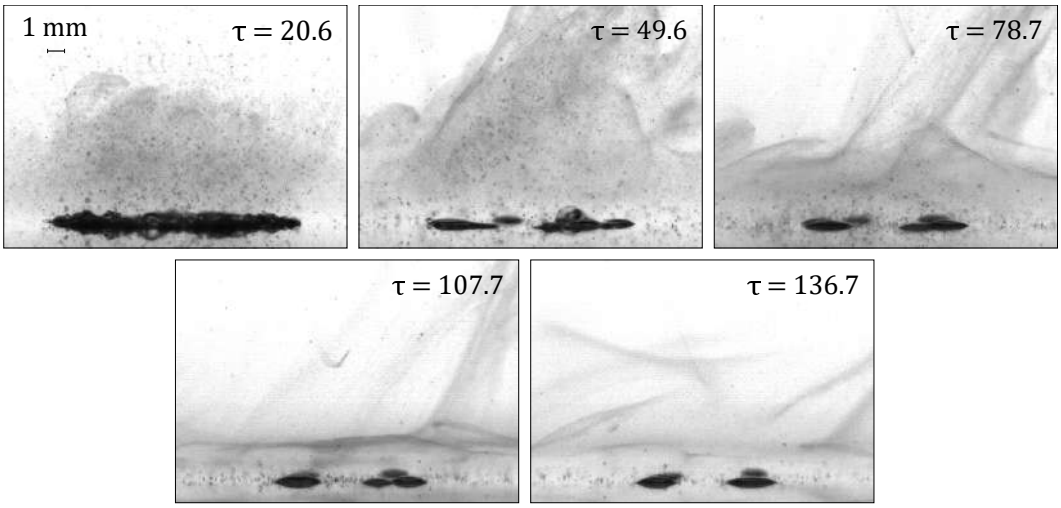

Figure 4.21: Nucleate boiling and formation of puddles of a mixture of 75% jet fuel with 25% HVO for $T_w = 240$°C.

ing ($\tau = 3.4$). After reaching its maximum spreading diameter, the droplet boils accompanied with secondary atomisation and puffing ($\tau = 44.1$).

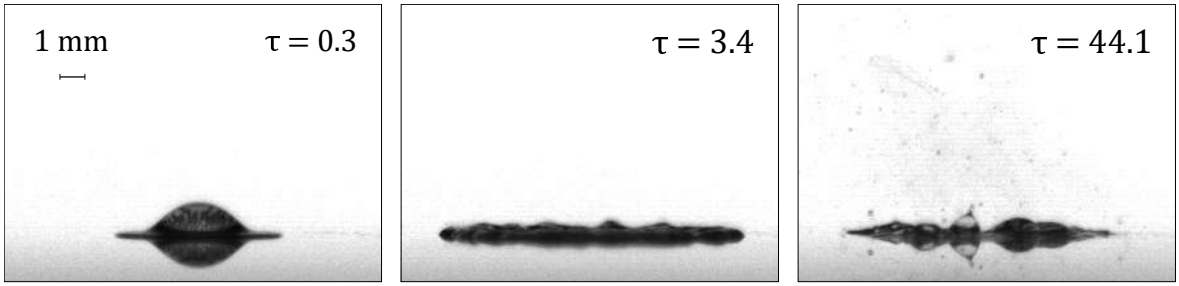

Figure 4.22: Mixture of 50% jet fuel with 50% HVO droplet impact ($We = 325$) onto an aluminium surface within the nucleate boiling regime ($T_w = 250$°C).

In the later stages of the impact, the same phenomenon occurs as it did for the 75% jet fuel with 25% HVO mixture. Since these two fluids have two different boiling points, the droplet is left on the heated plate in the film evaporation regime slowly evaporating. Pagoda-like bubbles were also reported for this temperature ($\tau = 44.1$).

4.1.2.5 100% HVO

At a wall temperature of $T_w = 285$°C (Fig. 4.23), the HVO droplet enters the nucleate boiling regime. This appears to be in the transition between nucleate boiling and the film evaporation regimes because at the early stages of impact, the droplet breaks up in the spreading phase into puddles ($\tau = 9.2$) and vapour bubbles form inside these puddles ($\tau = 30.6$). At later stages, the droplet starts boiling and producing secondary atomisation accompanied with puffing ($\tau = 64.4$).

Increasing wall temperature to $T_w = 300$°C (Fig. 4.24), in the nucleate boiling regime, after the droplet completely spreads, it breaks up into puddles ($\tau = 12.3$). Afterwards, the droplet remains on the heated surface evaporating, producing secondary atomisation and puffing

($\tau = 30.6 \; - \; \tau = 46.0$). It can be observed that for $\tau = 46.0$, the droplet is almost entirely evaporated, which implies that $T_w = 300$ºC is near the critical heat flux, therefore near the transition boiling regime.

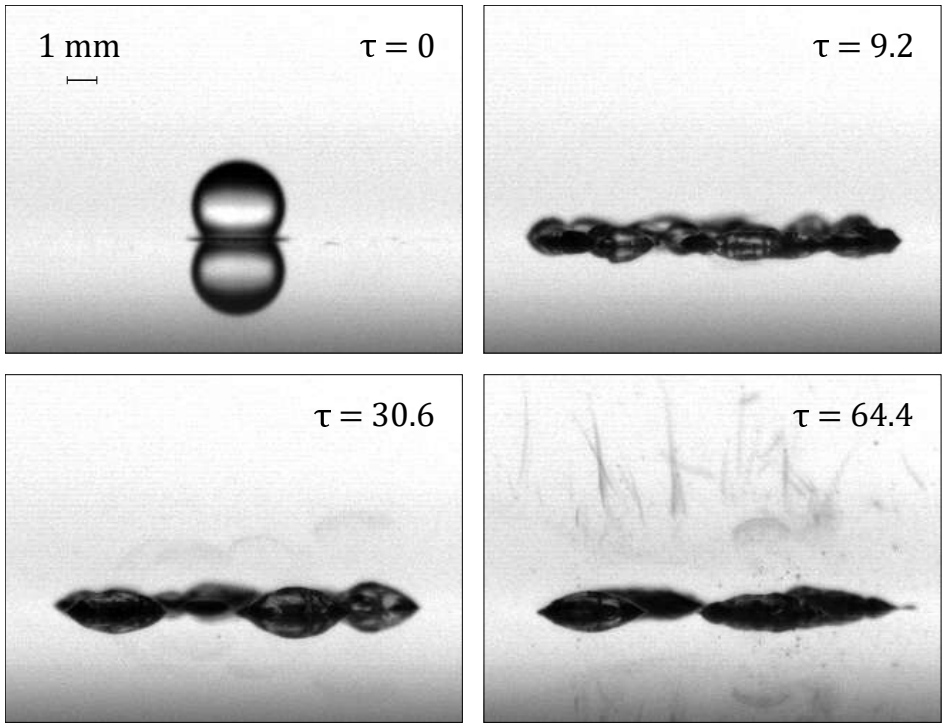

Figure 4.23: 100% HVO droplet impact ($We = 330$) onto an aluminium surface within the nucleate boiling regime ($T_w = 285$ºC).

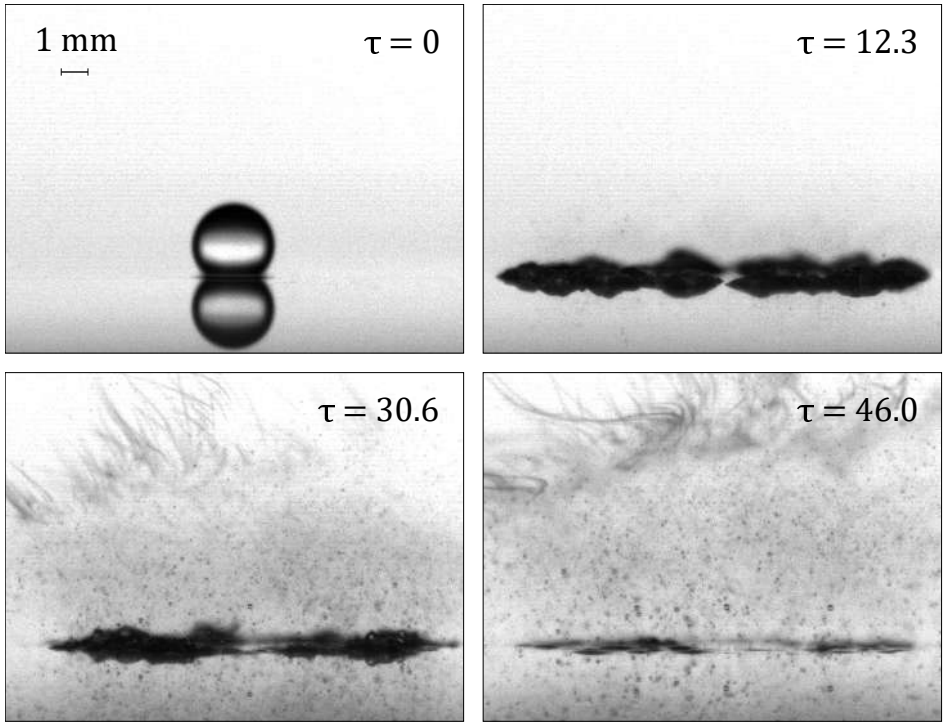

Figure 4.24: 100% HVO droplet impact ($We = 330$) onto an aluminium surface within the nucleate boiling regime ($T_w = 300$ºC).

4.1.3 Transition Boiling

4.1.3.1 H_2O

At $T_w = 135$ºC (Fig. 4.25), in the transition boiling regime, the droplet contacts with the surface intermittently. Here, the Leidenfrost phenomenon is visible and a tiny unstable vapour layer is formed beneath the droplet, which makes it possible to "levitate" and not evaporate immediately. However, this temperature does not represent the Leidenfrost temperature since, above T_{Leid}, there is no contact between the droplet and the wall.

After completely spreading and beginning the receding phase ($\tau = 3.0$), secondary atomisation is noticed at $\tau = 6.0$, and the liquid begins to form into bigger droplets, as seen at $\tau = 24.0$. After a short time ($\tau = 30.0$), there is no more secondary atomisation and the droplets rebound on the heated surface ($\tau = 48.0$). Vapour bubbles can be seen inside the droplets at all times after completely formed. After a short time rebounding, the bottom part of the droplet can burst because the heat is not enough to sustain the vapour layer (Fig. 4.26).

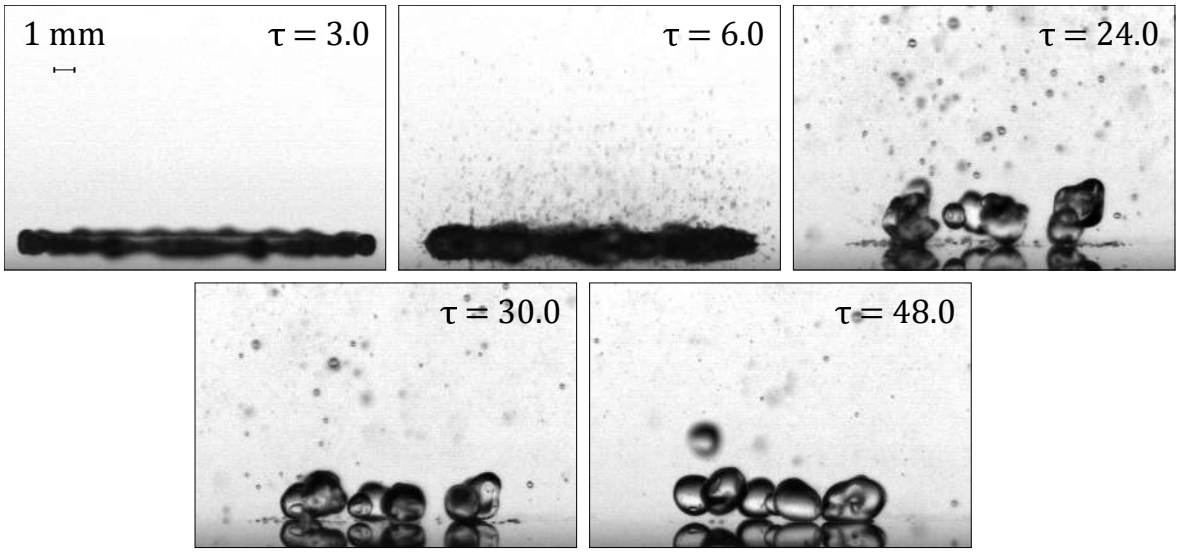

Figure 4.25: Water droplet impact ($We = 313$) onto an aluminium surface within the transition boiling regime ($T_w = 135$ºC).

In figure 4.27, it is represented the phenomenona of droplet impact at different temperatures in the transition boiling regime. As the temperature increases to $T_w = 150$ºC, in the transition boiling regime, the number of daughter droplets formed also increase and they are smaller in size (Fig. 4.27 (a)). The secondary atomisation at the moment of impact grows stronger until a wall temperature of $T_w = 250$ºC (Fig. 4.27 (b)), and then becomes weak again, $T_w = 300$ºC (Fig. 4.27 (c)), as the heated surface gets closer to the Leidenfrost temperature. Additionally, as the temperature increases, the number of droplets ejected in the radial direction increase, as opposed to the vertical ejected droplets, which increase up to $T_w = 250$ºC and then decrease until $T_w = 300$ºC. For these three temperatures, the only differences were in the first stages of impact regarding the projection of the secondary droplets.

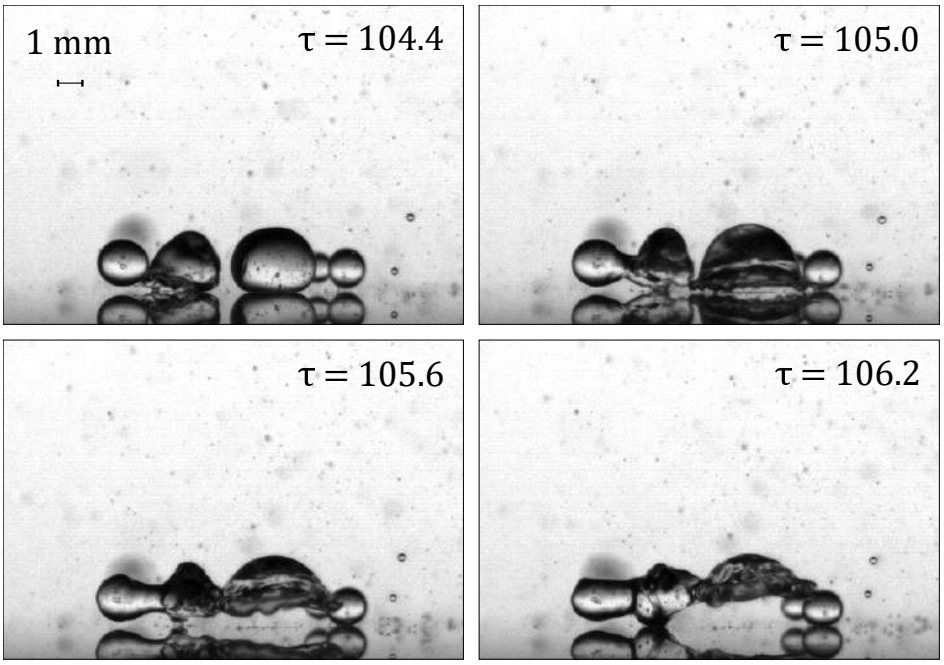

Figure 4.26: Water droplet burst on an aluminium surface within the transition boiling regime ($T_w = 135$°C).

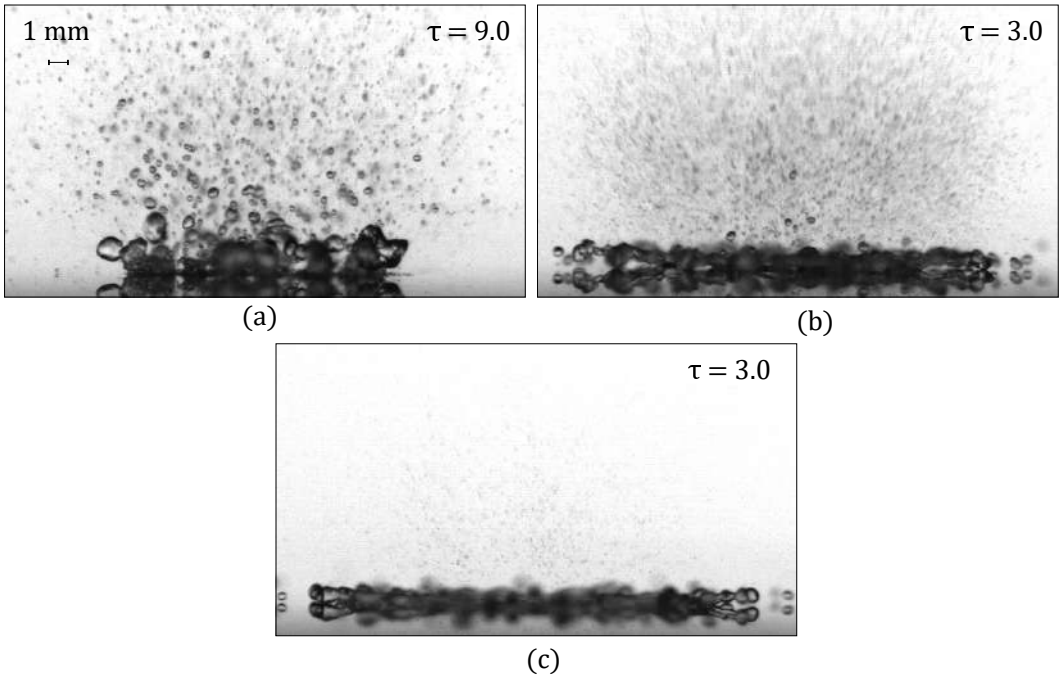

Figure 4.27: Water droplet impact at different wall temperatures in the transition boiling regime. (a) $T_w = 150$°C. (b) $T_w = 250$°C. (c) $T_w = 300$°C.

4.1.3.2 100% Jet Fuel

At $T_w = 200$°C (Fig. 4.28), the droplet impacts and, during the spreading phase, the vertical jet is witnessed again at $\tau = 1.6$. At $\tau = 6.6$, the droplet breaks up into tinier droplets accompanied with puffing. However, there is still contact with the surface, meaning that this is in the transition boiling regime. Secondary atomisation is also seen beginning at $\tau = 6.6$ and the new daughter droplets remain "levitating" on the unstable vapour layer. The direction of

these daughter droplets is mainly radial. However, some are still ejected vertically $\tau = 6.6$. This radial ejection during the spreading phase can be connected to a form of prompt splash, where the lamella breaks up due to the vapour layer. Vapour bubbles can be seen inside the tiny droplets ($\tau = 42.6$).

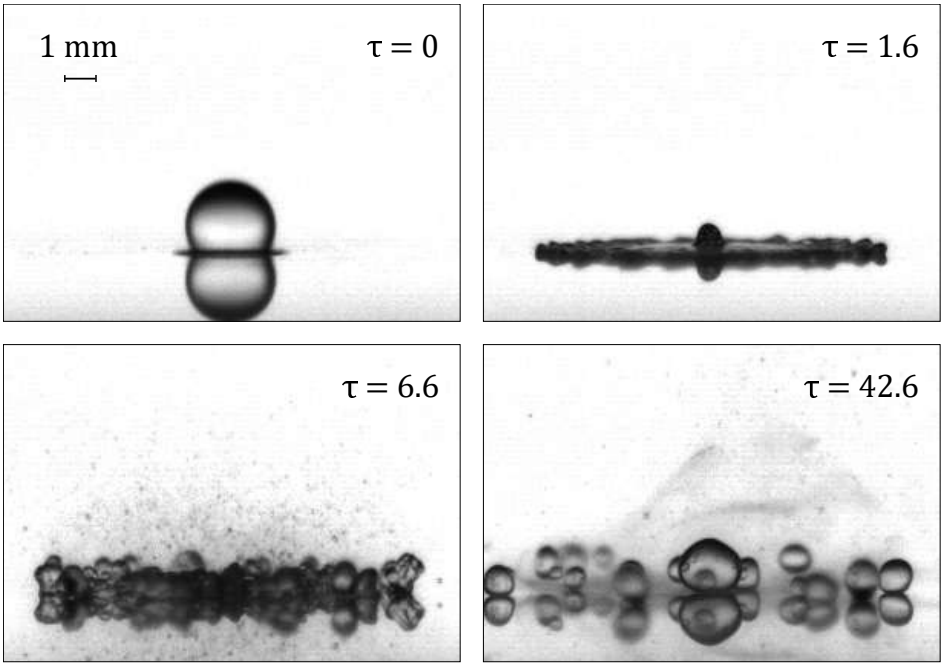

Figure 4.28: 100% jet fuel droplet impact ($We = 324$) onto an aluminium surface within the transition boiling regime ($T_w = 200$°C).

4.1.3.3 Jet Fuel (75%) - HVO (25%)

At $T_w = 260$°C (Fig. 4.29), from $\tau = 0$ to $\tau = 2.9$, the droplet spreads with fingering. The lamella breaks up and forms tiny droplets that levitate in an unstable vapour layer ($\tau = 11.6$), accompanied with puffing and secondary atomisation. The secondary droplets are projected radially and vertically. However, at this temperature, two different regimes can be seen – transition boiling and film boiling. This is because of different boiling points of these fluids. The wall temperature is in between two regimes of two different fluids, therefore, some part of the droplet will contact the wall and boil while the other will levitate on an unstable vapour layer ($\tau = 40.6$).

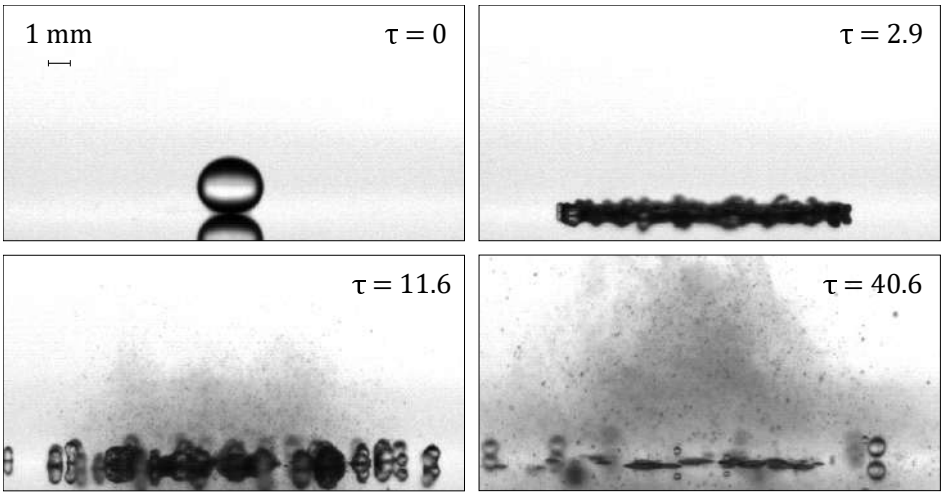

Figure 4.29: Mixture of 75% jet fuel with 25% HVO droplet impact ($We = 313$) onto an aluminium surface within the transition boiling regime ($T_w = 260$ºC).

4.1.3.4 Jet Fuel (50%) - HVO (50%)

At a $T_w = 275$ºC (Fig. 4.30), the droplet spreads with fingering and after reaching its maximum spreading diameter, it starts boiling violently, accompanied with puffing and secondary atomisation ($\tau = 6.8$). No receding phase was observed due to the instant boiling of the droplet. Just like the previous mixture, at this temperature, two different regimes can be observed: transition boiling and film boiling ($\tau = 33.9$). While some part of the liquid is boiling in contact with the wall, the droplets ejected from the explosions earlier will rebound on the vapour layer ($\tau = 50.9$).

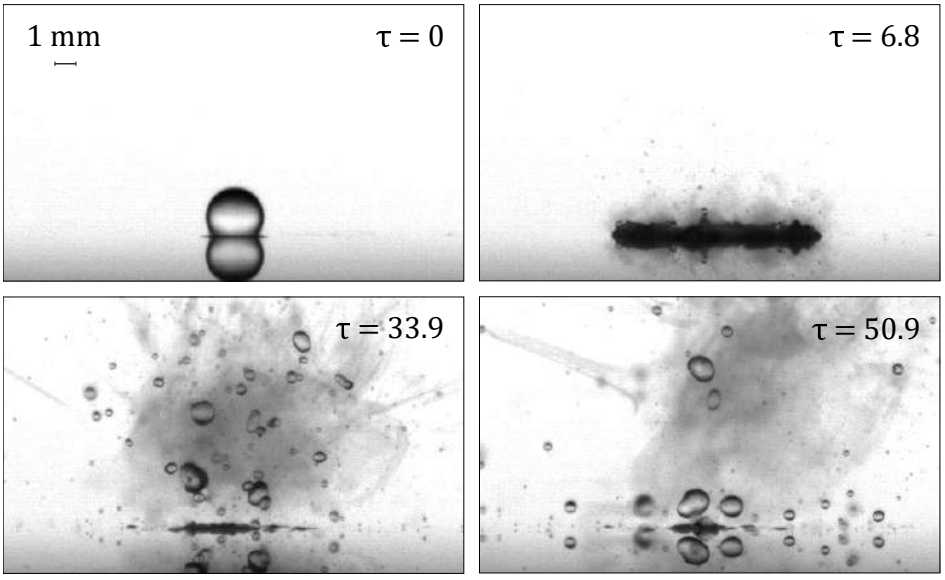

Figure 4.30: Mixture of 50% jet fuel with 50% HVO droplet impact ($We = 325$) onto an aluminium surface within the transition boiling regime ($T_w = 275$ºC).

At $T_w = 300$ºC (Fig 4.31), it is clearly seen the transition boiling regime. During the spreading phase ($\tau = 3.4$), the fingers of the lamella break. Additionally, the secondary atomisation produces tinier droplets that will be levitating on an unstable vapour layer ($\tau = 6.8$). There is

clearly contact with the wall as secondary atomisation and puffing occur ($\tau = 6.8 - \tau = 27.1$). It is possible to observe vapour bubbles inside the fully formed droplets ($\tau = 84.8$).

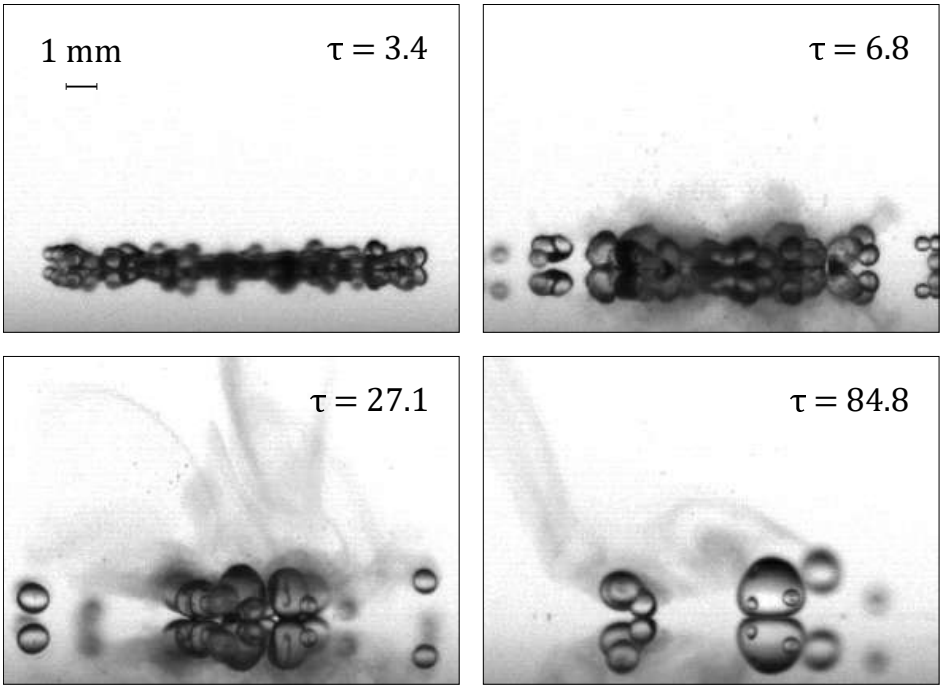

Figure 4.31: Mixture of 50% jet fuel with 50% HVO droplet impact ($We = 325$) onto an aluminium surface within the transition boiling regime ($T_w = 300$°C).

4.1.3.5 100% HVO

For this fluid at a wall temperature of $T_w = 315$°C (Fig. 4.32), the transition boiling regime is achieved. The droplet, after impact, spreads with fingering ($\tau = 3.1$) and these fingers break into small droplets ($\tau = 9.2$). These tiny droplets levitate on an unstable vapour layer and can eventually rapidly boil if the heat is not enough to sustain the vapour layer. This phenomenon occurred with secondary atomisation accompanied with puffing ($\tau = 27.6$). Additionally, for the same time, bubbles can be seen inside the secondary droplets.

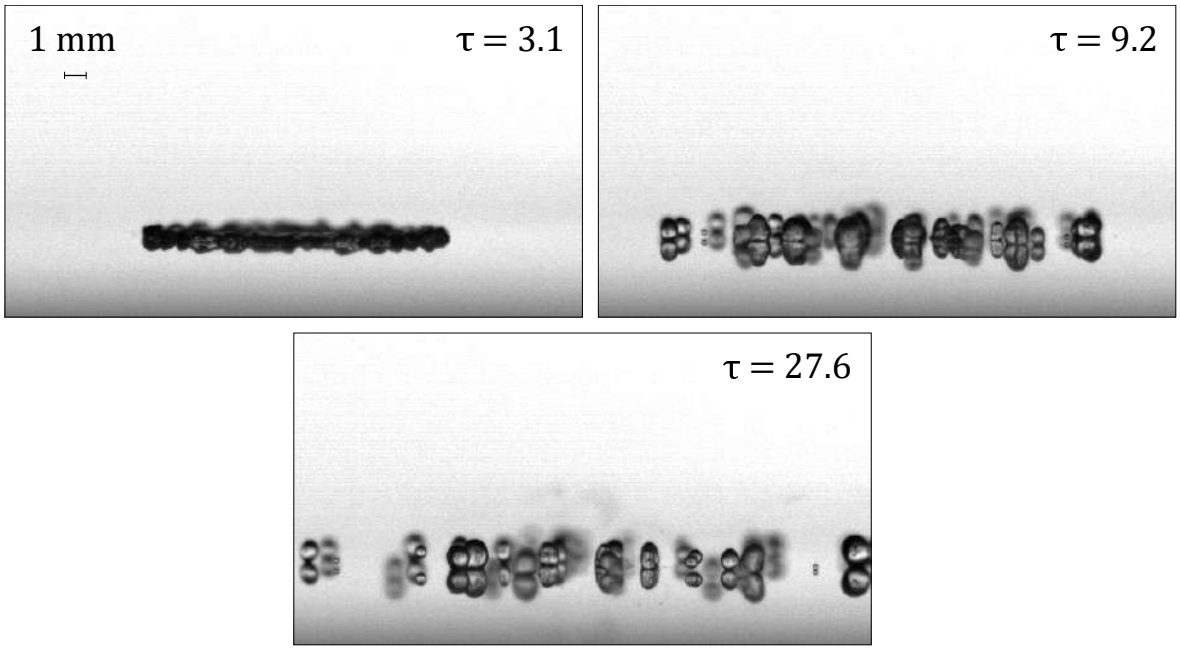

Figure 4.32: 100% HVO droplet impact ($We = 330$) onto an aluminium surface within the transition boiling regime ($T_w = 315$°C).

4.1.4 Film Boiling

4.1.4.1 H_2O

At $T_w = 320$°C (Fig. 4.33) at the moment of impact, the droplet completely shatters. Above the Leidenfrost temperature, there is no more liquid-solid contact as a result of the vapour layer formed between the two interfaces. Therefore, this absence of liquid-wall contact is responsible for the smaller droplets generated. At the moment of impact, the droplet undergoes a prompt splash ($\tau = 0.6$) and breaks up to form secondary droplets. Unlike lower temperatures, the droplets ejected are only in the radial direction ($\tau = 3.6 \ - \ \tau = 6.6$). This radial ejection is due to the increasing wall temperature. The higher the temperature, the more intense is the splashing and more tiny droplets are formed. The number of bubbles inside the daughter droplets are reduced significantly in this regime. However, some bubbles can still be seen within the daughter droplets at $\tau = 24.6$. In these experiments, no rebound of the entire droplet was seen because the Weber number was moderately high, which resulted in splashing in all tests done. While rebounding on the heated surface, the daughter droplets may coalesce to form a bigger droplet, as shown in figure 4.34.

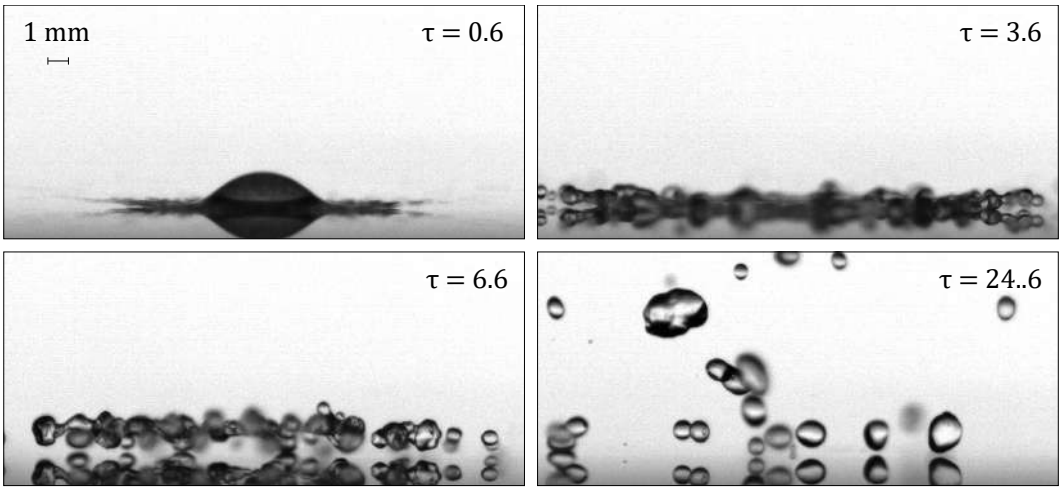

Figure 4.33: Water droplet impact ($We = 313$) onto an aluminium surface within the film boiling regime ($T_w = 320$ºC).

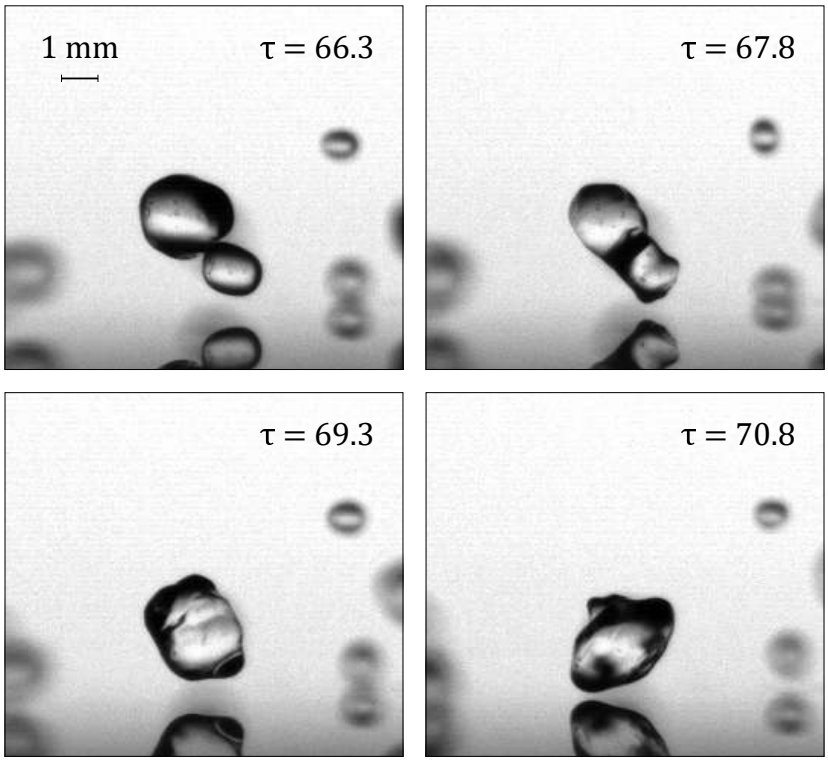

Figure 4.34: Water droplet coalescence while rebounding on the heated surface within the film boiling regime ($T_w = 320$ºC).

4.1.4.2 100% Jet Fuel

At a wall temperature of $T_w = 240$ºC (Fig. 4.35), the film boiling regime for 100% jet fuel is reached. The droplet levitates on a vapour layer formed right before impact, which reduces significantly the heat flux between the droplet and the wall. Thus, this temperature corresponds to the highest evaporation time. There is no solid-liquid contact and, for this reason, the droplet undergoes a prompt splash ($\tau = 0.7$) and breaks up into tinier secondary droplets ($\tau = 3.9 - \tau = 7.2$). The droplets are projected only in the radial direction and puffing does not occur, unlike what occurred in the transition boiling regime (Fig. 4.28),

where both phenomena would occur.

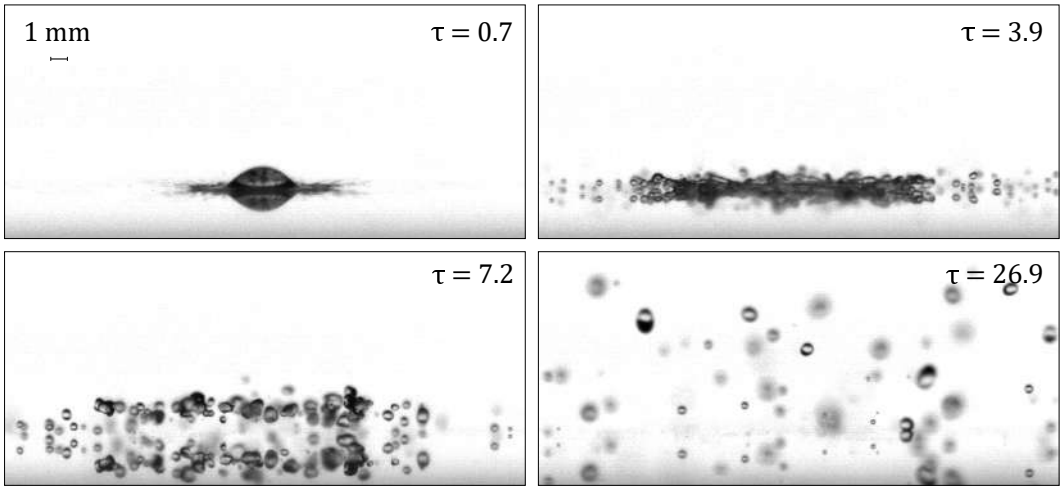

Figure 4.35: 100% jet fuel droplet impact ($We = 324$) onto an aluminium surface within the film boiling regime ($T_w = 240$ºC).

4.1.4.3 Jet Fuel (75%) - HVO (25%)

When wall temperature is set to $T_w = 275$ºC (Fig. 4.36), the droplet will enter the film boiling regime and the Leidenfrost phenomenon is clearly visible. The droplet will not contact the surface and, instead, it will levitate on a stable vapour layer, formed at the moment of impact, and bounce on the heated surface. At $\tau = 0.6$, it can be seen the prompt splash of the liquid lamella, breaking up into tiny droplets that are only projected radially ($\tau = 3.5$). For all experiments done, there was always a bigger droplet in the centre of the impact, as can be seen at $\tau = 23.2$. In this regime, puffing never occurred due to the absence of contact between the two interfaces. When wall temperature was set to $T_w = 320$ºC, there were no differences found in the impact, compared to the wall temperature of $T_w = 275$ºC.

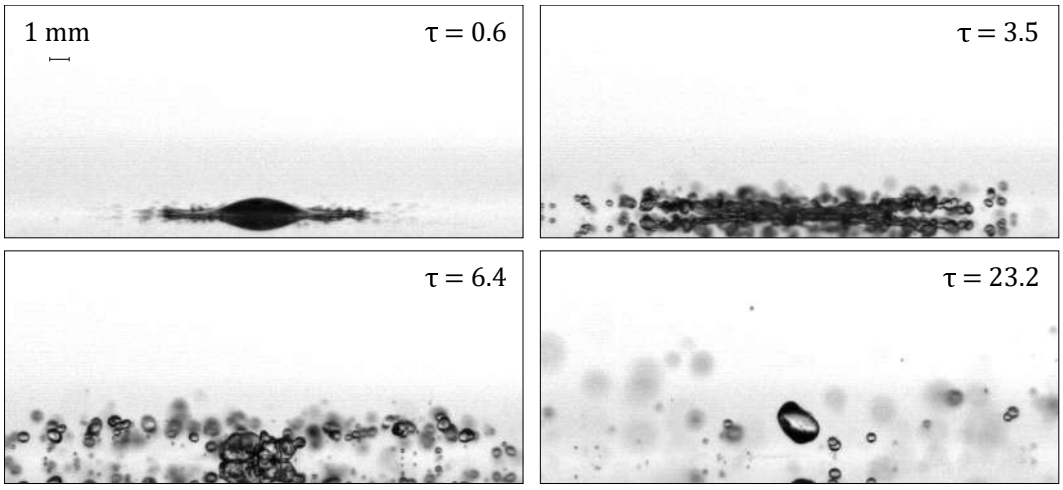

Figure 4.36: Mixture of 75% jet fuel with 25% HVO droplet impact ($We = 313$) onto an aluminium surface within the film boiling regime ($T_w = 275$ºC).

4.1.4.4 Jet Fuel (50%) – HVO (50%)

Increasing the wall temperature to $T_w = 320$ºC (Fig. 4.37), the film boiling regime is achieved. Just like the previous fluids in this regime, before impact, a tiny vapour layer is formed between the droplet and the surface. Therefore, the droplet never contacts the surface and bounces repeatedly on the heated surface. At the moment of impact, the droplet undergoes a prompt splash ($\tau = 0.7$). This splash produces many daughter droplets that are projected only in the radial direction ($\tau = 4.1$). At the centre of the impact, a higher concentration of bigger droplets was visible for all tests done ($\tau = 24.4$). Compared to lower temperatures, puffing never occurred in the film boiling regime due to the absence of contact between the surface and the droplet.

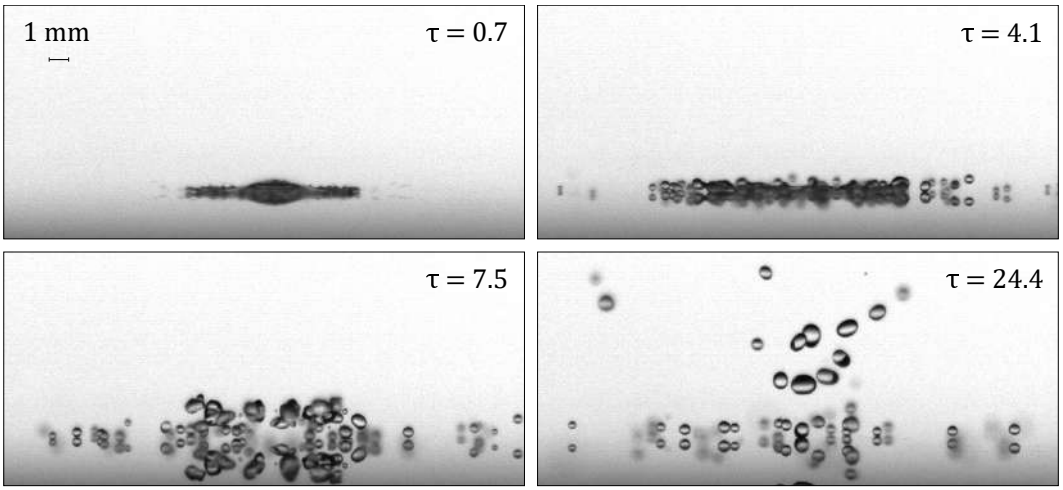

Figure 4.37: Mixture of 50% jet fuel with 50% HVO droplet impact ($We = 325$) onto an aluminium surface within the film boiling regime ($T_w = 320$ºC).

4.1.4.5 100% HVO

At $T_w = 330$ºC (Fig. 4.38), the film boiling regime is reached. Just like all other fluids, at this temperature, the droplet never wets the plate because it levitates on a stable vapour layer. Thus, the heat flux between the surface and the droplet is much lower. After impact, the droplet undergoes a prompt splash and breaks up in the radial direction into several tiny droplets ($\tau = 3.7 \; - \; \tau = 6.7$). The ejected droplets remain on the Leidenfrost effect and will never contact the wall like the main droplet. For this fluid, bigger droplets in the middle of the impact were observed ($\tau = 25.1$).

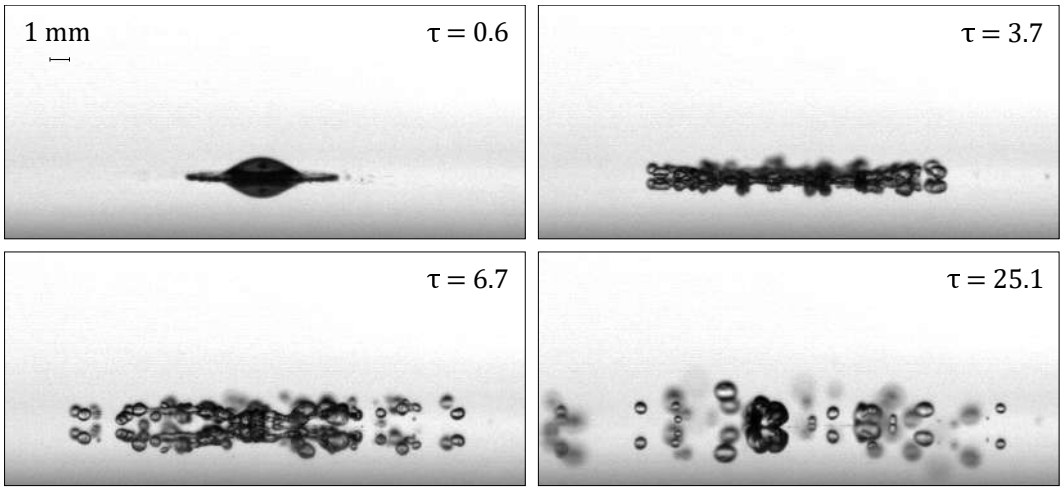

Figure 4.38: 100% HVO droplet impact ($We = 330$) onto an aluminium surface within the film boiling regime ($T_w = 330$ºC).

4.2 Summary

In this section, a brief summary of all the phenomena observed and the comparison between them will be done. A diagram representing the heat regimes and the respective transition temperatures will be presented (Fig. 4.39). Additionally, a table for each fluid, will be presented for easy understanding of the events depicted in the sections above (Table 4.1, Table 4.2, Table 4.3, Table 4.4, and Table 4.5).

All fluids behave similarly in the same regime, apart for some differences. The major difference from all the fluids is having a different boiling point. While for water, the boiling point is of $T = 100$ºC at ambient pressure, for the jet fuel mixture is around $T = 175$ºC, for 75% Jet Fuel with 25% HVO around $T = 200$ºC, for 50% Jet Fuel with 50% HVO is around $T = 250$ºC, and for HVO it is around $T = 285$ºC. This values do not represent the exact boiling point, and were obtained experimentally by observing when the fluid entered the nucleate boiling regime. These different boiling points translate into different heat regimes for the same temperature, which is why the experiments were not done for the same wall temperature for the different fluids.

In all tests for all fluids, there was always air entrapment at the moment of impact. In the film evaporation regime, for a surface temperature equal to the ambient temperature, the water droplet would spread and, in the receding phase, it would oscillate until it achieved an equilibrium state. Additionally, water was the only fluid to experience receding breakup. For the jet fuel, HVO and the jet fuel/biofuel mixtures, the droplet would not enter a receding phase. For all fluids, except for water, the droplet spreads without any fingers. This occurs due to the surface tension of water being almost three times higher than the other fluids. Approaching the nucleate boiling regime from the film evaporation, the fluids would start forming vapour bubbles and breaking up in the receding phase to form puddles, where they would vaporise slowly at its phase contact line, until the droplet is completely evaporated. Apart from water, all fluids evaporated fumes near the nucleate boiling regime (puffing).

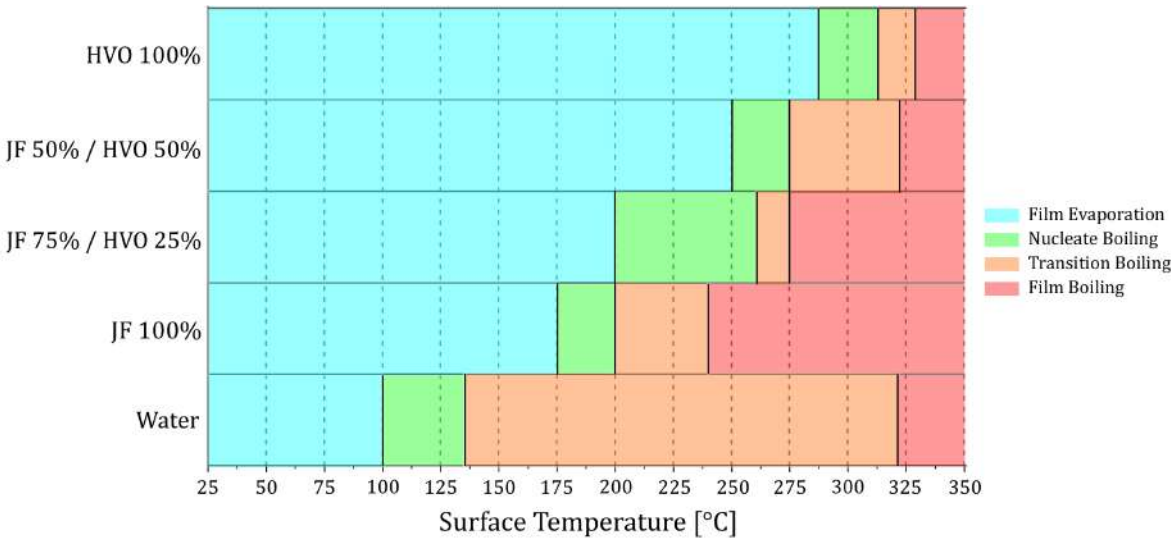

Figure 4.39: Regime map for the different fluids for the same Weber number.

In the nucleate boiling regime, the formation of vapour bubbles is more frequent at the droplet interface, ascending through the droplet and break through the droplet surface to form multiple secondary droplets. In all experiments, "pagoda-like bubbles" were reported for this regime. For jet fuel, a tiny jet in the impact point was observed, and puffing occurred for all fluids except water. For the mixtures of 50% jet fuel with 50% HVO and 75% jet fuel with 25% HVO, a multiple regime was observed. On impact, these two fluids would start boiling violently. At later stages of the impact, the droplet would remain in the film evaporation regime, slowly evaporating. Reason for this is that this mixture has two fluids with two different boiling points. The boiling point for jet fuel is around $T = 175$ºC, and for HVO is around $T = 285$ºC. Therefore, the jet fuel would boil while the HVO (below its boiling point) would only slowly evaporate. For the film evaporation and nucleate boiling regime, the droplets ejected were only vertically and never radially.

In the transition boiling regime, the vapour bubble formation increases rapidly. Therefore, the bubbles are constantly coalescing and form an unstable vapour layer on some portions of the areas between the droplet and the wall, while the rest of the droplet is in contact with the wall. Some authors report this phenomenon as "dancing" [21]. In this regime, the droplet would breakup on impact and form multiple daughter droplets that would levitate on this vapour layer. Every fluid, except water, experienced secondary atomisation accompanied with puffing, while water only experienced secondary atomisation. Since this vapour layer is very unstable, the droplets can stick to the wall and rapidly boil. For the mixtures of 75% jet fuel with 25% HVO, and 50% jet fuel with 50% HVO, the same phenomenon occurred as it did for the nucleate boiling regime. Due to different boiling points, the droplet on impact would eject secondary droplets that would levitate on the vapour layer in the film boiling regime. However, while below the boiling point of HVO, some part of the droplet would be in complete contact with the wall boiling, in the transition boiling regime.

Increasing the temperature above the Leidenfrost temperature, the film boiling regime is

reached. In this condition, the wall surface is covered with a stable vapour layer and the entire droplet never wets the surface (there is no liquid-solid contact). This temperature corresponds to the highest evaporation time of the droplet, because the heat flux from the surface to the droplet is highly reduced by the presence of the vapour layer. The droplet impact only projected droplets radially and never vertically. The droplet can rebound or splash in this regime. However, for rebound, the impact energy needs to be lower. Since these experiments had a moderately high Weber number (high impact energy), the droplet always experienced splashing for all fluids. For HVO and the jet fuel and biofuel mixtures, there was always a more concentrated droplet in the centre of the impact.

In figure 4.39, a visual representation of the heat regimes map for the five fluids is provided. This map was made according to the observable regime the fluid would be in, and the transition temperatures between regimes do not represent the exact transition temperature and are only estimates of the experimental work. However, they are not far away from the actual value because many tests were done to observe these transitions.

The film evaporation regime increases with increasing T_{sat}. Therefore, since water has the lowest boiling point, it also has the shortest range of temperatures for this regime, while HVO has the highest. For the nucleate boiling regime, the temperature variation is almost the same for all fluids, except for 75% jet fuel with 25% HVO mixture, which is slightly higher. The transition boiling also varied almost the same for all fluids except for water, in which it spanned a high range of temperatures. Jet fuel 100% has the lowest Leidenfrost temperature and, therefore, the film boiling regime is reached before the other mixtures. On the contrary, HVO has the highest Leidenfrost temperature, meaning that it had the highest wall temperature to achieve the film boiling regime. The Leidenfrost temperature of the mixtures of these two fluids was in the middle, being the one with the most HVO, the highest of these two.

One important aspect to mention is that two more regimes were needed to classify the impact for the mixtures of 75% jet fuel with 25% HVO and 50% jet fuel with 50% HVO. This is due to the presence of two different boiling points between the mixed fluids. While the boiling point of HVO is around $T_{sat} = 285$ºC, the boiling point for jet fuel is around $T_{sat} = 175$ºC. This discrepancy in these boiling points makes it possible to exist two different regimes at the same time. For example, for the mixture of 75% jet fuel with 25% HVO, in the nucleate boiling regime, the droplet would boil after impact. However, after a short time, a single droplet was left on the heated plate in the film evaporation regime, slowly evaporating. These two additional regimes are specific to the biofuel and fuel mixtures (75% jet fuel - 25% HVO, and 50% jet fuel - 50% HVO). The additional regimes for these two fluids are called ”wet boiling impact followed by the remaining of a sessile droplet on the surface after boiling completion”, and ”dry impact, bounce and wet boiling”. These regimes are based on the terminology of Kompinsky et al. [62]. The first regime is when the nucleate boiling and film evaporation regimes are present, and the second regime is when the transition and film boiling regimes coexist. Therefore, for the mixture of 75% jet fuel with 25% HVO, from $T_w = 220 - 240$ºC, the mixture is in the ”wet boiling impact followed by a remaining sessile droplet on the surface”

regime, and from $T_w = 260 - 275$°C the mixture experiences "dry impact, bounce and wet boiling". For the mixture of 50% jet fuel with 50% HVO, from $T_w = 250 - 275$°C, the mixture is in the "wet boiling impact followed by a remaining sessile droplet on the surface" regime, and from $T_w = 275 - 300$°C the droplet experiences "dry impact, bounce and wet boiling".

Table 4.1: Summary of the phenomena observed for H_2O for the four heat regimes.

Heat Regime	**T_w [°C]**	**Phenomenon Description**
Film Evaporation	25	Spreading w/ receding breakup, air entrapment, fingering
	85	Spreading w/ receding breakup, air entrapment, fingering, small formation of vapour bubbles, formation of puddles
Nucleate Boiling	100	Fingering, formation of puddles, formation and bursting of vapour bubbles, weak secondary atomisation;
	110	Formation and bursting of vapour bubbles, formation of puddles, secondary atomisation, pagoda-like bubbles.
Transition Boiling	135	Droplets projected radially and vertically, secondary atomisation, coalescence of the droplet, Leidenfrost effect, vapour bubbles form inside the daughter droplets;
	250	Droplets projected radially and vertically, violent secondary atomisation, Leidenfrost effect, vapour bubbles form inside the daughter droplets;
	300	Droplets projected radially and vertically, weak secondary atomisation, Leidenfrost effect, vapour bubbles form inside the daughter droplets;
Film Boiling	320	Droplets projected only radially, Leidenfrost effect, splashing

Table 4.2: Summary of the phenomena observed for 100% Jet Fuel for the four heat regimes.

Heat Regime	T_w [^oC]	Phenomenon Description
Film Evaporation	25	Spreading, no receding, air entrapment, no fingering;
	50	Spreading w/ receding, air entrapment, no fingering;
	150	Spreading, air entrapment, fingering, formation of vapour bubbles, formation of puddles, puffing.
Nucleate Boiling	175	Formation and bursting of vapour bubbles, vertical jet on impact, secondary atomisation, puffing, pagoda-like bubbles
Transition Boiling	200	Vertical jet on impact, droplets projected radially and vertically, puffing, secondary atomisation, Leidenfrost effect, vapour bubbles form inside the daughter droplets.
Film Boiling	240/320	Droplets projected only radially, Leidenfrost effect, splashing

Table 4.3: Summary of the phenomena observed for a mixture of 75% Jet Fuel with 25% HVO for the four heat regimes.

Heat Regime	T_w **[ºC]**	**Phenomenon Description**
Film Evaporation	25	Spreading, no receding, air entrapment, no fingering;
	100	Spreading w/ receding, air entrapment, no fingering;
	150	Spreading w/ receding, air entrapment, fingering, formation of vapour bubbles, puffing;
	175	Spreading, air entrapment, fingering, formation of vapour bubbles, formation of puddles, puffing.
Nucleate Boiling	200	Spreading, no receding, formation and bursting of vapour bubbles, formation of puddles, secondary atomisation;
	220	Formation and bursting of vapour bubbles, formation of puddles, secondary atomisation, puffing, pagoda-like bubbles, presence of two regimes - film evaporation and nucleate boiling.
	240	Formation and bursting of vapour bubbles, formation of puddles, secondary atomisation, puffing, pagoda-like bubbles, presence of two regimes - film evaporation and nucleate boiling.
Transition Boiling	260	Droplets projected radially and vertically, puffing, secondary atomisation, Leidenfrost effect, vapour bubbles form inside the daughter droplets, presence of two regimes - transition and film boiling
Film Boiling	275/320	Droplets projected only radially, impact point with a larger single droplet, Leidenfrost effect, splashing

Table 4.4: Summary of the phenomena observed for a mixture of 50% Jet Fuel with 50% HVO for the four heat regimes.

Heat Regime	T_w [ºC]	Phenomenon Description
Film Evaporation	25	Spreading, no receding, air entrapment, no fingering;
	100	Spreading w/ receding, air entrapment, no fingering;
	150	Spreading w/ receding, air entrapment no fingering, formation of vapour bubbles;
	180	Spreading w/ receding, air entrapment, fingering, formation of vapour bubbles, puffing;
	220	Spreading, air entrapment, fingering, formation of vapour bubbles, formation of puddles, puffing.
Nucleate Boiling	250	Formation and bursting of vapour bubbles, secondary atomisation, puffing, pagoda-like bubbles, presence of two regimes - film evaporation and nucleate boiling.
Transition Boiling	275	Droplets projected radially and vertically, puffing, secondary atomisation, Leidenfrost effect, vapour bubbles inside the daughter droplets, presence of two regimes - transition and film boiling;
	300	Droplets projected radially and vertically, puffing, secondary atomisation, Leidenfrost effect, vapour bubbles form inside the daughter droplets.
Film Boiling	320	Droplets projected only radially, impact point with larger and bigger droplets, Leidenfrost effect, splashing

Table 4.5: Summary of the phenomena observed for 100% HVO for the four heat regimes.

Heat Regime	T_w [ºC]	Phenomenon Description
Film Evaporation	25	Spreading, no receding, air entrapment, no fingering;
	50	Spreading w/ receding, air entrapment, no fingering;
	100	Spreading w/ receding, air entrapment no fingering, prompt splash;
	150	Spreading w/ receding, air entrapment, no fingering;
	200	Spreading w/ receding, air entrapment, fingering;
	250	Spreading, air entrapment, fingering, formation of vapour bubbles, formation of puddles, puffing.
Nucleate Boiling	285	Formation and bursting of vapour bubbles, secondary atomisation, puffing, formation of puddles
	300	Formation and bursting of vapour bubbles, secondary atomisation, puffing, pagoda-like bubbles.
Transition Boiling	315	Droplets projected radially and vertically, puffing, secondary atomisation, Leidenfrost effect, vapour bubbles form inside the daughter droplets
Film Boiling	330	Droplets projected only radially, impact point with larger and bigger droplets, Leidenfrost effect, splashing

Chapter 5

Conclusions and Future Work

In this chapter, two main topics will be discussed. The first one concerns the conclusions about the phenomena observed for this experimental work. The second topic will be about possible future works and improvements.

5.1 Conclusions

The objective of this experimental work was to visualise and describe the collision dynamics of a single droplet impact onto a heated wall with constant impact energy. Therefore, for the different fluids, the Weber number was kept at a constant value of about $We = 320$. The fluids tested were H_2O, Jet Fuel, a mixture of 75% Jet Fuel with 25% HVO, a mixture of 50% Jet Fuel with 50% HVO, and HVO. These fluids, apart from water, have similar physical properties, such as surface tension, but their viscosity varies notably. Additionally, the impact surface temperature varied from $T_w = 25$ºC to $T_w = 330$ºC in order to reach all heat regimes for all the fluids.

As mentioned in the experimental procedure, the installation and fluid properties were done and measured by Ribeiro [59]. To keep a constant Weber number, droplet size and impact velocity were varied. For the sake of consistency, the experiments for each fluid and for each temperature were done ten times. Additionally, when heating the surface to the desired experimental condition, a measurement of the surface temperature would be done until it stabilised. Besides that, every five tests made in each condition, another measurement of the surface temperature would be done, to ensure that every impact had the same condition.

The phenomenon of receding only occurred at room temperature for water. The other fluids only entered a receding phase when the plate was heated. However, water always had receding breakup and the other fluids did not. Additionally, water always experienced fingering in the spreading phase, in comparison with the other fluids that only experienced this when the plate was heated, and it was due to the incipience of boiling.

A prompt splash was observed for HVO in the film evaporation regime, at a wall temperature of $T_w = 100$ºC, while for the other fluids, never occurred. In an advanced film evaporation regime, the droplet would not undergo a receding phase and, instead, it would breakup into puddles. These puddles would slowly boil while ejecting bursting vapour bubbles that emerge to the surface of the droplet. The jet fuel/HVO mixtures, jet fuel, and HVO also experienced fumes evaporation which is called puffing. For every fluid, it was possible to observe the

phenomenon of the jets bursting on top of the ”pagoda-like bubbles”, as addressed by Liang et al. [28].

In the transition boiling regime, the droplet partially wets the wall and, therefore, it experiences both secondary atomisation and the Leidenfrost phenomenon, which is when a tiny vapour layer is formed between the droplet and the wall and it greatly reduces heat flux, increasing the droplet evaporation time by a significant amount. However, since this vapour layer is unstable, the droplet can rebound and eventually stick to the wall and completely boil.

In the film boiling regime, above the Leidenfrost temperature, the splashing phenomenon repeated itself for the fluids, with only some differences for the mixtures containing HVO. For these, a concentrated mass of a single droplet or droplets would rebound in the impact point. For water and jet fuel, this was not observed. However, all the fluids would undergo a prompt splash, where they would breakup in the rim of the spreading lamella, and the daughter droplets would be ejected in the radial direction. With the working impact energy, no complete rebound of the droplet was observed. Instead, the droplet always experienced splashing.

In this experimental study, it was possible to achieve all the four heat regimes (film evaporation, nucleate boiling, transition boiling, and film boiling) for all fluids, though their transition temperatures between regimes varied by a significant amount. Besides these four heat regimes, another two were observed. These are unique for the biofuel and fuel mixtures (75% jet fuel - 25% HVO, and 50% jet fuel - 50% HVO), and implies that two regimes are present at the same time due to different boiling points of the mixed fluids. They are wet boiling impact followed by the remaining of a sessile droplet on the surface after boiling completion, and dry impact followed by bounce and wet boiling [62]. The former occurs when the different fluids are between the nucleate boiling and film evaporation regimes, and the latter occurs when the fluids are between the transition and film boiling regimes.

5.2 Future Work

Through the analysis of this experimental work, some recommendations and suggestions for future work and its improvement can be advised.

First, it can be interesting to provide a more detailed heat regimes map for the fluids. In this work, the only parameter that changed was the wall temperature. Varying the Weber number and tracing a $We - T_w$ graph with the respective phenomenon for each fluid is of great interest. Also, providing a detailed analysis of the size of secondary droplets generated or varying the Weber number while keeping the Reynolds number constant can be of great interest.

Another interesting topic to approach is a detailed investigation on a single regime. For ex-

ample, analysing the maximum spreading diameter or the time it takes to achieve it, while increasing the wall temperature for a single regime. Additionally, using different surfaces, such as stainless steel for example, and compare the results for the aluminium surface in the same regime can be interesting. These studies are essential to compare them with the current literature, and perhaps, provide more information regarding these subjects.

Bibliography

[1] R. Luque, L. Herrero-Davila, J. M. Campelo, J. H. Clark, J. M. Hidalgo, D. Luna, J. M. Marinas, and A. A. Romero, "Biofuels: a technological perspective," *Energy & Environmental Science*, vol. 1, no. 5, pp. 542–564, 2008. 1

[2] ASTM International, "ASTM D7566-20b, Standard Specification for Aviation Turbine Fuel Containing Synthesized Hydrocarbons," West Conshohocken, Tech. Rep., 2020. 1

[3] D. B. van Dam and C. Le Clerc, "Experimental study of the impact of an ink-jet printed droplet on a solid substrate," *Physics of Fluids*, vol. 16, no. 9, pp. 3403–3414, 2004. 3

[4] M. Pasandideh-Fard, S. Aziz, S. Chandra, and J. Mostaghimi, "Cooling effectiveness of a water drop impinging on a hot surface," *International Journal of Heat and Fluid Flow*, vol. 22, no. 2, pp. 201–210, 2001. 3

[5] M. R. Panão and A. L. N. Moreira, "Flow characteristics of spray impingement in pfi injection systems," *Experiments in Fluids*, vol. 39, no. 2, pp. 364–374, 2005. 3

[6] V. Bergeron, D. Bonn, J. Y. Martin, and L. Vovelle, "Controlling droplet deposition with polymer additives," *Nature*, vol. 405, no. 6788, pp. 772–775, 2000. 3

[7] M. Visaria and I. Mudawar, "Application of two-phase spray cooling for thermal management of electronic devices," *IEEE Transactions on Components and Packaging Technologies*, vol. 32, no. 4, pp. 784–793, 2009. 3

[8] G. Liang and I. Mudawar, "Review of mass and momentum interactions during drop impact on a liquid film," *International Journal of Heat and Mass Transfer*, vol. 101, pp. 577–599, 2016. 3, 21, 22

[9] N. E. Ersoy and M. Eslamian, "Phenomenological study and comparison of droplet impact dynamics on a dry surface, thin liquid film, liquid film and shallow pool," *Experimental Thermal and Fluid Science*, vol. 112, p. 109977, 2020. 4, 7

[10] A. L. Yarin, "Drop impact dynamics: splashing, spreading, receding, bouncing...," *Annu. Rev. Fluid Mech.*, vol. 38, pp. 159–192, 2006. 5, 7

[11] C. Amiel, "Application de techniques optiques à l'étude du comportement dynamique et thermique de gouttes en interaction avec une paroi chauffée," Ph.D. dissertation, École nationale supérieure de l'aéronautique et de l'espace, 2003. 5

[12] R. Rioboo, C. Tropea, and M. Marengo, "Outcomes from a drop impact on solid sur-

faces," *Atomization and Sprays*, vol. 11, no. 2, 2001. 5, 6, 7, 8, 9, 10, 11

[13] J. D. Bernardin, I. Mudawar, C. B. Walsh, and E. I. Franses, "Contact angle temperature dependence for water droplets on practical aluminum surfaces," *International Journal of Heat and Mass Transfer*, vol. 40, no. 5, pp. 1017–1033, 1997. 6

[14] C. Josserand and S. T. Thoroddsen, "Drop impact on a solid surface," *Annual Review of Fluid Mechanics*, vol. 48, pp. 365–391, 2016. 7

[15] D. V. Rodrigues, "Numerical analysis of a single droplet impinging upon liquid films using the vof method," Master's thesis, Universidade da Beira Interior, 2018. 7

[16] N. F. C. Cunha, "Experimental study of a single droplet impinging on dry surface with and without a crossflow: Jet fuel and biofuel mixtures," Master's thesis, Universidade da Beira Interior, 2018. 8

[17] I. A. d. S. Ferrão, "Dynamic behavior of a single droplet impinging onto a sloped surface," Master's thesis, Universidade da Beira Interior, 2018. 9, 10

[18] H. Almohammadi and A. Amirfazli, "Droplet impact: Viscosity and wettability effects on splashing," *Journal of Colloid and Interface Science*, vol. 553, pp. 22–30, 2019. 10

[19] T. Mang, Ed., *Surface Tension*. Berlin, Heidelberg: Springer Berlin Heidelberg, 2014, pp. 2007–2007. [Online]. Available: https://doi.org/10.1007/978-3-642-22647-2_200474 10

[20] C. Bai and A. Gosman, "Development of methodology for spray impingement simulation," *SAE transactions*, pp. 550–568, 1995. 11

[21] I. Roisman, J. Breitenbach, and C. Tropea, "Thermal atomisation of a liquid drop after impact onto a hot substrate," *Journal of Fluid Mechanics*, vol. 842, p. 87, 2018. 12, 58

[22] V. Bertola, "An impact regime map for water drops impacting on heated surfaces," *International Journal of Heat and Mass Transfer*, vol. 85, pp. 430–437, 2015. 12, 13

[23] Y. Ko and S. Chung, "An experiment on the breakup of impinging droplets on a hot surface," *Experiments in Fluids*, vol. 21, no. 2, pp. 118–123, 1996. 13, 35

[24] M. Seki, H. Kawamura, and K. Sanokawa, "Transient temperature profile of a hot wall due to an impinging liquid droplet," *Journal of Heat Transfer*, vol. 100, no. 1, pp. 167–169, 1978. 14

[25] G. Liang and I. Mudawar, "Review of drop impact on heated walls," *International Journal of Heat and Mass Transfer*, vol. 106, pp. 103–126, 2017. 14, 18

[26] M. Di Marzo and D. D. Evans, "Evaporation of a water droplet deposited on a hot high thermal conductivity solid surface," National Bureau of Standards, Tech. Rep., 1986. 15

[27] S. Chandra, M. Di Marzo, Y. Qiao, and P. Tartarini, "Effect of liquid-solid contact angle on droplet evaporation," *Fire Safety Journal*, vol. 27, no. 2, pp. 141–158, 1996. 15

[28] G. Liang, X. Mu, Y. Guo, S. Shen, S. Quan, and J. Zhang, "Contact vaporization of an impacting drop on heated surfaces," *Experimental Thermal and Fluid Science*, vol. 74, pp. 73–80, 2016. 15, 66

[29] J. Fukai, Y. Shiiba, and O. Miyatake, "Theoretical study of droplet impingement on a solid surface below the leidenfrost temperature," *International Journal of Heat and Mass Transfer*, vol. 40, no. 10, pp. 2490–2492, 1997. 15

[30] Q. Cui, S. Chandra, and S. McCahan, "The effect of dissolving gases or solids in water droplets boiling on a hot surface," *Journal of Heat Transfer*, vol. 123, no. 4, pp. 719–728, 2001. 15

[31] A. Moita and A. Moreira, "Boiling morphology and heat removal of impinging coolant droplets," in *Proceedings of 22nd European Conference on Liquid Atomization and Spray Systems, ILASS2008, Como Lake, Italy*, 2008. 15

[32] S. Moghtadernejad, C. Lee, and M. Jadidi, "An introduction of droplet impact dynamics to engineering students," *Fluids*, vol. 5, no. 3, p. 107, 2020. 16

[33] T. Xiong and M. Yuen, "Evaporation of a liquid droplet on a hot plate," *International Journal of Heat and Mass Transfer*, vol. 34, no. 7, pp. 1881–1894, 1991. 16, 20

[34] S. G. Kandlikar and M. E. Steinke, "Contact angles and interface behavior during rapid evaporation of liquid on a heated surface," *International Journal of Heat and Mass Transfer*, vol. 45, no. 18, pp. 3771–3780, 2002. 16

[35] J. D. Bernardin, C. J. Stebbins, and I. Mudawar, "Mapping of impact and heat transfer regimes of water drops impinging on a polished surface," *International Journal of Heat and Mass Transfer*, vol. 40, no. 2, pp. 247–267, 1997. 16

[36] V. Nakoryakov, S. Y. Misyura, and S. Elistratov, "The behavior of water droplets on the heated surface," *International Journal of Heat and Mass Transfer*, vol. 55, no. 23-24, pp. 6609–6617, 2012. 16

[37] S. Akhtar, G. G. Nasr, and A. J. Yule, "Characteristics of water droplet impaction behavior on a polished steel heated surface: Part i," *Atomization and Sprays*, vol. 17, no. 8, 2007. 16, 21

[38] C. M. G. Rodrigues, “Modelling of spray-wall impingement,” Ph.D. dissertation, Universidade da Beira Interior, 2016. 16

[39] J. D. Bernardin and I. Mudawar, “A cavity activation and bubble growth model of the leidenfrost point,” *Journal of Heat Transfer*, vol. 124, no. 5, pp. 864–874, 2002. 17

[40] P. Testa and L. Nicotra, “Influence of pressure on the leidenfrost temperature and on extracted heat fluxes in the transient mode and low pressure,” *Journal of Heat Transfer*, vol. 108, no. 4, pp. 916–921, 1986. 17

[41] B. Gottfried, C. Lee, and K. Bell, “The leidenfrost phenomenon: film boiling of liquid droplets on a flat plate,” *International Journal of Heat and Mass Transfer*, vol. 9, no. 11, pp. 1167–1188, 1966. 17

[42] J. Senda, T. Kanda, M. Al-Roub, P. V. Farrell, T. Fukami, and H. Fujimoto, “Modeling spray impingement considering fuel film formation on the wall,” *SAE transactions*, pp. 98–112, 1997. 17, 18

[43] H. Chaves, A. M. Kubitzek, and F. Obermeier, “Dynamic processes occurring during the spreading of thin liquid films produced by drop impact on hot walls,” *International Journal of Heat and Fluid Flow*, vol. 20, no. 5, pp. 470–476, 1999. 19, 20, 38

[44] S. Chandra and C. Avedisian, “On the collision of a droplet with a solid surface,” *Proceedings of the Royal Society of London. Series A: Mathematical and Physical Sciences*, vol. 432, no. 1884, pp. 13–41, 1991. 19, 22, 35

[45] G. Cossali, M. Marengo, M. Santini, and J. Watanabe, “Secondary droplet atomisation from single drop impact on heated surfaces,” *ILASS-Europe 2002*, vol. 9, p. 11, 2002. 19

[46] G. Cossali, M. Marengo, and M. Santini, “Thermally induced secondary drop atomisation by single drop impact onto heated surfaces,” *International Journal of Heat and Fluid Flow*, vol. 29, no. 1, pp. 167–177, 2008. 20, 43

[47] G. Cossali, M. Marengo, and M. Santini, “Secondary atomisation produced by single drop vertical impacts onto heated surfaces,” *Experimental thermal and fluid science*, vol. 29, no. 8, pp. 937–946, 2005. 20, 42

[48] A. Moita and A. Moreira, “Drop impacts onto cold and heated rigid surfaces: morphological comparisons, disintegration limits and secondary atomization,” *International Journal of Heat and Fluid Flow*, vol. 28, no. 4, pp. 735–752, 2007. 20, 35

[49] A.-B. Wang, C.-H. Lin, and C.-C. Cheng, “Pattern analysis of a single droplet impinging

onto a heated plate," *Heat Transfer—Asian Research: Co-sponsored by the Society of Chemical Engineers of Japan and the Heat Transfer Division of ASME*, vol. 34, no. 8, pp. 579–594, 2005. 20

[50] V. Bertola and K. Sefiane, "Controlling secondary atomization during drop impact on hot surfaces by polymer additives," *Physics of Fluids*, vol. 17, no. 10, p. 108104, 2005. 20

[51] A.-L. Biance, C. Clanet, and D. Quéré, "Leidenfrost drops," *Physics of Fluids*, vol. 15, no. 6, pp. 1632–1637, 2003. 21

[52] F. Celestini, T. Frisch, and Y. Pomeau, "Take off of small leidenfrost droplets," *Phys. Rev. Lett.*, vol. 109, p. 034501, Jul 2012. [Online]. Available: https://link.aps.org/doi/10.1103/PhysRevLett.109.034501 21

[53] N. Hatta, H. Fujimoto, K. Kinoshita, and H. Takuda, "Experimental study of deformation mechanism of a water droplet impinging on hot metallic surfaces above the leidenfrost temperature," *Journal of Fluids Engineering*, vol. 119, no. 3, pp. 692–699, 1997. 21

[54] L. Wachters and N. Westerling, "The heat transfer from a hot wall to impinging water drops in the spheroidal state," *Chemical Engineering Science*, vol. 21, no. 11, pp. 1047–1056, 1966. 21, 23

[55] S.-L. Chiu and T.-H. Lin, "Experiment on the dynamics of a compound drop impinging on a hot surface," *Physics of Fluids*, vol. 17, no. 12, p. 122103, 2005. 21

[56] A.-L. Biance, F. Chevy, C. Clanet, G. Lagubeau, and D. Quéré, "On the elasticity of an inertial liquid shock," *Journal of Fluid Mechanics*, vol. 554, p. 47, 2006. 22

[57] J. Yong Park, A. Gardner, W. P. King, and D. G. Cahill, "Droplet impingement and vapor layer formation on hot hydrophobic surfaces," *Journal of Heat Transfer*, vol. 136, no. 9, 2014. 23

[58] E.-S. R. Negeed, M. Albeirutty, S. F. Al-Sharif, S. Hidaka, and Y. Takata, "Dynamic behavior of a small water droplet impact onto a heated hydrophilic surface," *Journal of Heat Transfer*, vol. 138, no. 4, 2016. 23

[59] D. F. S. Ribeiro, "Experimental study of a single droplet impinging upon liquid films: Jet fuel and biofuel mixtures," Master's thesis, Universidade da Beira Interior, 2018. 30, 65

[60] J. H. Moon, D. Y. Kim, and S. H. Lee, "Spreading and receding characteristics of a non-

newtonian droplet impinging on a heated surface," *Experimental thermal and fluid science*, vol. 57, pp. 94–101, 2014. 37

[61] C. Cen, H. Wu, C.-f. Lee, L. Fan, and F. Liu, "Experimental investigation on the sputtering and micro-explosion of emulsion fuel droplets during impact on a heated surface," *International Journal of Heat and Mass Transfer*, vol. 132, pp. 130–137, 2019. 38

[62] E. Kompinsky, G. Dolan, and E. Sher, "Experimental study on the dynamics of binary fuel droplet impacts on a heated surface," *Chemical Engineering Science*, vol. 98, pp. 186–194, 2013. 59, 66

Appendix A

A.1 Blueprint of the Impact Surface

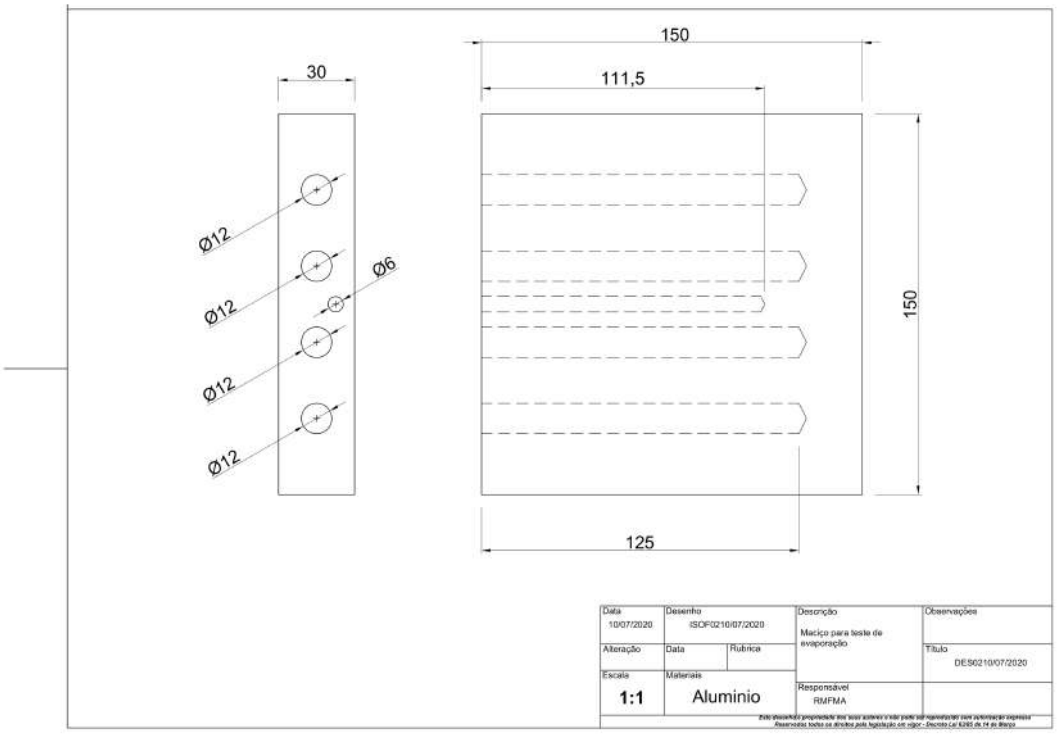

Figure A.1: Blueprint of the impact surface.